IMPROVING THE EFFICACY AND EXPANDING THE APPLICATION OF NQO1-BIOACTIVATED THERAPEUTICS

APPROVED BY SUPERVISORY COMMITTEE

David A. Boothman, Ph.D. (Mentor)

Rolf A. Brekken, Ph.D. (Chair)

Jinming Gao, Ph.D.

Pier Paolo Scaglioni, M.D.

DEDICATION

For Madison.

IMPROVING THE EFFICACY AND EXPANDING THE APPLICATION OF NQO1-BIOACTIVATED THERAPEUTICS

by

ZACHARY RAY MOORE

DISSERTATION

Presented to the Faculty of the Graduate School of Biomedical Sciences

The University of Texas Southwestern Medical Center at Dallas

In Partial Fulfillment of the Requirements

For the Degree of

DOCTOR OF PHILOSOPHY

The University of Texas Southwestern Medical Center at Dallas

Dallas, Texas

Degree Conferral May, 2018

IMPROVING THE EFFICACY AND EXPANDING THE APPLICATION OF NQO1-BIOACTIVATED THERAPEUTICS

Publication No. _____

Zachary Ray Moore, Ph.D.

The University of Texas Southwestern Medical Center at Dallas, 2015

Supervising Professor: David A. Boothman, Ph.D.

Abstract

NADPH:quinone oxidoreductase-1 (NQO1)-bioactivated drugs, such as ß-lapachone (ß-lap), are powerful therapeutics for tumor-specific therapy. They react with NQO1, which is highly overexpressed in most solid tumors, to cause a futile redox cycle that results in devastating oxidative DNA damage and energy depletion in the form of ATP, NAD(H) and NADP(H) loss specifically in tumor cells. However, ß-lap suffers from inherent limitations shared by quinone therapeutics, most notably

methemoglobinemia at high doses caused by non-specific oxidation of hemoglobin. My goal was to increase the efficacy of ß-lap at lower, well-tolerated doses without increasing normal tissue toxicity.

Targeting the NAD^+ synthesis pathway by inhibiting NAMPT prevented cells from surviving the metabolic stress of NAD^+ and ATP depletion induced by PARP1 hyperactivation secondary to ß-lap treatment. This resulted in synergistic cancer cell death at normally sublethal doses of both ß-lap and NAMPT inhibitors, occurring through the same NAD^+-Keresis mechanism as with ß-lap alone. On the other hand, synergy with PARP inhibitors occurred due to an increased accumulation of DNA double strand breaks, which was a result of inhibited repair of ß-lap-induced single strand breaks. In contrast to synergy observed with NAMPT inhibition, PARP inhibitors combined with ß-lap caused canonical caspase-mediated apoptosis.

In addition to providing new treatments for further preclinical and clinical development, these studies elucidated the importance of NAD^+ and ATP depletion in cell death induced by ß-lap. Furthermore, these treatment strategies increase the tumor specificity and widen the use of both NAMPT and PARP inhibitors, since in combination with ß-lap they are effective against all NQO1-overexpressing tumor cells. As a study in expanding the application of NQO1-bioactivated therapeutics, I have also demonstrated NQO1 overexpression and ß-lap sensitivity in atypical teratoid rhaboid tumors (ATRTs), a rare but deadly pediatric malignancy that can be targeted with NQO1-bioactivated therapeutics.

TABLE OF CONTENTS

PRIOR PUBLICATIONS

1. Chakrabarti, C. **Moore, Z**., Luo, X., Ilcheva, M., Ali, A., Fattah, F., Padanad, M., Zhou, Y., Xie, Y., Lyssiotis, C., Scaglioni, P., Kimmelman, A., DeBerardinis, R., Cantley, L., Boothman, DA. **Targeting KRAS-reprogrammed glutamine metabolism sensitizes pancreatic cancer to NQO1-bioactivatable drugs.** *Submission Pending*

2. Chakrabarti, G., Silvers, M., Ilcheva, M., Liu, Y., **Moore, Z.**, Luo, X., Gao, J., Anderson, G., Liu, L., Gerber, D., Burma, S., DeBerardinis, RJ., Gerson, SL., Boothman, DA. **Tumor-selective use of DNA base excision repair inhibition in pancreatic cancer using the NQO1 bioactivatable drug, β-lapachone.** *Submission Pending*

3. **Moore, Z.**, Chakrabarti, G., Luo, X., Ali, A., Hu, Z., Fattah, F.J., Vemireddy, R., DeBerardinis, R.J., Brekken, R.A., and Boothman, D.A. (2015). NAMPT inhibition sensitizes pancreatic adenocarcinoma cells to tumor-selective, PAR-independent metabolic catastrophe and cell death induced by beta-lapachone. Cell death & disease *6*, e1599.

4. Ma, X., Huang, X., **Moore, Z.**, Huang, G., Kilgore, J.A., Wang, Y., Hammer, S., Williams, N.S., Boothman, D.A., and Gao, J. (2015). Esterase-activatable beta-lapachone prodrug micelles for NQO1-targeted lung cancer therapy. Journal of controlled release: official journal of the Controlled Release Society *200*, 201-211.

5. Cao, L., Li, L.S., Spruell, C., Xiao, L., Chakrabarti, G., Bey, E.A., Reinicke, K.E., Srougi, M.C., **Moore, Z.**, Dong, Y*., et al.* (2014). Tumor-Selective, Futile Redox Cycle-Induced Bystander Effects Elicited by NQO1 Bioactivatable Radiosensitizing Drugs in Triple-Negative Breast Cancers. Antioxidants & redox signaling *21*, 237-250.

6. Bey, E.A., Reinicke, K.E., Srougi, M.C., Varnes, M., Anderson, V.E., Pink, J.J., Li, L.S., Patel, M., Cao, L., **Moore, Z.***, et al.* (2013). Catalase abrogates beta-lapachone-induced PARP1 hyperactivation-directed programmed necrosis in NQO1-positive breast cancers. Molecular cancer therapeutics *12*, 2110-2120.

7. Huang, G., Chen, H., Dong, Y., Luo, X., Yu, H., **Moore, Z.**, Bey, E.A., Boothman, D.A., and Gao, J. (2013). Superparamagnetic iron oxide nanoparticles: amplifying ROS stress to improve anticancer drug efficacy. Theranostics *3*, 116-126.

LIST OF FIGURES

CHAPTER ONE

CHAPTER TWO

LIST OF ABBREVIATIONS

2-DG – 2-deoxy-D-glucose

ADP – adenosine diphosphate

AIF – apoptosis inducing factor

ATP – adenosine triphosphate

ATRT - atypical teratoid rhabdoid tumor

DER – dose enhancement ratio

Dic – dicoumarol

DNQ - deoxyniboquinone

DSB - double strand break

ECAR – extracellular acidification rate

F6P – fructose 6-phosphate

FK – FK866

G6P – glucose 6-phosphate

GA3P – glyceraldehyde 3-phosphate

GAPDH – glyceraldehyde 3-phosphate dehydrogenase

GEM – genetically engineered mouse

GSH – glutathione (reduced)

HDAC - histone deacetylase

IB-DNQ - isobutyl-deoxyniboquinone

IHC - immunohistochemistry

INI1 - integrase interactor 1

MNNG – methylnitronitrosoguanidine

MRT - malignant rhabdoid tumor

NAD – nicotinamide adenine dinucleotide

NAMPT – nicotinamide phosphoribosyltransferase

NMN – nicotinamide mononucleotide

NQO1 – NADPH:quinone oxidoreductase

NSCLC - non-small cell lung cancer

Oligo - oligomycin

PAR – poly(ADP ribose)

PARP1 – poly(ADP ribose) polymerase 1

PD - pharmacodynamics

PDA – pancreatic ductal adenocarcinoma

PK – pharmacokinetics

RFLP - restriction fragment-length polymorphism

RNS – reactive nitrogen species

ROS – reactive oxygen species

ß-lap – ß-lapachone

SSB - single strand break

STS – staurosporine

TUNEL - terminal deoxynucleotidyl nick end labeling

Chapter One
Introduction and Overview

1.1 Targeted Cancer Therapeutics

Rapid technological achievements have exposed the inner workings of the cancer cell, but clinicians still lack the tools to make cancer a problem of the past. The 5-year survival rate for patients diagnosed with pancreatic cancer is about 6% (R. Siegel, Naishadham, & Jemal, 2013). Lung cancer, another deadly malignancy, is the leading cause of cancer death among both men and women, with 158,040 deaths in the United States expected in 2015 (R. L. Siegel, Miller, & Jemal, 2015). If surgery does not cure patients with solid tumors, the prognosis is dismal; the typical outcome from treating advanced cancers with most current chemotherapeutics is a nominal survival increase, often only a few months (Conroy et al., 2011).

Many of the chemotherapeutics frequently used today, such as methotrexate and fluorouracil, are relics of early discoveries that DNA damaging agents and antimetabolites kill rapidly dividing cancer cells. Unfortunately, they are also toxic to healthy proliferating cells in the GI tract and the bone marrow (Farber & Diamond, 1948; Vaitkevicius, Brennan, Beckett, Kelly, & Talley, 1961). These chemotherapeutics work well for some cancers, but for more recalcitrant diseases we have come up mostly empty-handed for better options, though not for lack of trying. Over decades of study, researchers have uncovered many of the molecular drivers that initiate and promote the progression of cancer with the hope of locating an “Achilles heel” to shoot with a “magic bullet”. The dream of designing highly specific drugs to target the individual drivers of cancer was realized by the tyrosine kinase inhibitor imatinib, which

was a great success in treating chronic myelogenous leukemia while causing only minimal side effects (Sawyers, 2004). Dozens of targeted therapeutics have since been developed, with varying levels of success (Janku, Stewart, & Kurzrock, 2010; Scott, Wolchok, & Old, 2012). Unfortunately, drugs have not been successfully developed to target some of the most ubiquitous oncogenes and tumor suppressors such as Ras and p53 due to intractable technical challenges. On the other hand, therapy with even the most specific and potent targeted agents suffers from inherent limitations. For example, a promising clinical trial of a BRAF inhibitor in melanoma was at first wildly successful, with many patients experiencing dramatic shrinking of metastatic tumors (Flaherty et al., 2010). However, in almost all patients, the tumors returned and developed drug resistance (Flaherty et al., 2010). The same problem plagues EGFR inhibitors for lung cancer, HER2 antibodies for breast cancer, and virtually all other targeted cancer therapies (Kobayashi et al., 2005; Nahta, Yuan, Zhang, Kobayashi, & Esteva, 2005).

Cancer cells are very robust, and a rapid growth rate and high mutation frequency amplifies their ability to adapt to the selective pressure of exposure to targeted drugs. Mechanisms of resistance include altered drug metabolism, expression of drug efflux pumps, and suppression of apoptosis (Gottesman, 2002; Holohan, Van Schaeybroeck, Longley, & Johnston, 2013). By regulating compensatory signaling pathways and cultivating mutations that provide resistance to targeted agents, cancer readily circumvents small molecule inhibitors and antibodies (Gorre et al., 2001; Hynes & Lane, 2005; Kobayashi et al., 2005; Villanueva et al., 2010).

Two paradigms for dealing with resistance include re-testing recurrent cancers for new mutations and gene expression changes to guide the selection of follow-up therapeutics, which amounts to an expensive and unwieldy game of whack-a-mole, or treating from the onset with a cocktail of different therapeutics while carefully monitoring side effects and drug interactions (Kamb, Wee, & Lengauer, 2007; Meric-Bernstam, Farhangfar, Mendelsohn, & Mills, 2013). A common problem with targeted therapeutics is a trade-off between tumor specificity and development of resistance. This stems from the reliance of most targeted therapeutics on inhibition or activation of particular signaling pathways to prevent cancer cell growth or induce apoptosis (Maloney, Smith, & Rose, 2002; Weinstein & Joe, 2008). Highly specific targeted agents often have fewer side effects but are also more easily obviated by tumor cell resistance. On the other hand, using a copious number of agents in combination or applying agents with mixed target specificity may decrease the probability of resistance but limit dosing due to more toxicity to normal tissue.

This paradigm can be shifted by decoupling the means of achieving target specificity from the method of inducing tumor cell death. A new class of drugs known as NQO1-bioactivated therapeutics shows great promise for achieving high cancer cell specificity in a variety of tumor types based on the wide therapeutic window provided by NQO1 overexpression, while avoiding the pitfall of relying on oncogene addiction to a particular signaling pathway by inducing a robust form of cell death without known resistance mechanisms.

1.2 NQO1, a biomarker in solid tumors

NADPH:quinone oxidoreductase 1 (NQO1) is a phase II detoxifying enzyme that catalyzes the two electron reduction of target quinones to promote their neutralization and removal from the cell (Ross et al., 2000). Endogenous quinones are important electron carriers in metabolic reactions, but both endogenous and exogenous quinones can generate toxic reactive oxygen species (ROS) that damage DNA, proteins, and lipids. Historically, the detoxification of carcinogenic molecules has been defined by a two-step process catalyzed by phase I and phase II enzymes (Williams, 1967). Phase I enzymes, like NADPH:cytochrome P450 reductase (P450r) and NADH:cytochrome b_5 reductase (b5R), catalyze the one-electron reduction of quinones, which produces reactive semiquinone intermediates. Phase II enzymes, such as glutathione-s-transferase, conjugate these reactive intermediates to specialized substrates like glutathione which neutralizes their reactivity, improves their solubility, and allows them to be efficiently exported from the cell (Talalay, 2000). NQO1 bypasses the formation of reactive intermediates by performing a two-electron reduction and instead generates a hydroquinone from the parent quinone that is typically much more stable and can still be conjugated by other phase II enzymes for cellular export (Cadenas, 1995).

The kinetic mechanism of this two-electron reduction is called “ping pong bi-bi”: NADH or NADPH (either can be used with equal efficiency) first binds NQO1 and reduces its FAD cofactor, NAD^+ or $NADP^+$ is released, and finally the quinone binds and is reduced in one step to the hydroquinone (Preusch, Siegel, Gibson, & Ross, 1991). The active site of NQO1 is a flexible hydrophobic pocket that can accommodate

consecutive binding of NADH/NADPH and a variety of quinones with a diversity of structures (Faig et al., 2001; Nolan, Timson, Stratford, & Bryce, 2006). Dicoumarol, a vitamin K analog that was used clinically as an anticoagulant, is a potent inhibitor of NQO1 and binds tightly in the active site to the oxidized form of the enzyme (Preusch et al., 1991).

NQO1 is present in animals, plants and bacteria, with expression in humans seen primarily in epithelial cells, especially lung and GI epithelium (Nolan et al., 2006; D. Siegel & Ross, 2000). The expression of NQO1 is tightly regulated as it is typically only transiently induced in normal tissue when reactive oxygen species (ROS) stress is occurring or when exogenous quinones or polycyclic aromatic hydrocarbons are present (Ross et al., 2000). For example, cigarette smoke can rapidly and transiently increase NQO1 expression in the lung, and polyphenolic compounds from plants also increase NQO1 levels (Gebel et al., 2004; Tanigawa, Fujii, & Hou, 2007). NQO1 expression is primarily regulated by the Nrf2-KEAP1 signaling pathway; oxidative stress causes KEAP1 and Nrf2 to disassociate due to direct post-translational modification by superoxide, allowing nuclear translocation of Nrf2, where it acts as a transcription factor to drive expression of NQO1 and other genes containing an antioxidant response element (ARE) in their promoters, thereby activating a concerted response to ameliorate potential causes of ROS stress in the cell (Motohashi & Yamamoto, 2004).

NQO1 is a specialized component of a large antioxidant program driven by Nrf2; the only phenotype reported from NQO1 knockout in mice is hypersensitivity to menadione (a quinone that is normally neutralized by NQO1) and benzene toxicity

(Bauer et al., 2003; Radjendirane et al., 1998). In fact, two relatively common polymorphisms lead to a complete lack of functional NQO1 in the human population. The C609T mutation, referred to as NQO1*2, results in an amino acid change that yields an inactive form of NQO1 that cannot bind FAD and is rapidly degraded (Ross et al., 2000). Loss of NQO1 protein level and enzyme activity is only present in individuals who are homozygous for this polymorphism, which occurs at different rates depending on ethnicity, from 5% in Caucasians to 20% in Asians (Kelsey et al., 1997). Another polymorphism with a lower frequency is C465T (NQO1*3), which also results in loss of functional NQO1 in homozygous individuals (Gaedigk et al., 1998). There have been many studies to determine the clinical relevance of these polymorphisms with mixed findings. Some studies show higher lung cancer risk or a null association with the wild-type allele, whereas others show that cancer risk associated with polymorphic alleles can be either increased or decreased depending on race or smoking status (Lawson, Woodson, Virtamo, & Albanes, 2005) (Chao, Zhang, Berthiller, Boffetta, & Hashibe, 2006). There is also evidence that NQO1 polymorphism status may be a prognostic factor for response to chemotherapy, which may be related to its ability to activate or inactivate certain chemotherapeutic molecules as well as secondary effects caused by the ability of wild-type NQO1 to bind and stabilize p53 (Asher, Lotem, Kama, Sachs, & Shaul, 2002; Fagerholm et al., 2008).

Renewed interest in NQO1 was sparked by the discovery that it is overexpressed in solid tumors from a variety of cancer types (Awadallah et al., 2008; Belinsky & Jaiswal, 1993; Srivastava, Khurana, & Sugadev, 2012). NQO1 is markedly overexpressed in non-small cell lung cancer (NSCLC), breast, colon, and prostate

cancer (Schlager & Powis, 1990; D. Siegel, Franklin, & Ross, 1998). Up to 90% of pancreatic cancer cases exhibit 12-fold overexpression of NQO1 on average (Lewis et al., 2005). Reports on NQO1 often focus on its potential use as a biomarker that could aid diagnosis, since it appears to be overexpressed very early in cancer progression, and even in precancerous lesions (Awadallah et al., 2008). The mechanism of NQO1 overexpression in solid tumors is still not fully understood, and likely varies depending on the molecular context in each individual cancer type. For example, frequent mutations in NSCLC disrupt the KEAP1-Nrf2 interaction and drive NQO1 expression, whereas in pancreatic ductal adenocarcinoma (PDA), K-ras mutations increase Jun dimerization with Nrf2 to promote transcription of NQO1 (DeNicola et al., 2011; Singh et al., 2006).

The widespread overexpression of NQO1 in solid tumors makes it a good cancer biomarker, but its role in tumor growth, cancer progression, and metastasis has not been elucidated. There is at least one report that an NQO1 inhibitor slows the growth of PDA xenografts, but in general it does not appear that NQO1 expression is strictly necessary for the growth of tumor cells (Dehn, Siegel, Moody, Steiner, & Ross, 2005). Treatment with NQO1 inhibitors is probably not a viable strategy for cancer therapy, but the overexpression of NQO1 in cancer can be targeted a different way: with a class of NQO1-bioactivatable quinone drugs that are only toxic when metabolized by NQO1.

1.3 ß-Lapachone, an NQO1-bioactivated therapeutic

ß-lapachone (ß-lap) was the first therapeutic compound found to have a mechanism of action dependent on an NQO1 catalyzed futile cycle. Originally, ß-lap was isolated from the bark of the Pink Lapacho tree (*Handroanthus impetiginosus*), and exhibited anti-trypanosomal and anti-bacterial properties (Boveris, Docampo, Turrens, & Stoppani, 1978; Cruz, Docampo, & Boveris, 1978). Later, it was discovered to cause lethality to cancer cells, especially when combined with DNA damaging agents like ionizing radiation (IR), but the mechanism was hypothesized to be DNA damage repair inhibition, which is now known to be a secondary effect of its primary mechanism (Boothman, Trask, & Pardee, 1989). It wasn't until treatment times were reduced from 24 hours and longer to 2-4 hours that the NQO1 specificity of ß-lap was finally elucidated (Pink, Planchon, et al., 2000).

ß-Lap is a 1,2 napthoquinone substrate for NQO1, which catalyzes a 2-electron reduction. What makes ß-lap unique compared to other quinones that are neutralized by NQO1 is that the resulting hydroquinone form of ß-lap is exceptionally unstable. Instead of being conjugated and removed from the cell, the hydroquinone form of ß-lap spontaneously reacts with oxygen in two steps: first, an oxidization to the semiquinone form, and second, a reversion back to the parent quinone. Each of the spontaneous oxidation steps generates a superoxide anion radical. In sum, these reactions form a futile redox cycle in which ß-lap is converted to a hydroquinone by NQO1, oxidizing NADH and NADPH, and the hydroquinone reverts back to ß-lap, generating superoxide (**Figure 1-1**) (Pink, Planchon, et al., 2000). This cycle occurs very rapidly in cells that

express NQO1; one mole of ß-lap can cause 60 moles of NAD(P)H to be consumed and 120 moles of free radicals to be generated in less than ten minutes (Pink, Planchon, et al., 2000). Furthermore, ß-lap toxicity is completely dependent on NQO1 activity, as it is blocked by inhibition of NQO1 with dicoumarol or with RNAi mediated knockdown of NQO1 expression (Li et al., 2011; Planchon et al., 2001).

Rapid generation of superoxide and consumption of NAD(P)H are potently destructive to NQO1-overexpressing cells that are treated with ß-lap. The superoxide radicals generated directly from the futile cycle are reactive and short lived, but they are converted to other more stable reactive oxygen species (ROS), including hydrogen peroxide. These reactions are catalyzed by manganese superoxide dismutase (MnSOD) and spontaneous chemical processes. Hydrogen peroxide is membrane permeable and has a 1000-fold longer half life than the superoxide anion, allowing it to diffuse from the cytoplasm (where the NQO1-mediated futile cycle occurs) to the nucleus, where it is then converted back to superoxide through the Fenton reaction and reacts with DNA (Docampo, Cruz, Boveris, Muniz, & Esquivel, 1979; Imlay, Chin, & Linn, 1988). The DNA damage caused by ß-lap consists of single strand breaks and base oxidation, with a notable lack of double strand breaks compared to ionizing radiation (Bentle, Reinicke, Dong, Bey, & Boothman, 2007).

ß-lap induces apoptosis-like cell death in cancer cells that overexpress NQO1 as a result of two primary causes: a rapid burst of DNA damage that exceeds the repair capacity of the cell, and acute energy depletion resulting from the loss of NADP(H) and NAD^+, caused by both the redox futile cycle and PARP1 hyperactivation. PARP1 attempts to repair the single strand break DNA lesions by binding to the sites of

damage and catalyzing the poly(ADP ribosylation) of target DNA repair proteins to recruit and activate them (Beck, Robert, Reina-San-Martin, Schreiber, & Dantzer, 2014; Haince et al., 2008). However, due to the large number of lesions rapidly caused by ß-lap treatment, PARP1 is overwhelmed and completely consumes the available pool of NAD^+, which has been supplemented by the oxidation of NADH in the futile cycle, to form long chains of poly(ADP ribose) (PAR) (Bey et al., 2007). ß-Lap treatment is also associated with release of calcium from the endoplasmic reticulum and the subsequent activation of µ-Calpain (Pink, Wuerzberger-Davis, et al., 2000; Tagliarino, Pink, Dubyak, Nieminen, & Boothman, 2001). Much like members of the caspase family, µ-calpain is a cysteine protease that initiates cell death through cleavage of target proteins, including PARP1 (Tagliarino et al., 2003). Apoptosis inducing factor (AIF) translocates from the mitochondrial membrane to the nucleus and contributes to chromatin condensation, DNA fragmentation, and death (Bey et al., 2013; E. J. Park et al., 2014). The result is cell death with the following characteristics: PAR formation, ATP and NAD^+ depletion, caspase independence, µ-calpain cleavage, atypical PARP1 cleavage, and TUNEL staining (Bentle, Reinicke, Bey, Spitz, & Boothman, 2006; Bey et al., 2007; X. Huang et al., 2012; Tagliarino et al., 2003). The sequence of this cell death process is depicted in (**Figure 1-2**). Cell death exhibiting similar biomarkers is observed in other contexts, including glutamine excitotoxicity in neurons, and ischemia reperfusion in neurons and heart tissue (van Wijk & Hageman, 2005; Ying, Sevigny, Chen, & Swanson, 2001). There are some contrasting reports about cell death after ß-lap treatment occurring through caspase-dependent apoptosis, but this has only been observed after long-term treatment (8-74 hours versus 2-4 hours), which likely occurs through a different

mechanism since NQO1 dependence is also reduced with these longer treatment times (M. T. Park et al., 2011; Woo & Choi, 2005).

1.4 Limitations of ß-lap

ß-Lap is a promising therapeutic for cancer therapy. Many tumors overexpress NQO1, providing a large therapeutic window, and ß-lap induces cell death that is not affected by resistance to apoptosis or oncogene dependence. Unfortunately, there are some factors that may limit its clinical application. Both in the clinic and when used in animal models, the dose limiting toxicities of ß-lap are methemoglobinemia and hemolytic anemia (Hartner et al., 2007). Attempts to address these issues include the development of micelle formulations to reduce the amount of the potentially toxic vehicle 2-hydroxypropyl-beta-cyclodextrin (HPßCD) and improve tumor delivery by the enhanced permeability and retention (EPR) effect (Blanco et al., 2010). Esterase-activated ß-lap prodrug nanoparticles can be tolerated at much higher doses; RBCs are protected from circulating ß-lap since the prodrug is activated by esterases in the tumor microenvironment (Ma et al., 2015). Nanoparticle delivery systems can also be tuned to synergize with ß-lap's mechanism of action, as is the case with iron oxide nanoparticles that increase the formation of ß-lap induced ROS in tumor cells (G. Huang et al., 2013). Tumor-implantable polymer millirods are an example of another delivery strategy to provide localized ß-lap delivery while reducing circulating drug levels (Dong et al., 2009).

Despite advances in drug delivery technology, methemoglobinemia remains an issue that is difficult to address. Hemoglobin oxidation is a common feature of quinone

therapeutics since they are targeted for 1-electron reductions by the multitude of NADH and NADPH reductases in RBCs, including b5R and P450r. These reactions result in the formation of ROS and oxidization of the iron in hemoglobin (P. O'brien, 1991). Predictably, this toxicity has been observed with ß-lap, its derivatives, and other NQO1 bioactivatable therapeutics. Though ß-lap and other NQO1 bioactivatable drugs are effective against mouse xenografts of human cancers, they must be used at doses near or at the maximum tolerated dose (MTD) in order to achieve a sufficiently high intratumoral drug concentration (approximately 4 μM for ß-lap) to achieve anti-tumor efficacy (Blanco et al., 2010; X. Huang et al., 2012). This suggests that when used in monotherapy, toxicity will have to be carefully managed in order to achieve efficacy in clinical trials.

The tumor specific DNA damage caused by ß-lap makes it a promising candidate for combination therapy. ß-Lap can be combined with low doses of ionizing radiation (IR) to yield much greater efficacy (H. J. Park et al., 2005; Reddy, Li, Boothman, Sumer, & Yordy). Ionizing radiation normally does not generate a sufficient density of single strand breaks to cause PARP1 hyperactivation, but when used in combination with ß-lap, enough additional DNA damage is caused in tumor cells to enhance PARP1 hyperactivation at normally sublethal ß-lap doses and result in synergy (Dong et al., 2010). Other chemotherapeutic agents that cause DNA damage are similarly being explored for synergistic effects with the added tumor specificity provided in combination with ß-lap (D'Anneo et al., 2010; Terai et al., 2009). These combination treatments may help advance the application of ß-lap in clinical trials, but

a thorough examination of potential treatment strategies is necessary to improve the efficacy of NQO1-bioactivated drugs at low doses.

1.5 Project Overview

My work focused on developing combination treatment strategies based on the mechanism of cell death induced by ß-lap in order to increase the efficacy of ß-lap and other NQO1-bioactivated drugs while preventing toxicity to normal tissue. Others have previously identified the general sequence of signaling events that occur during ß-lap induced cell death. In order to select agents that would effectively synergize with ß-lap I formulated a hypothesis and related corollaries about the relevance and cause versus effect relationships of events in the cell death pathway, which are listed below.

Hypothesis: *ß-Lap induces substantial DNA damage, but the resulting cell death is driven primarily by energy depletion and metabolic catastrophe. Effective tumor-specific synergy strategies will branch in their downstream effects based on whether they enhance or prevent ATP and NAD^+ depletion.*

Corollary 1: *ß-Lap will exhibit tumor-specific synergy with NAMPT inhibitors since NAD^+ and ATP depletion will be enhanced. Cell death will occur through the same mechanism as with ß-lap alone, but at lower doses.*

Corollary 2: *ß-Lap will exhibit tumor-specific synergy with PARP inhibitors due to a lack DNA damage repair at normally sublethal doses and an increase in conversion of*

unrepaired single strand lesions to double strand breaks. However, cell death will not occur through the same mechanism as with ß-lap alone, since energy depletion will not occur.

Both of these corollaries are addressed in chapters 2 and 3, respectively. Based on their connection to the initial hypothesis, findings in these studies have improved the understanding of the unique pathway of cell death initiated by ß-lap in NQO1-expressing cells in addition to providing novel, clinically relevant therapeutic strategies. Chapter 4 explores the application of ß-lap to a rare but devastating pediatric cancer called atypical teratoid rhabdoid tumors (ATRTs). There is no effective chemotherapeutic treatment for this type of cancer, and my report of NQO1 elevation and ß-lap sensitivity in a panel of patient derived cell lines shows promise for future clinical application. Furthermore, the unique genetic landscape of these tumors provides an excellent opportunity to explore the mechanism for increased NQO1 expression in tumor versus normal tissue. In sum, my work advances the understanding of ß-lap induced cell death, expands the application of NQO1-bioactivated therapeutics to a new cancer type, and provides new combination therapeutic strategies for further preclinical and clinical development.

Chapter 1 Figures

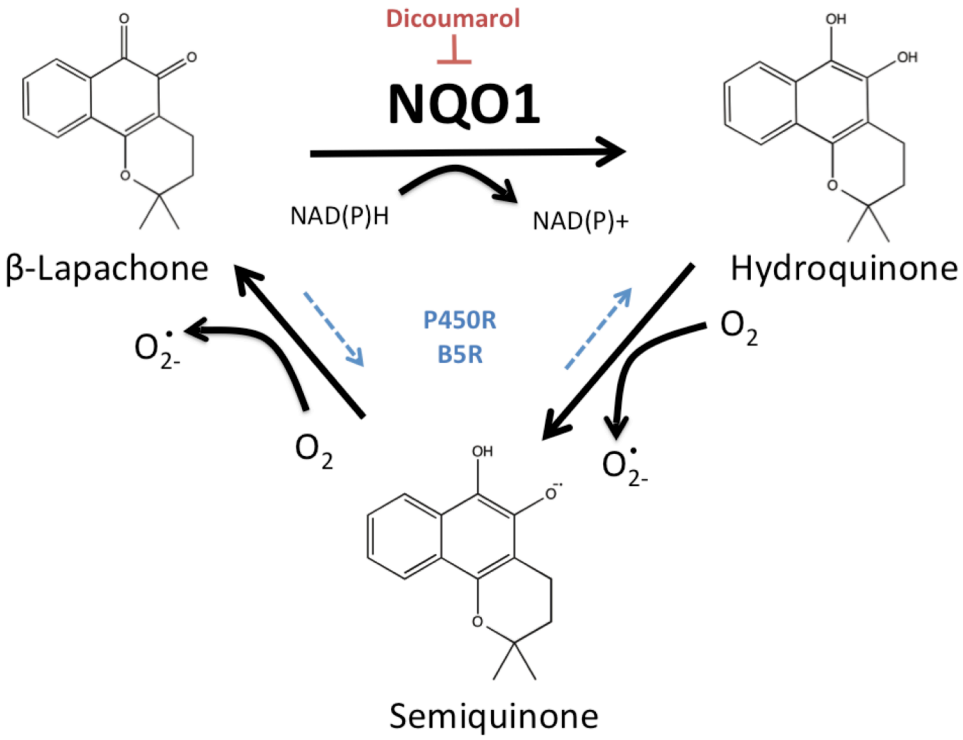

Figure 1-1. Redox futile cycle between NQO1 and ß-lap. NQO1 oxidizes NADPH or NADH to reduce ß-lap to a hydroquinone, which spontaneously reacts with oxygen to revert to the parent compound through the semiquinone intermediate. P450R and B5R catalyze the less efficient 1-electron reductions. Dicoumarol is a specific inhibitor of NQO1.

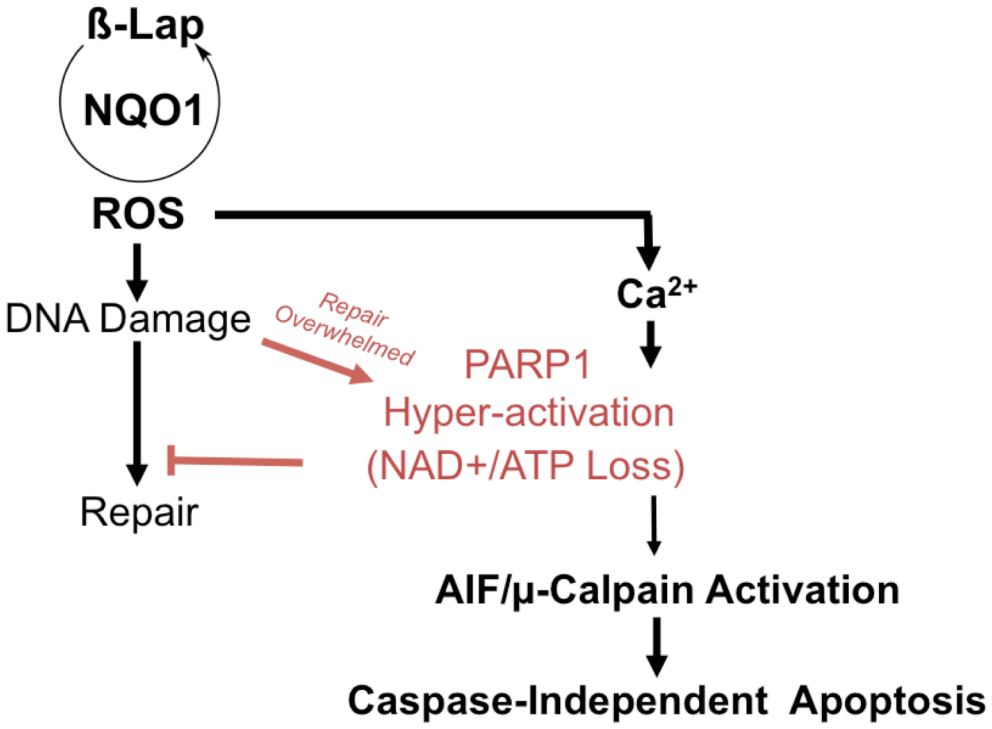

Figure 1-2. Cell death induced by ß-lap. The NQO1-mediated futile cycle generates ROS, which causes single strand DNA damage and hyperactivation of PARP1. PARP1 hyperactivation results in rapid NAD and ATP depletion, AIF and µ-Calpain are activated by Ca^{2+} release into the cytoplasm, and cells undergo caspase-independent apoptosis.

Chapter Two
ß-Lapachone synergizes with NAMPT inhibition to induce tumor-specific metabolic catastrophe

2.1 Notes and Acknowledgements

Chapter 2 was adapted and expanded from a published manuscript (Moore et al., 2015). I performed all experiments in this chapter with assistance as follows: Dr. Edward A. Motea: Flow Cytometry sample processing, Dr. Zeping Hu and Claire Klimko: metabolomics sample processing and mass spectrometry, Dr. Aktar Ali: extracellular flux analysis. I completed data analysis, figure design, and manuscript composition.

2.2 Abstract

Nicotinamide phosphoribosyltransferase (NAMPT) inhibitors (e.g., FK866) target the most active NAD^+ synthetic pathway in tumor cells, but lack tumor-selectivity. ß-Lapachone (ß-lap, ARQ761 in clinical form) is specifically bioactivated in a futile redox cycle mediated by overexpressed (10- to 200-fold) NAD(P)H:quinone oxidoreductase-1 (NQO1) levels in >80% pancreatic adenocarcinoma (PDA) cells. Synergy with FK866 + ß-lap was NQO1-dependent, tumor-selective, mediated by poly(ADP-ribose, PAR) polymerase 1 (PARP1) with simultaneously decreased NAD^+ synthesis and elevated NAD^+ consumption. Profound and long-lasting $NAD(P)^+$ depletion, inhibition of glycolysis at the level of GAPDH and dramatic reductions in ATP pools prevented recovery noted with either agent alone. Cell death is mediated by μ-calpain activity and

independent of PAR accumulation, a process referred to as NAD^+-Keresis. Reducing NAD^+ pools to prime NQO1+ PDA cells for sensitization to PARP1-dependent cell death using NQO1 bioactivatable drugs is a novel therapeutic strategy to treat pancreatic and other NQO1+ solid tumors.

2.3 Introduction

An emerging metabolic target for the treatment of recalcitrant cancers, such as pancreatic adenocarcinoma (PDA) is their reliance on NAD^+ synthesis, particularly through the nicotinamide recycling pathway (Chini et al., 2014; Olesen, Hastrup, & Sehested, 2011; Srivastava et al., 2012). Warburg originally discovered NADH and its essential role in fermentation in the 1930s. The NAD^+/NADH and related $NADP^+$/NADPH redox pairs are critical for generating ATP in both glycolysis and mitochondrial respiration. They are also necessary for an array of normal metabolic processes, including fatty acid and nucleic acid synthesis (Natter & Kohlwein, 2013). The robust anabolism that must support rapid growth and proliferation of cancer cells necessitates an increased burden on NAD^+ synthesis to sustain these metabolic processes. This is compounded by the utilization of NAD^+ in several signaling pathways. In contrast with metabolic redox reactions that reversibly oxidize or reduce the NAD^+/NADH pair, ADP ribosylation by signaling proteins like PARP1 and protein deacetylation by members of the sirtuin family irreversibly consume NAD^+, requiring it to be regenerated from precursor molecules (Chiarugi, Dolle, Felici, & Ziegler, 2012).

In order to take advantage of the increased utilization of NAD^+ in cancer cells for both metabolism and signaling, the biosynthetic pathways of NAD^+ generation may be targeted. NAD^+ can be synthesized from niacin, an essential nutrient consisting of both nicotinamide (Nam) and nicotinic acid (NA), or *de novo* from tryptophan. In the most active recycling pathway, Nam is converted to a mononucleotide by combining it with phosphoribosylpyrophosphate (PRPP) through the action of Nam phosphoribosyltransferase (NAMPT) (Chiarugi et al., 2012). The pathways for NAD^+ synthesis from a variety of substrates converge at the formation of a dinucleotide, which is catalyzed by NMN adenylyltransferases (NMNATs), of which there are multiple isoforms with different tissue and organelle distributions (F. Berger, Lau, Dahlmann, & Ziegler, 2005). In the classic pathway of NAD^+ synthesis from NA described by Preiss and Handler, NAD^+ synthetase and glutamine are required for the final conversion of the nicotinic acid adenine dinucleotide to NAD^+ (Preiss & Handler, 1958a, 1958b). This additional energy-consuming step is not required when Nam is used as a starting material.

The function of NAMPT is critical in the most common and energy-efficient salvage pathway, since the utilization of NAD^+ in poly-ADP ribosylation and protein deacetylation results in substantial Nam generation (Hassa & Hottiger, 2008; Houtkooper, Canto, Wanders, & Auwerx, 2010). Without salvaging Nam, the recommended daily niacin intake of about 15 mg does not begin to approach the demand for NAD^+ synthesis, which occurs on the order of grams in the liver alone (Chiarugi et al., 2012; Medicine, 1998). Since salvaging Nam is critical, inhibiting NAMPT is the most effective means of reducing steady state NAD^+ levels. Specific

NAMPT inhibitors have been designed, including FK866, which progressed through phase II clinical trials. There is still much to be learned about the pleiotropic effects of NAMPT inhibition, but it has been found to reduce proliferation and induce apoptosis in a variety of cancer cell lines (Bi et al., 2011; Cea et al., 2009; Travelli et al., 2011). In preclinical animal studies NAMPT inhibitors reduce tumor growth and increase overall survival (Munk Jensen et al., 2013; Nahimana et al., 2009). The specificity of NAMPT inhibition relies on overexpression of NAMPT in cancer cells due to an increased reliance on NAD^+ recycling (Olesen et al., 2011; Srivastava et al., 2012). However, since the NAMPT pathway is also important in virtually all healthy tissue, inhibition of NAMPT is not sufficiently tumor specific to avoid potentially serious side effects such as thrombocytopenia or GI toxicity even at sub-effective doses of the inhibitors (von Heideman, Berglund, Larsson, & Nygren, 2010). Since FK866 has a short half-life in circulation, prolonged infusions were also required. The failure of FK866 and other NAMPT inhibitors in patients suggested that NAMPT inhibitors do not demonstrate sufficient tumor-selectivity to achieve clinical success as single agents (von Heideman et al., 2010). Due to this lack of specificity, there has been a push to identify combination treatment strategies that may synergize with NAMPT inhibitors to target cancer cells and cause fewer side effects.

Elevated NQO1 has been identified in patient tissue from pancreatic ductal adenocarcinoma (PDA), making pancreatic cancer an especially appealing target for therapy using NQO1 bioactivatable drugs, such as ß-lap (Awadallah et al., 2008; Lewis et al., 2005; Li et al., 2011; Logsdon et al., 2003). However, dose-limiting methemoglobinemia caused by non-specific ROS generation at high ß-lap doses limits

the efficacy of ß-lap as monotherapy (L. P. Hartner, 2007). Strategies for increasing cancer cell cytotoxicity while maintaining NQO1 specificity could greatly enhance the use of ß-lap for therapy against PDA, as well as other solid cancers that overexpress NQO1.

Examining cell death pathways induced by ß-lap, with or without FK866 treatment, is also a novel tool to elucidate mechanisms of lethality mediated by NAD^+ loss, since cell death by PARP1 hyperactivation occurs in other contexts. Notably, cell death induced by ischemia/reperfusion shares many characteristics with ß-lap induced cell death, including ROS induction, PARP1 hyperactivation, calcium release, AIF translocation, and caspase-independence (van Wijk & Hageman, 2005; Zhang, Xie, Munoz, Lau, & Monks, 2014). Similarly, treatment with MNNG (a DNA alkylating agent) or induction of neuronal excitotoxicty causes PARP1 hyperactivation and cell death, but without futile cycle-induced ROS production (N. A. Berger, 1985; Mandir et al., 2000; Ying et al., 2001). Recent studies promote an important role for accumulated free PAR polymer that can directly activate μ-calpain, activate and release AIF, and inhibit glycolysis (Andrabi et al., 2014; N. A. Berger, 1985; David, Andrabi, Dawson, & Dawson, 2009; Vanden Berghe, Linkermann, Jouan-Lanhouet, Walczak, & Vandenabeele, 2014; Virag, Robaszkiewicz, Rodriguez-Vargas, & Oliver, 2013). By combining ß-lap and FK866, NAD^+ and ATP depletion is uncoupled from the robust formation of PAR noted with ß-lap alone, revealing the function of PAR formation in ß-lap-induced cell death.

ß-Lap and FK866 have distinct, but highly complementary mechanisms of action. ß-Lap induces tumor-selective NAD^+ depletion specifically in cancer cells that

express high levels of NQO1. FK866 primes cancer cells for cell death by lowering NAD^+/NADH pools and prevents recovery by inhibiting NAD^+ synthesis from nicotinamide liberated by activated PARP1. I have shown that increased dependence of PDA cells on glycolysis is specifically targeted by ROS-induced NAD^+ depletion caused by exposure to both drugs. Glycolytic inhibition, ATP depletion, and cell death is independent of PAR formation, strongly suggesting that PAR accumulation is not directly involved. The use of ß-lap with NAMPT inhibitors resulted in synergistic NQO1 and PARP1-dependent antitumor activity, allowing the use of lower doses and shorter treatment times for both therapeutics.

2.4 Results

FK866 pretreatment sensitizes PDA cells to ß-lap. I hypothesized that pretreatment of NQO1-overexpressing PDA cells with FK866 would sensitize them to subsequent ß-lap exposure by lowering the available NAD^+ pools, thereby increasing the ability of PARP1 to fully deplete the remaining NAD^+ when stimulated by NQO1-induced ROS generation (**Figure 2-1**). MiaPaca2 cells were pretreated with FK866 for 24 h, then exposed to ß-lap + FK866 for 2 h. Pre-treatment with FK866 resulted in increased sensitivity to ß-lap, at normally sub-lethal and higher doses of the drug (**Fig. 2-2A**). At LD_{90} levels of ß-lap, FK866 pretreatment led to a dose enhancement ratio (DER) of 1.6, which was saturated by 4 nM FK866 (p=.0018). I observed similar results in colony formation assays (**Figure 2-2B**), indicating that the loss of viability corresponds with loss of proliferative capacity. While FK866 is lethal to MiaPaca2 cells at low nanomolar concentrations with a long-term 72 h treatment (**Figure 2-2C**), a short-term (24h + 2h)

treatment had no effect on viability (**Figure 2-2A**, all results normalized to untreated cells). Using GMX1778, an alternative small molecule NAMPT inhibitor, yielded a similar sensitization to ß-lap in MiaPaca2 (**Figure 2-2D**).

Synergy reduces required treatment times and is effective in a variety of cancer cell types. I optimized the ability of FK866 to sensitize PDA cells to ß-lap, examining dose response and time-course exposures. It was previously determined that the minimum exposure time to induce cell death for ß-lap was ~2 h with LD_{50} values of ~3 μM in most cells, where NQO1+ cells are eliminated regardless of cell cycle position or p53 status (Bentle et al., 2006). Interestingly, the minimum ß-lap treatment time required to induce cell death was decreased to 1 h with FK866 and ß-lap combination treatment (**Figure 2-3A**). Synergy was also dependent on the dose of FK866 used, with increasing effects up to 16 nM (**Figure 2-3B**). For MiaPaca2, I chose 8 nM FK866 as a conservative clinically relevant dose, as described in the discussion. In contrast to synergy observed in MiaPaca2, normal human IMR-90 embryonic lung fibroblasts that express low levels of NQO1 remained resistant to ß-lap, with or without FK866 pretreatment (**Figure 2-3C**), suggesting that toxicity to normal cells was not promoted by FK866 pretreatment (Bey et al., 2007). As with MiaPaca2 cells, the survival of other PDA cells showed similar hypersensitivity to ß-lap + FK866 compared to either drug alone (**Figure 2-3D).** Furthermore, other NQO1-overexpressing cancer types, such as A549 NSCLC, showed synergistic lethality with this combination treatment.

Other NQO1-bioactivated drugs exhibit varying efficacy when combined with FK866. Deoxyniboquinone (DNQ) is an NQO1-bioactivated therapeutic with a markedly different structure than ß-lap (X. Huang et al., 2012). Though it is known to work through the same mechanism as ß-lap, DNQ does not synergize with FK866 (**Figure 2-4A**). Isobutyl-deoxyniboquinone (IB-DNQ), a derivative that has increased solubility for *in vivo* use, also does not synergize to the same extent as ß-lap at sublethal doses (**Figure 2-4B**). In contrast, GB59, a derivate of ß-lap, does effectively synergize with FK866 (**Figure 2-4C**). Based on *in vitro* recycling assays, DNQ cycles through the NQO1-mediated redox reactions much more rapidly than ß-lap, requiring more oxygen and NADH to sustain the futile cycle (X. Huang et al., 2012). For this reason, pretreating with FK866 to reduce NAD^+ levels in cells prior to co-treatment does not allow for effective synergy with DNQ and IB-DNQ as it does for ß-lap. On the other hand, GB59 is a structural derivative of ß-lap and engages in the futile cycle in a similar fashion, demonstrating synergy with FK866.

FK866 + ß-lap synergy is NAMPT and NQO1-dependent. A series of small molecule and genetic experiments were used to better define the target specificity of FK866 + ß-lap combination therapy. Dicoumarol, a small molecule inhibitor of NQO1, completely prevented the cytotoxicity of MiaPaca2 cells treated with ß-lap alone or FK866 + ß-lap (**Figure 2-5A**). NAMPT specificity was explored by adding nicotinamide mononucleotide (NMN, 500 μM), the product of the NAMPT-catalyzed reaction, which rescued FK866-dependent hypersensitivity to ß-lap (**Figure 2-5B**). Notably, NMN

addition did not rescue combination cytotoxicity above that induced by ß-lap alone, suggesting that the capacity for additional NAD^+ synthesis does not spare cells from ß-lap treatment (**Figure 2-5B**). Additionally, treating with nicotinic acid (NA, 500 μM) did not rescue MiaPaca2 cells from the effects of combination treatment (**Figure 2-5C**). This supports the specificity of combination treatment for the NAMPT pathway since nicotinic acid is also a precursor of NAD^+, but cannot be utilized by MiaPaca2 due to a lack of nicotinate phosphoribosyltransferase (NAPT) expression in this cell line (W. Wang et al., 2014). Furthermore, depletion of NAMPT mRNA and protein levels using specific siRNAs (**Figure 2-5D**, inset) increased sensitivity to ß-lap, and this hypersensitivity was rescued to basal ß-lap sensitivity levels with NMN (**Figure 2-5D**). Thus, NAMPT inhibition and NQO1-dependent bioactivation of ß-lap are necessary and sufficient for the observed synergistic lethality.

Genetic Models confirm NQO1 and tumor specificity of combination treatment. Since dicoumarol is an NADH mimic and may have off-target effects, I used genetically matched NQO1+ and NQO1- PDA cells from parental NQO1 polymorphic S2-013 cells prepared as described (Pink, Planchon, et al., 2000). Briefly, the S2-013 cell line, which does not express NQO1 due to a homozygous *2 polymorphism, was infected with retrovirus containing an NQO1 or empty CMV-driven expression vector and subsequently subcloned for protein level and enzyme activity. Note that ATP depletion caused by FK866 alone was not dependent on NQO1 expression, while ß-lap-induced cytotoxicity and synergy only occurred in NQO1+, and not in NQO1-, S2-013 cells (**Figure 2-6A**) ($p=0.00012$). IMR-90 cells were transfected with an empty or NQO1

containing expression vector, and exposed to combination or single agent treatment with ß-lap and FK866 (**Figure 2-6B**). NQO1 expression did result in ATP loss both with single agent ß-lap and combination treatment. However, unlike results obtained in S2-013 cancer cells, IMR-90 did not exhibit synergy with FK866 inhibition. Normal immortalized pancreatic ductal cells (hTERT-HPNE) were somewhat sensitive to ß-lap but also did not exhibit synergy with FK866 (**Figure 2-6C**). In contrast with IMR-90, HPNE cells exhibit NQO1 expression that is higher than expected for normal pancreas tissue, which explains their sensitivity to ß-lap. This is a feature also observed in immortalized human bronchial endothelial cells (HBEC), and appears to be a result of NQO1 upregulation that occurs during the immortalization process. Nevertheless, neither HPNE nor IMR-90 NQO1+ cells exhibit synergy with FK866. These results suggest that normal cells are less sensitive to FK866 synergy due to a decreased reliance on NAD^+ synthesis via NAMPT. Based on these *in vitro* studies, a high therapeutic window for combination treatment is expected, even taking into consideration the possibility that some normal cells may have transiently elevated NQO1 expression. Additionally, these findings show that genetic models of NQO1 loss and overexpression confirm the NQO1 specificity results obtained from the use of dicoumarol.

FK866 pretreatment enhances energy depletion and reduces glutathione levels. ß-Lap treated cells exhibit severe NQO1-dependent NAD^+/NADH depletion at lethal doses as a result of a two-step process: (i) NQO1-dependent conversion of NADH to elevated pools of NAD^+ with accompanying dramatic elevation of ROS levels; and (ii)

rapid depletion of NAD^+ levels due to ROS-stimulated PARP1 hyperactivation (Bey et al., 2007; Bey et al., 2013; Dong et al., 2010; X. Huang et al., 2012; Li et al., 2011). When MiaPaca2 cells were exposed to FK866 + ß-lap, a significantly greater NAD^+/NADH depletion was noted as a result of the smaller NAD+ pool size caused by inhibition of NAMPT-catalyzed nicotinamide recycling (**Figure 2-7A**), with similar results in other PDA cell lines. While low doses of ß-lap (1-2 μM) cause PARP1 activation and NAD^+ consumption, NAD^+ synthesis compensates to maintain the pool size. However, when NAD^+ synthesis was inhibited by FK866, the shoulder region where NAD^+/NADH levels were maintained with low doses of ß-lap was eliminated (**Figure 2-7A**). Addition of NMN spared, to some extent, loss of NAD^+/NADH total pools caused by FK866 + ß-lap (**Figure 2-7A**). Though complete nucleotide rescue with NMN was not observed, the functional relevance of partial rescue is evident in the NMN viability rescue from combination treatment observed under the same treatment conditions (**Figure 2-5B**). $NADP^+$/NADPH losses measured after the same treatment conditions followed similar trends, but with less overall depletion (**Figure 2-7B**), most likely because $NADP^+$ is not directly consumed by PARP1, but is synthesized from NAD^+.

Since glutathione is oxidized to neutralize reactive oxygen species (ROS) generated by ß-lap, I examined the effects FK866 + ß-lap combination therapy on glutathione. Significant depletion of reduced glutathione (GSH) levels occurred in ß-lap-exposed MiaPaca2 cells, which was lower after combination treatment and rescued with NMN (**Figure 2-7C**) (Reinicke et al., 2005). Additional loss of GSH levels

could be a result both of decreased glutathione reductase activity due to low NADPH levels (**Figure 2-7B**) and less *de novo* glutathione synthesis caused by ATP loss noted with ß-lap (Bentle et al., 2006; Suzuki & Kurata, 1992). Indeed, total glutathione levels were also lower following combination treatment, with rescue provided by NMN up to the level of ß-lap alone (**Figure 2-7D**). These findings are consistent with reduced glutathione synthesis, which could result from depletion of ATP levels after treatment.

Energy depletion and recovery inhibition caused by FK866 + ß-lap. Marked ATP loss was noted in MiaPaca2 cells exposed to FK866 (8 nM) + ß-lap (2.5 μM) compared to either agent alone (**Figure 2-8A**). Surprisingly, substantial ATP depletion was observed with 24 h FK866 treatment alone (~40%), though this treatment does not result in the loss of cell viability (**Figure 2-2A**), so I performed a recovery experiment, in which I treated cells for 24 h with or without FK866, added ß-lap or vehicle for a 2 h co-treatment, and then washed off the drug-containing media and assayed ATP (**Figure 2-8B**), NAD^+/NADH (**Figure 2-8C**) or $NADP^+$/NADPH (**Figure 2-8D**) levels at various times up to 4 h after treatment. Despite substantial initial depletion, complete recovery of all nucleotide pools occurred rapidly after removal of FK866 when used as a single agent, exemplifying a robust metabolic recovery after treatment that normally serves to prevent toxicity except in the case of prolonged FK866 exposure. However, this recovery was blocked in a dose-dependent manner when ß-lap was used in combination with FK866 (**Figure 2-8B, 2-8C, 2-8D**). In addition to increased ß-lap dose-dependent depletion of these nucleotides, ATP, NAD(H), and NADP(H) levels do

not recover from combination treatment over the same time course. This suggests that substantial metabolic perturbations occurred in combination treated cells relative to cells treated with FK866 alone.

Metabolic catastrophe results from glycolytic inhibition. Since dramatic alterations in ATP levels were noted with combination treatment, I examined MiaPaca2 cells for alterations in glycolytic activity after ß-lap + FK866 treatment. Analysis of extracellular acidification rate (ECAR) with the XF Flux Analyzer revealed that basal glycolysis and glycolytic reserve capacity of ß-lap-exposed cells were reduced immediately after drug exposure (**Figure 2-9A**). Prior reports have shown that long-term FK866 treatment inhibited glycolysis by reducing glyceraldehyde 3-phosphate dehydrogenase (GAPDH) activity due to low NAD^+ levels (Rovito & Oblong, 2013; Tan et al., 2013). I found that short-term (24 h) treatment with FK866 followed by removal of the drug resulted in no ECAR reduction (**Figure 2-9A**). Nevertheless, FK866 pre-treatment markedly decreased ECAR following ß-lap co-treatment, to a significantly greater extent than ß-lap alone. Since GAPDH can be reversibly inhibited by ROS-induced oxidation or irreversibly by post-translational modifications (e.g., PARylation) (Colussi et al., 2000; Du et al., 2003; Grant, Quinn, & Dawes, 1999; Hwang et al., 2009), I examined the effects of ß-lap and combination treatment on GAPDH activity. Indeed, GAPDH activity was inhibited in MiaPaca2 cells following ß-lap exposure, and rescued by the addition of dicoumarol (**Figure 2-9B**). Excess NADH was added to the assay buffer, so the moderate GAPDH inhibition shown in **Figure 2-9B** was independent of NAD^+ depletion, but is likely not enough to be solely responsible for the substantial ECAR reduction

from **Figure 2-9A**. Importantly, FK866 pretreatment did not reduce GAPDH inhibition caused by ß-lap exposure, but it also did not synergize with ß-lap in this assay **(Figure 2-9B)**. These data suggest that ß-lap caused ROS mediated post-translational modification of GAPDH, and increased glycolytic inhibition observed with combination treatment was secondary to the increased NAD^+ depletion (**Figures 2-7A**). Inhibition of GAPDH was strongly supported by a ~12 fold accumulation of glyceraldehyde 3-phosphate (GA3P), the substrate of GAPDH, and a lesser accumulation of the upstream metabolites glucose-6-phosphate/fructose-6-phosphate (G6P/F6P) in ß-lap + FK866 treated cells (**Figure 2-9C**). Additional accumulation of these metabolites in ß-lap + FK866 treated versus ß-lap alone treated MiaPaca2 cells ($p < .01$) is consistent with the reduced ECAR seen with combination treatment due to lower NAD^+ pools despite the similar (and overall lower) level of NAD^+-independent enzyme inhibition observed in **Figure 2-9B**. Next, I explored whether the inhibition of glycolysis with FK866 + ß-lap treatment was durable, since recovery of ATP, NAD(H) and NADP(H) occurred in the hours following removal of FK866 (**Figure 2-8**). Inhibition of lactate production and glucose utilization was noted following drug removal after combination treatment (but before cells begin to die at 12-48 h), demonstrating that the combined effects of ß-lap on GAPDH inhibition and both drugs on NAD^+ depletion result in substantial inhibition of glycolysis in PDA cells (**Figures 2-9D, 2-9E**).

FK866 + ß-lap combination therapy results in reduction of PAR formation. Our group previously reported that ß-lap-induced lethality was caused upstream by PARP1

hyperactivation and dramatic loss of NAD^+ pools in NQO1+ cancer cells, including PDA (Bey et al., 2013). Since others have shown that the PAR polymer itself is critical for signaling and lethality in other forms of PARP1 hyperactivation-mediated cell death (e.g. from MNNG exposure) (Virag et al., 2013), I sought to define the distinct contributions of PARP1 activity and PAR formation in the synergy noted with FK866 + ß-lap combination treatment. Surprisingly, ß-lap and FK866 combination treatment of MiaPaca2 or AsPC1 cells resulted in no increase in PAR formation by western blot, in contrast to the elevated PAR levels typically noted in ß-lap-treated NQO1-expressing cancer cells (**Figure 2-10A**). PAR formation in combination treated cells was rescued by restoring NAD^+ levels with NMN. Despite decreased NAD^+ pools caused by FK866 pretreatment, exposure of ß-lap-treated MiaPaca2 cells to the PARP1 inhibitor, Rucaparib (AG014699), or addition of BAPTA-AM to chelate Ca^{2+} (which is required for ß-lap-induced PARP1 hyperactivation) (Bentle et al., 2006; Tagliarino et al., 2001), prevented additional ATP depletion caused by ß-lap treatment in combination with FK866 (**Figure 2-10B**). These findings show that reduction of NAD^+ pools by FK866 treatment increases the ability of PARP1 to completely exhaust NAD^+ pools after ß-lap treatment, without generating substantial PAR formation. Once NAD^+ levels were exhausted, PARP1 would not be capable of properly repairing DNA lesions created by the high levels of ROS induced by ß-lap, resulting in more rapid conversion to DNA double strand breaks (DSBs). Indeed, delayed γH2AX induction normally seen with ß-lap treatment alone appeared more rapidly in MiaPaca2 cells exposed to FK866 + ß-lap, forcing cells to deal with potentially lethal DNA damage in addition to metabolic catastrophe driven by PARP1 activity during combination treatment (**Figure 2-10C**).

ROS formation and the mechanism of cell death. One concern in lowering NAD^+/NADH levels is that the NQO1-dependent futile cycle could be compromised, which would suggest that the increased cell death observed with combination treatment occurred through a non-ROS induced mechanism. However, I noted that H_2O_2 levels generated in MiaPaca2 cells after ß-lap treatments with or without FK866 (8 nM, pre- and co-administration) were identical (**Figure 2-11A**). Furthermore, addition of pegylated-catalase (150 U/mL) partially rescued lethality in MiaPaca2 cells exposed to ß-lap + FK866 (**Figure 2-11B**) in a manner similar to rescue reported in cells treated with ß-lap alone (Bey et al., 2013; Cao et al., 2014). In sum, this supports the hypothesis that the ß-lap futile redox cycle is maintained even after FK866 pretreatment, but there is not an increase in ROS production that is responsible for the synergy between these two compounds.

I hypothesized that cancer cells exposed to FK866 + ß-lap would die by the same caspase-independent, but apoptosis-like programmed cell death pathway that occurs in ß-lap-treated NQO1+ cancer cells (Pink, Planchon, et al., 2000). MiaPaca2 cells exposed to 4 μM ß-lap for 2 h exhibited significant apoptosis (41%), though they lacked caspase cleavage (Bey et al., 2007), and demonstrated μ-calpain activation by the formation of the 23 kDa active form of the small subunit of μ-calpain 48 h post-treatment (**Figure 2-11C**). Atypical cleavage of p53 catalyzed by μ-calpain was also observed in both ß-lap and combination treated cells (**Figure 2-11D)** (Tagliarino et al., 2003). Overall, exposing MiaPaca2 cells to FK866 + ß-lap resulted in significant levels of apoptotic cells (>50%) that appear to die by the same mechanism as noted with a lethal dose of ß-lap (Bey et al., 2007; Li et al., 2011). Treatment of MiaPaca2 cells with

FK866 (8 nM, 24h) alone did not cause substantial apoptosis (**Figure. 2-11C**). Since PAR accumulation was not noted in the cell death induced by FK866 + ß-lap, free PAR does not appear to be necessary in this NAD^+ loss-dependent cell death pathway (**Figures 2-10, 2-11**).

Depletion of NAD(H), NADP(H), and ATP occurred to a greater extent with ß-lap + FK866 combination treatment than with ß-lap alone (**Figures 2-7, 2-8**), which could promote necrosis, so I assayed cell membrane permeability after treatment. I found that membrane permeability after exposure to FK866 + ß-lap did not surpass that of cells treated with ß-lap alone, and both were comparable to cells undergoing canonical apoptosis induced by the apoptosis-inducing agent, staurosporine (STS) (**Figure 2-11E**).

Cell cycle analysis and morphology of cell death. After combination treatment with FK866 + ß-lap, MiaPaca2 cells were analyzed for total DNA content by flow cytometry (**Figure 2-12A**). At 48 h after treatment, many of the dying cells (53%) have entered a subG1 population as a result of the cell death pathway initiated by µ-calpain and AIF (Bey et al., 2007; Bey et al., 2013). However, the distribution of cells in the other cell cycle phases was relatively unchanged, as shown by the 2N/4N ratios (**Figure 2-12A**). This supports the cell cycle independence of combination treatment, as there is no evidence of a particular population of cells being depleted or cell cycle arrest occurring. Furthermore, the morphology of MiaPaca2 cells 48 h after treatment with ß-

lap + FK866 is characteristic of apoptosis-like death; the nuclei were condensed and became more round, and the cytoplasmic area decreased.

Pharmacodynamics of combination treatment *in vivo*. The focus of my studies has been to elucidate the PARP1 induced cell death mechanism and metabolic perturbations induced by ß-lap and combination treatment, but also to determine if combination treatment with FK866 and ß-lap may prove to be a viable clinical strategy for targeting NQO1-expressing cancer. In order to determine if this treatment strategy would be viable for further preclinical characterization, I treated mice bearing MiaPaca2 subcutaneous xenografts for 1 day with FK866 followed by a single FK866 and ß-lap injection. Based on PAR formation 1 h after treatment, combination treated mice exhibited reduced PAR formation versus ß-lap treated mice (**Figures 2-13A, 2-13B**). This biomarker of response is consistent with *in vitro* results demonstrating reduced PAR formation with FK866 + ß-lap vs ß-lap alone (**Figure 2-10**).

2.5 Discussion

Addition of ß-lap to short-term FK866 treatment resulted in enhanced tumor-specificity and efficacy not typically found with FK866 treatment alone. This combination resulted in elevated DNA lesions, more extensive NAD^+/ATP loss mediated by PARP1, and metabolic catastrophe. My work has defined the metabolic effects of this combination treatment in order to relate the mechanism of this treatment strategy to other drugs. MNNG, an alkylating agent that causes DNA damage and PARP1 hyperactivation, is reported to block glycolysis through a free PAR moiety-

mediated mechanism of hexokinase inhibition (Andrabi et al., 2014). In contrast, ß-lap exposure caused inhibition of GAPDH even in the presence of excess NADH, which could be a result of oxidative stress- or PARylation-induced post-translational modification (Du et al., 2003). However, free PAR did not accumulate in cells co-treated with FK886 + ß-lap, yet persistent GAPDH inhibition was noted to the same extent as cells exposed to ß-lap alone. While the mechanism by which GAPDH is inhibited by combination treatment is not definitively known, there are a few probable processes. Our group previously reported NQO1-dependent, ROS-induced S-nitrosylation and nuclear translocation of GAPDH in various NQO1 cancer cells after ß-lap treatment (Bey et al., 2013) and reactive nitrogen species (RNS)-mediated irreversible inhibition of GAPDH has also been previously shown *in vitro* (Chuang, Hough, & Senatorov, 2005). Regardless of the specific mechanism, the inhibition of GAPDH by ß-lap is enhanced by the additional NAD^+ depletion caused by combination treatment with FK866, as seen by markedly increased accumulation of GA3P, and has long-term effects on glycolytic activity. Additionally, this data strongly suggests that free PAR accumulation is not a critical component of the cell death signaling pathway. Without active ATP synthesis, cancer cells cannot recover from depleted NAD^+ pools or repair the extensive DNA lesions caused by ß-lap, resulting in cell death (Bentle et al., 2006).

Addition of FK866 + ß-lap to NQO1 overexpressing cancer cells caused a burst of ROS-induced DNA damage and NAD^+/ATP depletion in a near-identical manner to the caspase-independent, μ-calpain-mediated cell death pathway induced by lethal doses of ß-lap alone, despite the additional energy depletion. There are reports of ß-lap inducing caspase-mediated apoptosis, but this is noted only after long-term

continuous treatment with ß-lap, which also significantly reduces specificity for NQO1+ overexpressing cells (M. T. Park et al., 2011; Shah et al., 2008; Woo & Choi, 2005). There are also reports that PAR polymers directly influence μ-calpain activation, and are critical for inducing cell death under conditions where PARP1 hyperactivation occurs, such as with MNNG treatment or ischemia-reperfusion (Vanden Berghe et al., 2014; Virag et al., 2013). With ß-lap + FK866 treatment, PARP1 activity is stimulated with ß-lap, but extensive PAR formation does not occur due to low NAD^+ levels, and rescuing PAR formation and NAD^+ levels with NMN decreases cytotoxicity. Nevertheless, μ-calpain activation/proteolysis and caspase-independent apoptosis still occurs, demonstrating that PARP1 activity to deplete energy stores is more important than the formation and accumulation of extensive PAR polymers. My findings with ß-lap are consistent with a report that NAMPT inhibition synergizes with pemetrexed in a PARP1 dependent manner with an associated reduction in PAR formation (Chan et al., 2014). I found that severe NAD^+/NADH depletion induced by ß-lap caused metabolic catastrophe, ATP depletion, and cell death that was not dependent on PAR accumulation and was promoted by NAMPT inhibition. As expected from the observed extensive energy depletion and DNA damage, cancer cells were committed to death after only a brief period of combination treatment (1-2 h) regardless of cell cycle status. I propose to refer to this mode of cell death as NAD^+-Keresis, after the death spirits in Greek mythology called Keres, who pull the life out of those who die violently, in this case through severe NAD^+/NADH depletion.

Novel therapies are desperately needed for patients with PDA. By combining NAMPT inhibitors (e.g., FK866) and NQO1 bioactivatable drugs (e.g., ß-lap, ARQ761)

we exploit the reliance of PDA on rapid NAD^+ synthesis, as well as the tumor-selective overexpression of NQO1 through the use of agents that are bioactivated to induce cell death. Combination treatment with NAMPT inhibitors + ß-lap addresses issues associated with either agent alone, since the combination can enhance antitumor efficacy at well-tolerated doses of these drugs. I noted that FK866 + ß-lap combination treatment was most effective with FK866 pretreatments followed by ß-lap co-treatment. This was consistent with my hypothesis that lowered NAD^+/NADH levels caused by FK866 would sensitize NQO1+ tumor cells to rapid futile redox cycling initiated by ß-lap. Importantly, cytotoxicity of these drugs to normal cells was not increased with combination treatment; elevated NQO1 expression was still required to achieve cell death. Furthermore, the ß-lap doses used in my studies are relevant to those achievable *in vivo* (Savage et al., 2008). When used in clinical trials, the maximum tolerated dose of FK866 yielded a 14 nM steady state plasma concentration, which is in the effective synergy range for combination treatment with ß-lap (Holen, Saltz, Hollywood, Burk, & Hanauske, 2008). However, for single agent treatment it was administered continuously for 96 hours. Combination treatment with ß-lap significantly reduced the required FK866 treatment time, which should increase the feasibility of its clinical application. Preliminary *in vivo* studies showed PAR formation that mirrored *in vitro* results, suggesting that these drugs may be applicable to mouse models. Next-generation NAMPT inhibitors currently in development demonstrate better PK profiles are expected to similarly benefit from combination treatment, with reduced need for long-term infusion and more effective clinical application (T. O'Brien et al., 2013). This treatment strategy will be pursued in future preclinical studies to explore potential

clinical application and to further elucidate the pathways and mechanism of NAD^+-Keresis.

Chapter 2 Figures

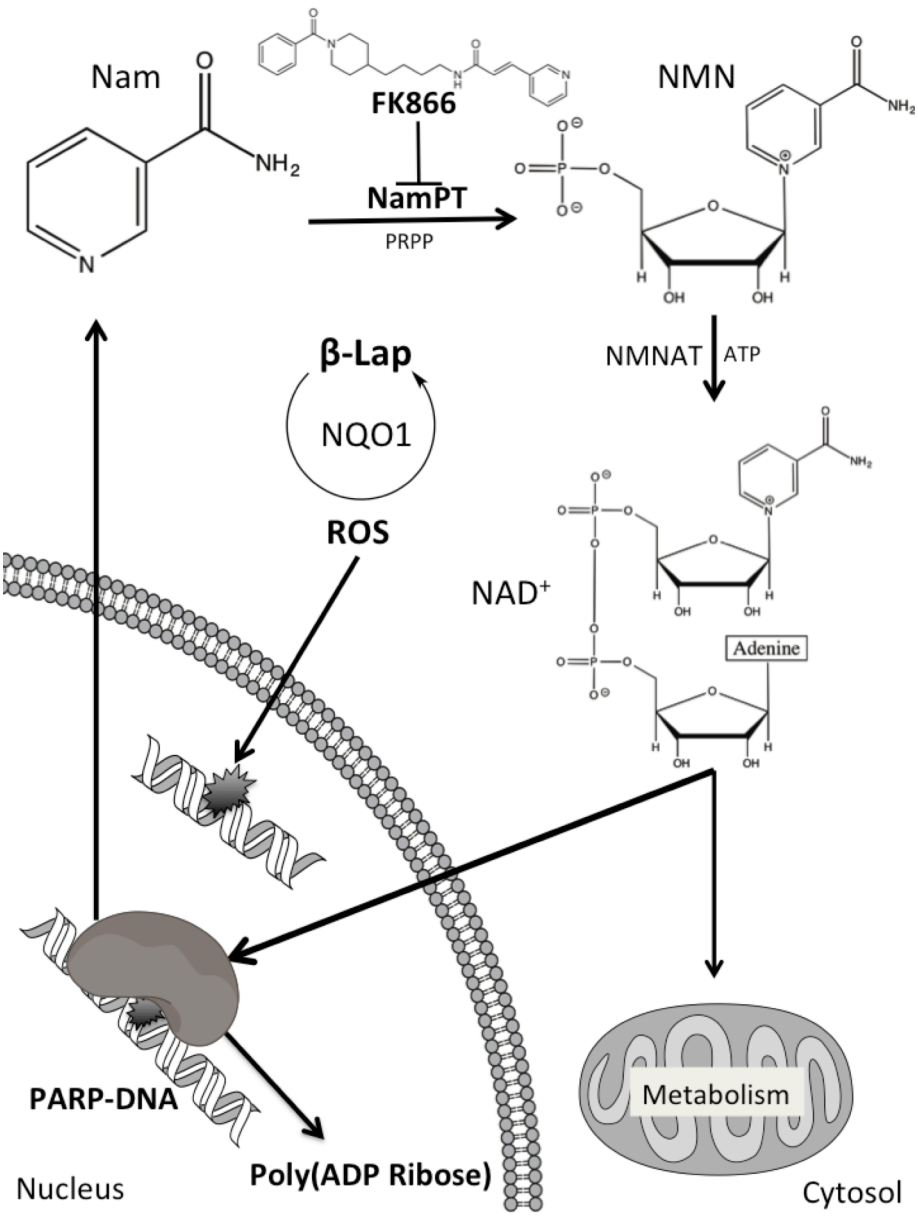

Figure 2-1. Treatment schematic for ß-lap + FK866. ß-lap engages in a futile redox cycle with NQO1, oxidizing NAD(P)H and generating reactive oxygen species. PARP1 is activated in response to ROS-induced DNA damage and causes PAR formation, consuming NAD^+ and liberating Nam. FK866 prevents the synthesis of NAD^+ from Nam by blocking NAMPT, the rate-limiting enzyme. This treatment strategy kills NQO1+ cancer cells by increasing NAD^+ consumption and decreasing NAD^+ synthesis, resulting in metabolic catastrophe.

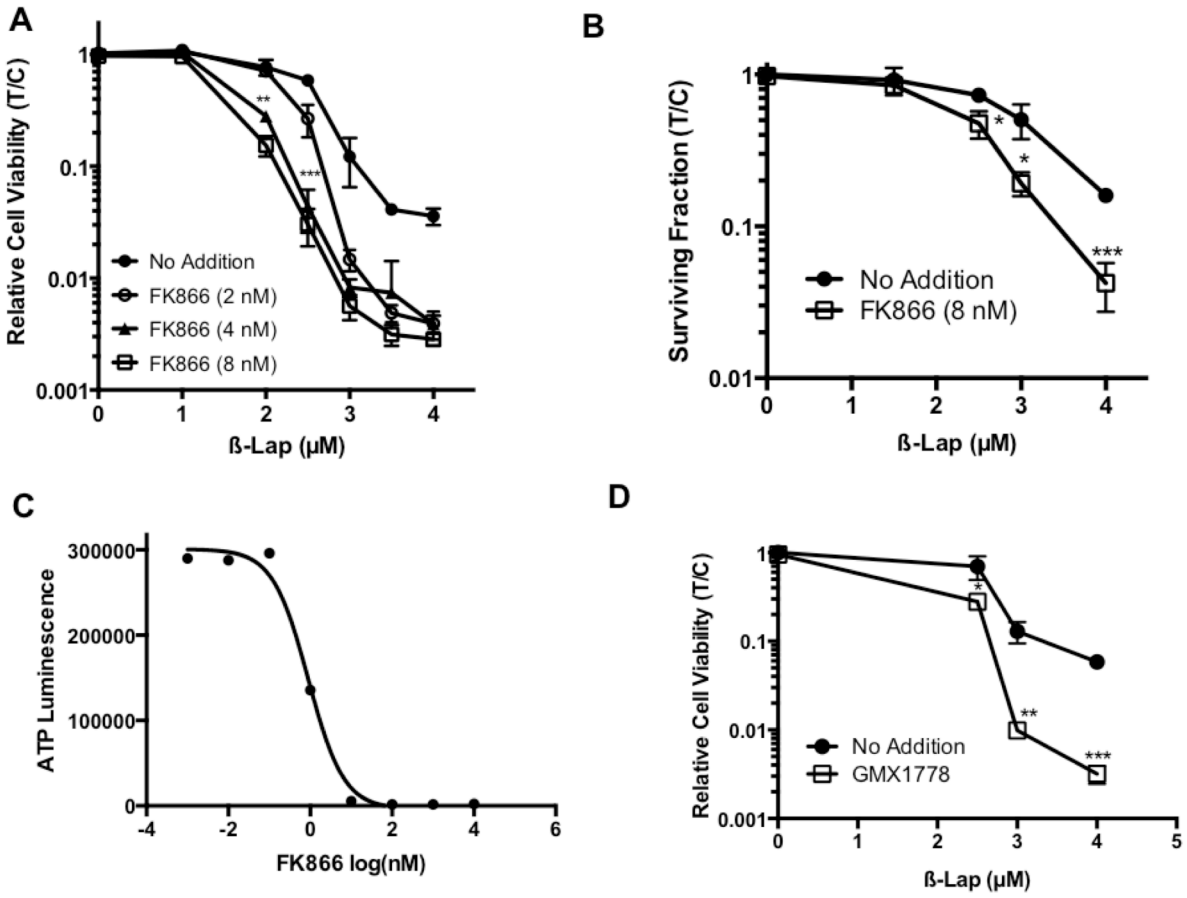

Figure 2-2. FK866 pre- and co-treatment sensitizes PDA cells to ß-lap. **A)** MiaPaca2 cells were pretreated for 24 h with FK866 or vehicle alone at indicated doses. Cells were washed and then exposed to ß-lap for 2 h, with or without FK866, as indicated. Relative cell viability (T/C) was monitored by CellTiter-Glo 24 h later. All luminescence values were normalized to untreated cells (no FK866 or ß-lap). **B)** Colony formation ability of MiaPaca2 cells was tested after treatment as in '**A**' with 8 nM FK866 pre-treatment and then ß-lap co-treatment. **C)** MiaPaca2 cells were treated long-term (72 h) with FK866 alone, followed by ATP viability assays. **D)** An alternative NAMPT inhibitor, GMX1778 (16 nM), was used in combination with ß-lap as described in 'A'. Results were compared using Student's t-tests (n=3 with mean +/- standard deviation) as indicated. **p<0.05;**p<.01; ***p<0.001*.

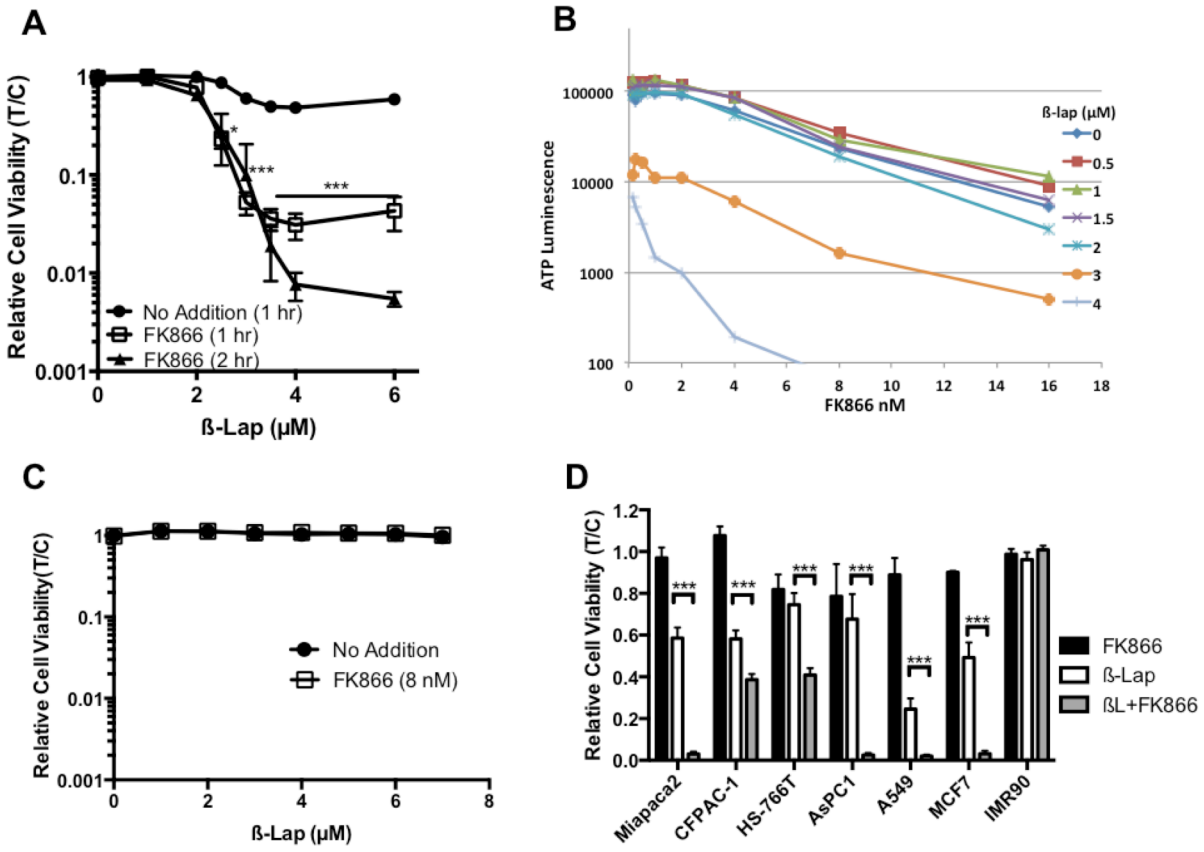

Figure 2-3. Reduced co-treatment time and sensitivity of other cancer cell lines. **A)** FK866 pre- and co-treatment markedly reduced the minimum effective treatment time for ß-lap. MiaPaca2 cells were treated with 8 nM FK866 and then exposed to ß-lap for 1 or 2 h in the presence or absence (no addition) of 8 nM FK866. Drugs were removed and relative cell viability (T/C) was assessed 24 h later. **B)** FK866 dose response with combination treatment. MiaPaca2 cells were pretreated with the indicated doses of FK866 followed by a 2 h co-treatment with ß-lap and viability assay 24 h later. **C)** Normal fibroblast IMR90 cells, which do not express NQO1, were pretreated with FK866 and co-treated with ß-lap at the indicated doses, followed by a viability assay 24 h later. **D)** Additional NQO1+ PDA cell lines (CFPAC-1, HS766T and AsPC1), as well as breast (MCF7) and non-small cell lung (A549) cancer cells were treated with FK866 alone, ß-lap alone, or with the combination as in '**C**' and assessed for relative cell viability (T/C) as in '**C**'. All results were compared using Student's t-tests (n=3 with mean +/- standard deviation) as indicated. **p<0.05;**p<.01; ***p<0.001*.

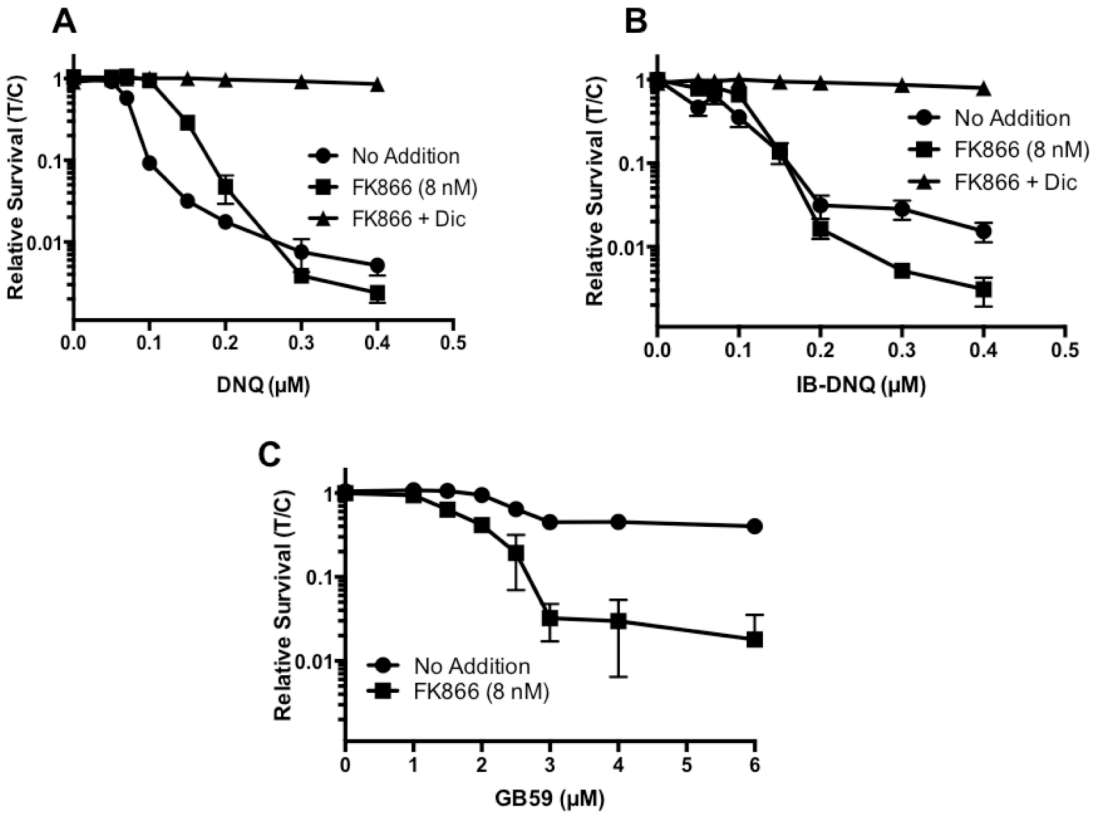

Figure 2-4. Performance of other NQO1-bioactivated drugs in combination with FK866. **A)** DNQ, a potent NQO1-bioactivated drug that engages a more rapid futile redox cycle than ß-lap, was added to MiaPaca2 cells with FK866 for two hours following 24 h FK866 pre-treatment. Synergy was not observed in viability assays 24 h after co-treatment. **B)** IB-DNQ, a derivative of DNQ with similar efficacy, also does not exhibit synergy with ß-lap under the same treatment conditions as in '**A**'. **C)** GB59 is a more potent derivative of ß-lap that did exhibit synergy with FK866.

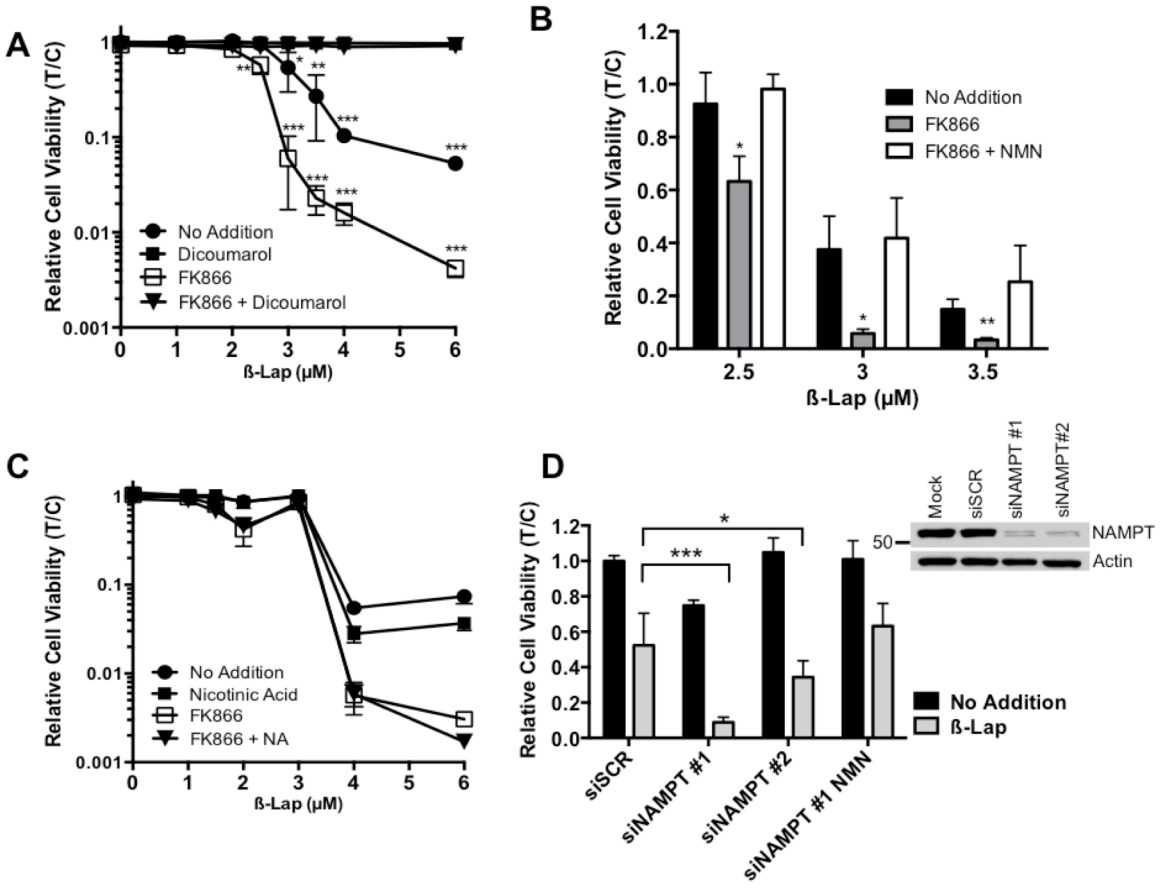

Figure 2-5. NQO1 and NAMPT specificity of combination treatment. **A)** MiaPaca2 cells were pre-treated with or without FK866 (8 nM), washed, and then exposed to various doses of ß-lap (μM) with or without 8 nM FK866 in the presence or absence of dicoumarol (50 μM) for 2 h. Viability assays were performed to monitor survival 24 h after treatment. **B)** Nicotinamide mononucleotide (NMN, 500 μM), which bypasses the NAMPT catalyzed reaction to rescue NAMPT inhibition, was added during FK866 pre-treatment and ß-lap exposure as in '**A**'. NMN prevented sensitization by FK866, but did not spare ß-lap-induced lethality. **C)** Nicotinic acid (NA, 500 μM) was added during co-treatment analogous to NMN treatment in '**B**'. Rescue of FK866 + ß-lap synergy was not observed since MiaPaca2 cells lack NAPT. **D)** Knockdown of NAMPT increased sensitivity to ß-lap. Two unique siRNAs specific for the coding region of NAMPT were used to suppress expression of NAMPT (inset). Cells were then treated with ß-lap (3 μM, 2 h) and viability assays were performed 24 h later. Results were compared using Student's t-tests (n=3 with mean +/- standard deviation), **p<0.05; **p<0.01; ***p<0.001*.

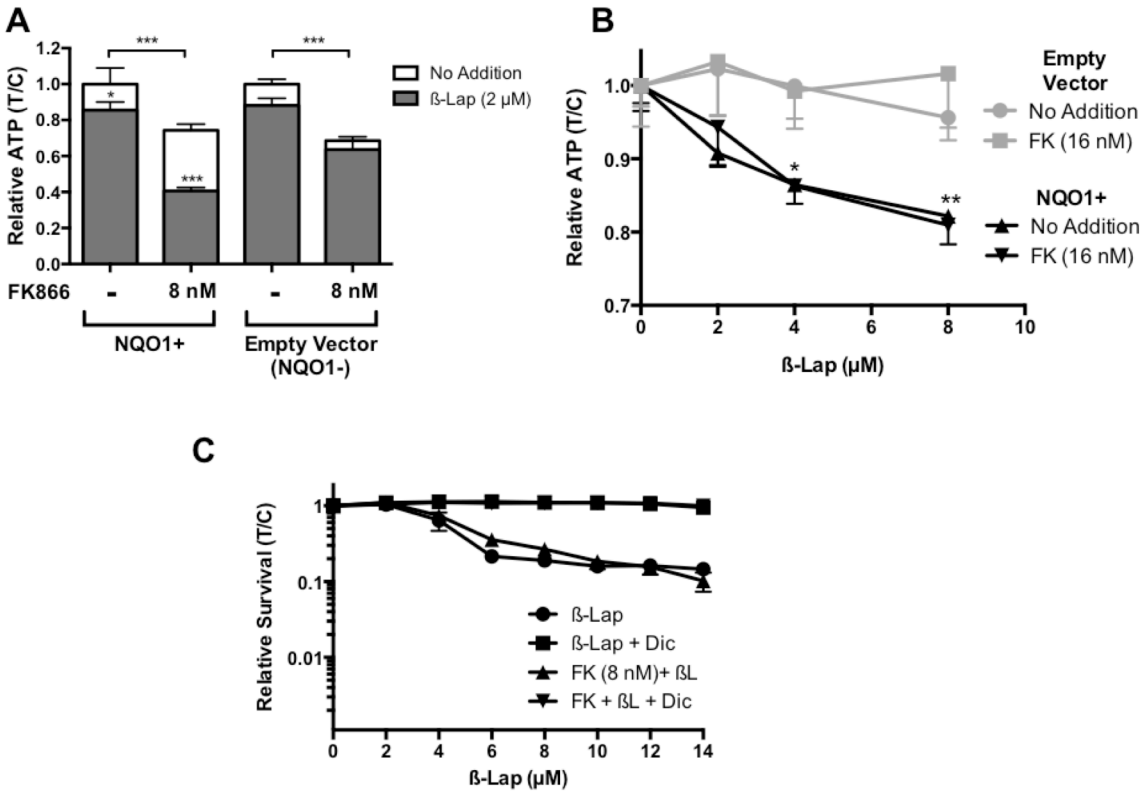

Figure 2-6. Normal and tumor cell genetic models of NQO1 specificity. **A)** S2-013 (NQO1-) PDA cells were corrected for NQO1 expression by CMV-NQO1 stable transfection. Cells were treated with FK866 and ß–lap and assessed for relative ATP content (T/C) 2 h later. **B)** NQO1 was expressed in IMR-90 normal fibroblasts and cells were treated as in '**A**' with an ATP assay performed 2 h after co-treatment. Though NQO1 overexpression caused ß-lap sensitivity, synergy with FK866 was not observed. **C)** Normal immortalized pancreatic ductal cells (hTERT-hPNE) were pretreated with FK866 (8 nM) for 24 h followed by co-treatment with ß-lap for 2 h and removal of both drugs. Viability assays were performed 24 h later. Due to increased expression of NQO1 in immortalized cells, ß-lap sensitivity was observed, but synergy with FK866 did not occur. Results were compared using Student's t-tests (n=3 with mean +/- standard deviation), **p<0.05; **p<0.01; ***p<0.001*.

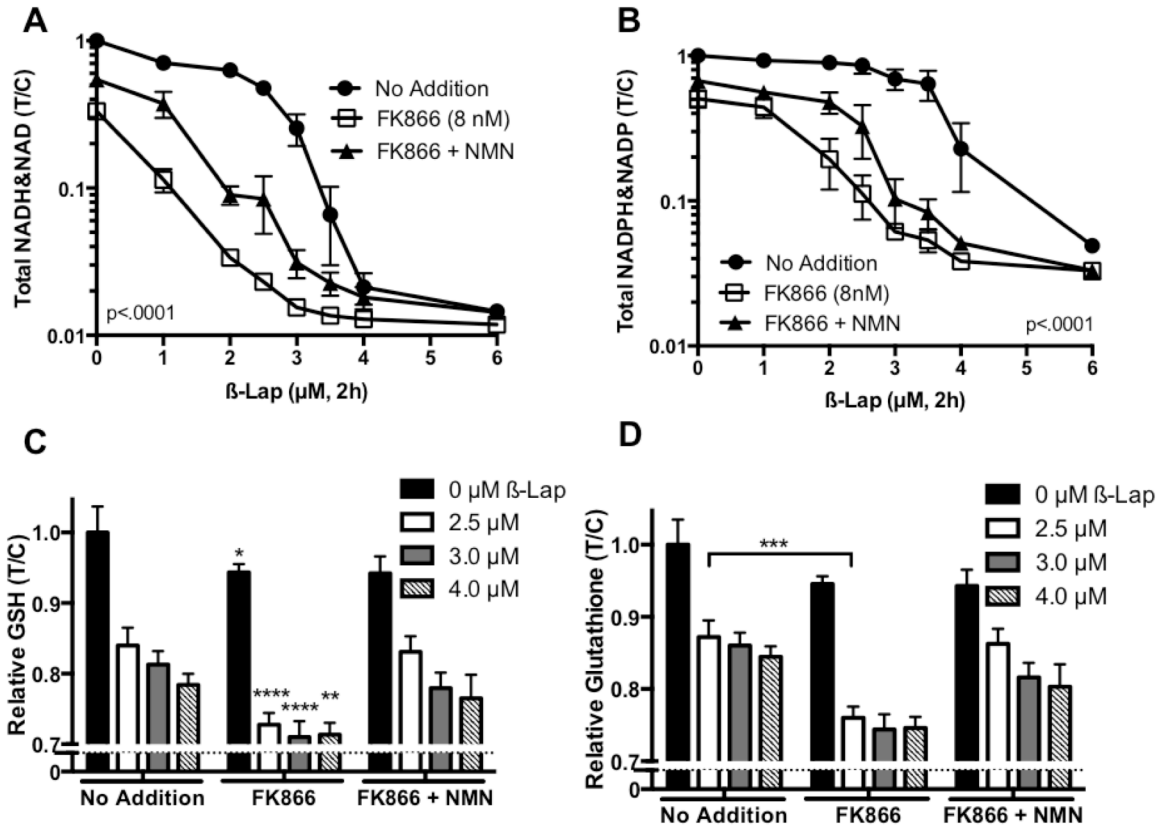

Figure 2-7. FK866 + ß-lap treatment caused depletion of NAD⁺/NADH, NADP⁺/NADPH, and glutathione. A, B) MiaPaca2 cells were pre-treated with FK866 (8 nM, 24 h), with or without NMN (500 µM) and then exposed or not to various doses of ß-lap (µM, 2 h with or without FK866 +/- NMN). Total NADH & NAD^+ (**A**) or NADPH & $NADP^+$ (**B**) pools were assayed at 2 h when drugs were removed. NMN addition partially rescued depletion of both sets of nucleotides. Results were analyzed by ANOVA (n=3 +/- standard deviation) comparing ß-lap alone (no addition) to FK866 + ß-lap. **C, D**) MiaPaca2 cells were treated as in '**A, B**' and relative reduced glutathione (GSH) (**C**) and total glutathione (**D**) levels (T/C) were monitored. Results were compared using Student's t-tests (n=3 with mean +/- standard deviation), ***p<0.01; ***p<0.001; ****p<0.0001*.

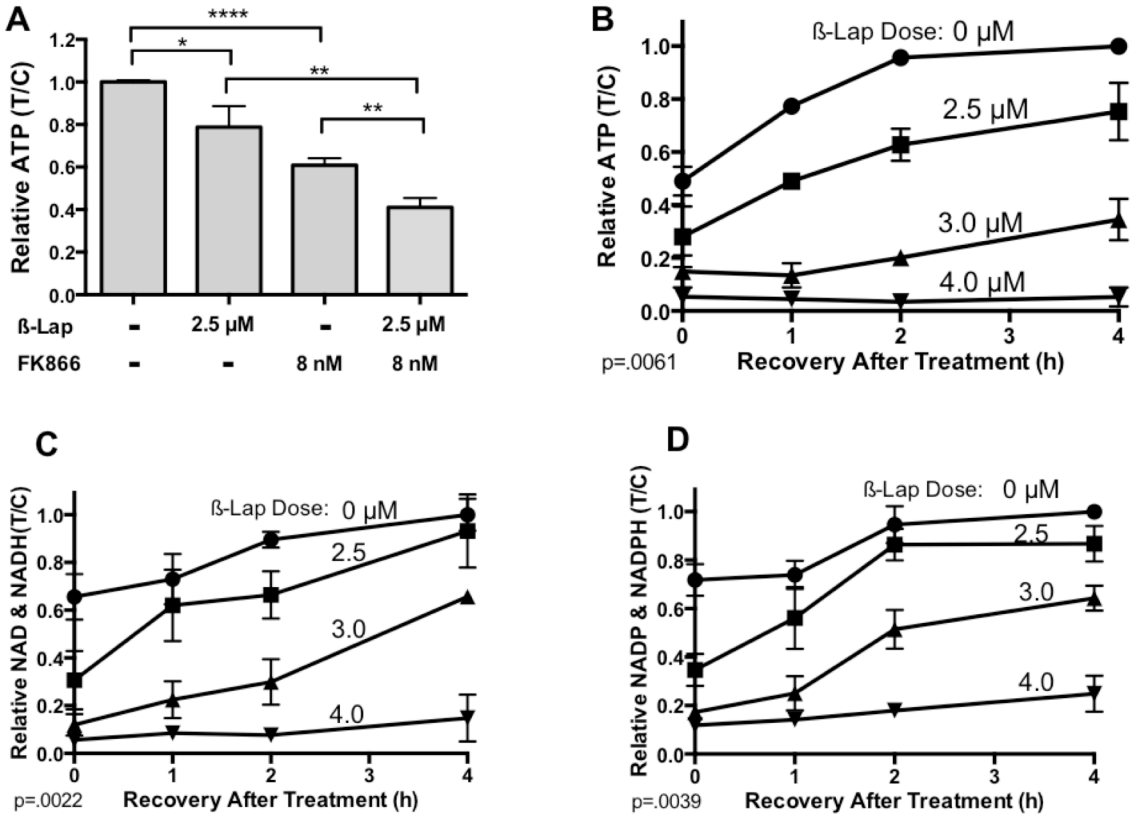

Figure 2-8. Combination treatment caused ATP depletion and prevented recovery after FK866 treatment. A) MiaPaca2 cells were pretreated with FK866 (8 nM) and then co-treated with ß-lap (2.5 µM) for 2 h and relative ATP pools were assessed. Results were compared using Student's t-tests (n=3 with mean +/- standard deviation), **p<0.05; **p<0.01; ****p<0.0001*. **B, C, D, E**) After combination treatment as in '**A**', ATP (**B**), NAD(H) (**C**), and NADP(H) (**D**) levels were measured at the indicated time points starting at t=0 after both drugs were removed. Results were compared with ANOVA (n=3 +/- standard deviation at each time point).

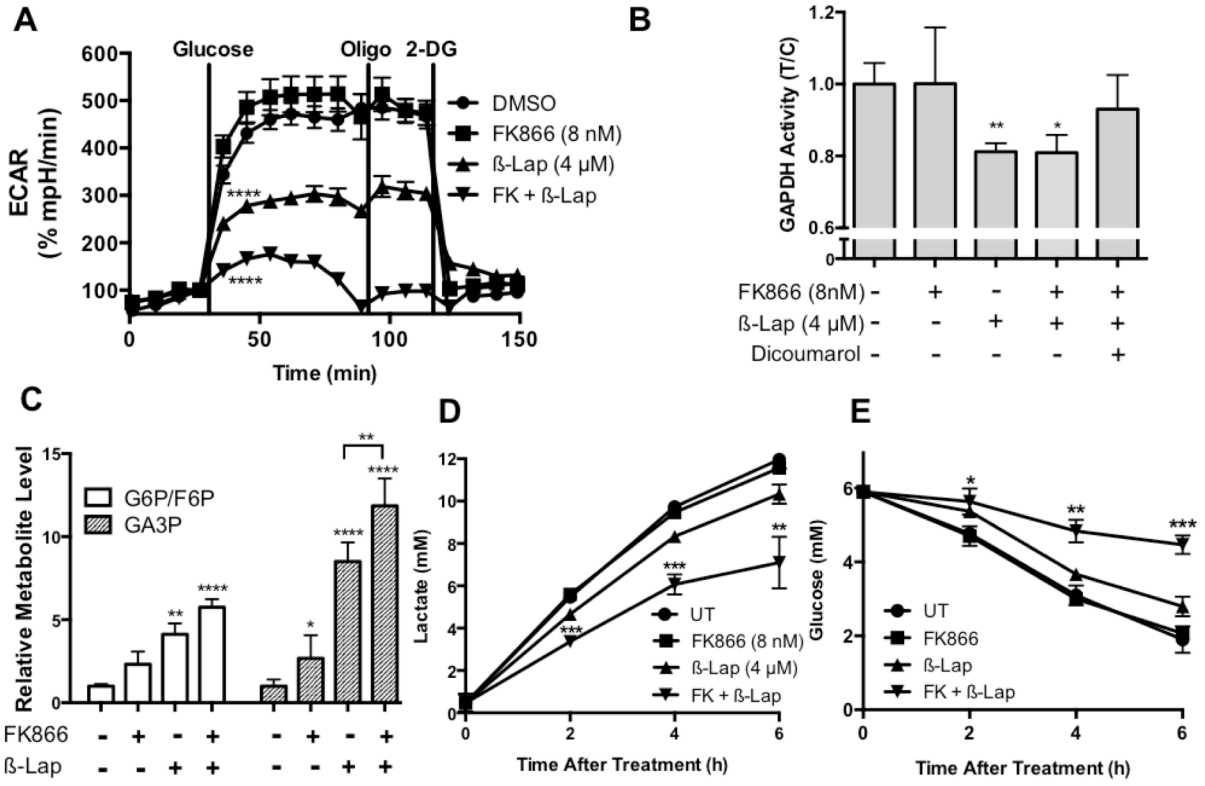

Figure 2-9. Combination treatment disrupts cancer cell glycolytic activity through GAPDH inhibition. A) Glycolytic stress tests were performed using the Seahorse XF bioanalyzer to measure the glycolytic capacity of MiaPaca2 cells pretreated with or without FK866 (8 nM), ß-lap (4 µM) alone or the combination therapy of FK866 (8 nM) + ß-lap (4 µM). Analyses were performed immediately following 2 h ß-lap exposures. Results were compared using ANOVA (n=4). ****$p<.0001$. **B)** GAPDH enzyme activities were measured from lysates of MiaPaca2 cells with or without FK866 (8 nM), and then exposed or not to ß-lap in the presence or absence of dicoumarol (50 µM) for 2 h. Extracts were prepared and enzyme activities (µmol NADH min^{-1}) were monitored and normalized to untreated samples. Data were expressed as relative GAPDH activity (T/C) and results were compared using Student's t-tests (n=6, +/- standard deviation) *$p<0.05$; **$p<0.01$. **C)** Glucose 6-phosphate/fructose 6-phosphate (G6P/F6P) and glyceraldehyde 3-phosphate (GA3P) were quantified in MiaPaca2 cells 30 min after treatment as described in methods. **D,E)** MiaPaca2 cells were treated as in 'A' and extracellular lactate **(D)** or glucose **(E)** levels in culture media were quantified using a Nova Bioprofile Analyzer at the indicated times after both removal of drugs. Results were compared using Student's t-tests (n=3 +/- standard deviation) *$p<.05$; **$p<.01$; ***$p < .001$; ****$p<.0001$.

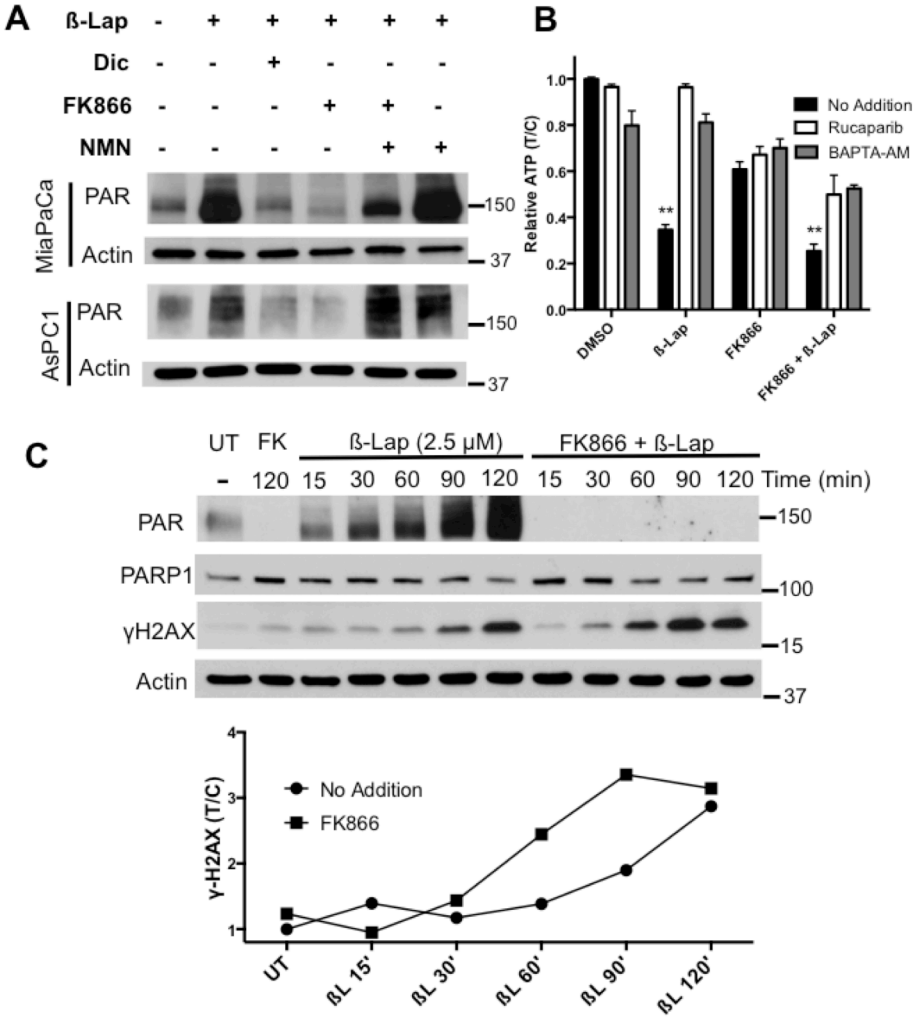

Figure 2-10. FK866 addition abrogated PAR formation and increased DSBs in ß-lap-treated MiaPaca2 cells A) NQO1+ MiaPaca2 or AsPC1 PDA cells were pre-treated with FK866 (8 nM, 24 h), then ß-lap (2.5 µM) was added in the presence or absence of dicoumarol (Dic, 50 µM) or NMN (500 µM) for 20 mins. Cell extracts were analyzed for PAR formation. Dicoumarol inhibits NQO1 activity thereby preventing PARP1 hyperactivation. ß-Lap-induced PAR formation was abrogated by FK866 (8 nM) and rescued with NMN (500 µM). Actin levels were monitored as loading controls. **B)** MiaPaca2 cells were pretreated with or without FK866 (8 nM) and then exposed to ß-lap (3 µM) in the presence or absence of (i) a PARP1 inhibitor (Rucaparib (AG014699), 20 µM) or (ii) a calcium chelator (BAPTA-AM) for 2 h; Rucaparib or BATPA-AM treatments prevent PARP1 hyperactivation in ß-lap-treated cells [16, 29, 42]. ATP levels were measured after the 2 h co-treatment. Student's t-tests were performed comparing ß-lap or FK866 + ß-lap *versus* addition of Rucaparib (AG014699) (n=3 +/- standard deviation). ***p <0.01*. **C)** MiaPaca2 cells were pretreated or not with FK866 (8 nM, 24 h), then exposed to ß-lap (2.5 µM) and PAR and γ-H2AX formation were monitored at various times during the 2 h exposure by western blot. Mean γH2AX band intensities, as a measure of DNA double strand break formation, were normalized to actin and levels graphed over time. Low PARP1 activity, as a result of lowered NAD^+ levels from FK866 exposure, resulted in more rapid induction of γ-H2AX.

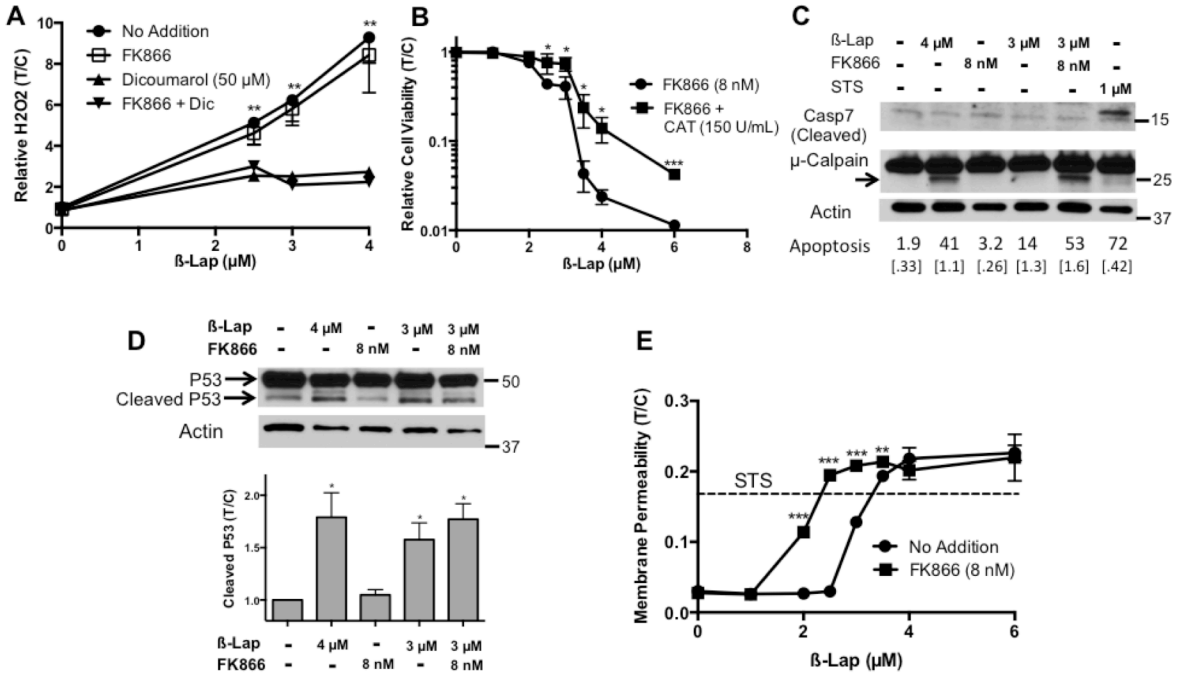

Figure 2-11. Exposure of NQO1+ MiaPaca2 cells to FK866 + ß-lap leads to NQO1-dependent, µ-calpain-mediated cell death. A) H_2O_2 levels, resulting from NQO1-dependent futile cycling of ß-lap, were monitored in MiaPaca2. FK866 pre- and co-treatment with ß-lap (µM) did not alter H_2O_2 production over the 2 h treatments. **B)** Addition of pegylated catalase (150 U/mL) neutralized H_2O_2 formation in FK866 (8 nM) + ß-lap-exposed MiaPaca2 cells over a 2 h treatment period, which partially rescued combination treatment lethality. **C**) Proteolytic cleavage of caspase-7 and the small subunit (27 kDa, arrow) of µ-calpain as indicators of activation were monitored by western blot 48 h post-treatment in MiaPaca2 cells pretreated with FK866 (8 nM), with or without ß-lap (4 µM) for 2 h. Staurosporin (1 µM, 18 h) treatment of MiaPaca2 cells served as a positive control for classic apoptosis. Flow cytometry analysis of sub G1 cells after the same treatment conditions was performed (standard deviation in brackets). **D**) Atypical p53 proteolysis, as expected with µ-calpain-induced cell death, was observed 48 h after exposure to ß-lap alone or after combination FK866 + ß-lap treatment. Band intensity was quantified and normalized to actin band intensity as indirect quantification of µ-calpain activity. **E)** MiaPaca2 cells were pre- and co-treated with or without FK866 (8 nM, 24 h) and then exposed or not to FK866 + ß-lap (µM) for 2 h. Membrane permeability was measured 24 h after drug treatment using CellTox Green, a membrane impermeable dye that measures extracellular DNA. Cells were lysed with SDS for 100% permeability normalization. For comparison, STS induced intrinsic apoptosis, but not necrosis. All indicated results were compared with Student's t-test (n=3, +/- standard deviation). **p<0.05; **p<0.01; ***p<0.001.*

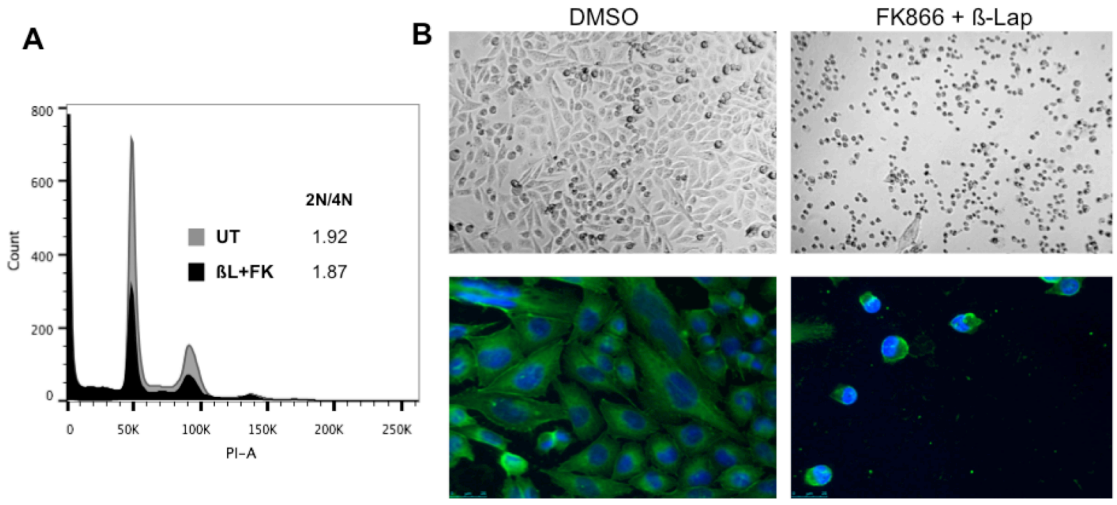

Figure 2-12. Cell cycle analysis and morphology after FK866 + ß-lap treatment. **A**) 48 h after treatment with FK866 + ß-lap, MiaPaca2 cells were stained with PI and cell cycle analysis was performed using flow cytometry. The ratio of cells with 2N and 4N DNA was calculated in FlowJo. **B)** After treatment as in 'A', MiaPaca2 cells were fixed and stained for actin (green) and DAPI (blue) for immunofluorescence. Images were captured in both phase contrast (above) and IF (below).

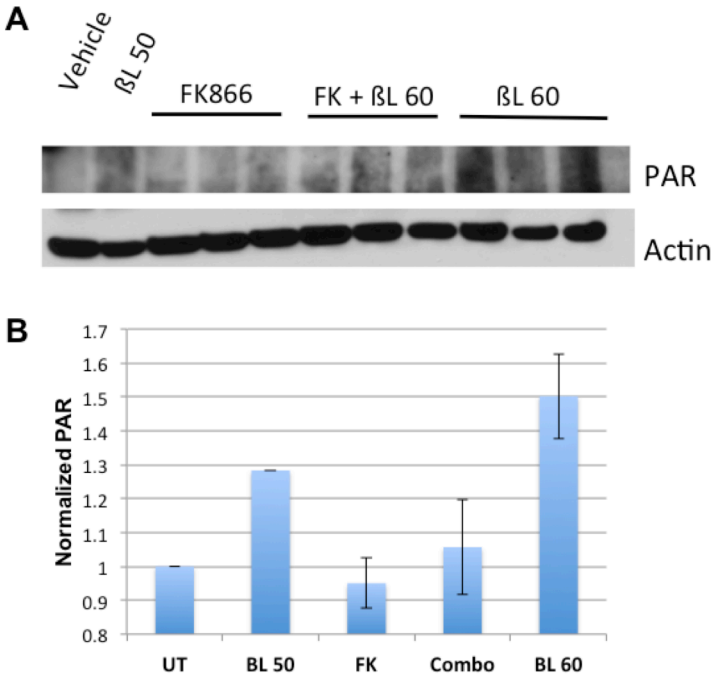

Figure 2-13. Pharmacodynamics of FK866 and ß-lap *in vivo*. A) MiaPaca2 subcutaneous tumors were established in athymic nude mice. Mice were injected I.P. with FK866 (15 mg/kg) or vehicle 1 day prior to co-injection with FK866 and ß-lap in HPßCD (50 mg/kg or 60 mg/kg). Tumor tissue was collected 2 h later and assayed for PAR formation. **B)** PAR intensity in '**A**' was normalized to actin and plotted (mean +/- standard deviation), showing a lack of PAR formation in tumor tissue with combination ß-lap + FK866 treatment *in vivo*.

Chapter Three
PARP1 inhibition in combination with ß-lapachone treatment results in increased DNA damage and apoptotic tumor cell death

3.1 Notes and Acknowledgements

The following chapter was adapted from a manuscript in preparation for submission. Dr. Xiumei Huang completed the majority of experiments in this chapter and is co-first author on the manuscript. Dr. Glenda Anderson performed the expression analysis, and Dr. Erik Bey analyzed human tissue samples for catalase expression and NQO1 protein level and activity and tested the NSCLC panel for drug sensitivity. I curated and assembled the results, analyzed the findings, and wrote the manuscript.

3.2 Abstract

DNA repair inhibitors, including drugs that block poly(ADP-ribose) polymerase 1 (PARP1) activity, are effective against cancers with rare genetic vulnerabilities, (e.g., BRCA1/2 deficiencies) but lack tumor specificity and efficacy for more general application. Patients with recalcitrant non-small cell lung cancer (NSCLC) and pancreatic cancer overexpress the two-electron oxidoreductase, NAD(P)H:quinone oxidoreductase 1 (NQO1), and have concomitantly low catalase levels compared to associated normal tissue. NQO1-bioactivatable drugs exploit the NQO1/Catalase therapeutic windows to elicit tumor-selective, NQO1-dependent futile redox cycling that causes extensive DNA base damage and single-strand breaks. Dramatic NAD(H)/ATP losses via PARP1 hyperactivation ensue and programed cell death is

independent of oncogenic driver or passenger mutations. The findings below describe synergistic interactions between PARP1 inhibitors and ß-lapachone (clinical form, ARQ761) wherein exposed NQO1+ cancer cells exhibit marked increases in DNA lesions that are not repaired due to PARP1 inhibition. Synergistic apoptosis was noted in all NQO1+ cancers tested, including NSCLC, pancreatic, and triple-negative breast cancers. Increased antitumor efficacy and survival were observed in orthotopic A549 NSCLC xenograft models. This drug combination greatly expands the use and tumor-specific efficacy of PARP1 inhibitors for cancer therapy.

3.3 Introduction

Poly(ADP-ribose) polymerase-1 (PARP1) is a crucial component of multiple DNA repair pathways for both single strand break (SSB) and double strand break (DSB) repair (Dantzer et al., 2000; Dantzer et al., 1999; M. Wang et al., 2006). In the single strand break repair (SSBR) pathway, PARP1 binds single strand breaks and consumes NAD^+ to catalyze the formation of long chains of poly(ADP ribose) (PAR) on histones, target DNA repair proteins, and itself (Helleday, Petermann, Lundin, Hodgson, & Sharma, 2008; E. J. Park et al., 2014). The activity of PARP1 recruits repair and scaffolding proteins to the site of damage (El-Khamisy, Masutani, Suzuki, & Caldecott, 2003; Lindahl, Satoh, Poirier, & Klungland, 1995; Underhill, Toulmonde, & Bonnefoi, 2011). PARP1 also binds double strand breaks and is a component of an alternative pathway of non-homologous end joining (NHEJ) (Beck et al., 2014; Haince et al., 2008; Langelier, Planck, Roy, & Pascal, 2012; M. Wang et al., 2006). The discovery that a DNA repair defect in BRCA1/2 mutant cancers yields hypersensitivity to PARP

inhibition caused a rush to develop new PARP inhibitors for targeted therapy in breast and ovarian cancer, where these mutations are found in a hereditary cancer syndrome (Farmer et al., 2005; Fong et al., 2010; Sandhu et al., 2013; Turner, Tutt, & Ashworth, 2005; Underhill et al., 2011). This class of cancers exhibits defective homologous recombination repair; therefore, when PARP1 inhibitors are used to block repair of spontaneous single strand DNA damage, the damage is converted to double strand breaks, which then must be repaired by low fidelity pathways such as NHEJ, resulting in genomic instability and cell death (Farmer et al., 2005). Furthermore, the disruption of PARP1-mediated alt-NHEJ also contributes to the resulting breakdown of the DNA repair response (Ceccaldi et al., 2015; Mateos-Gomez et al., 2015). The high specificity of PARP inhibitors has yielded good safety and tolerability, but their applicability is limited for use as a single agent treatment. Olaparib is the first PARP1 inhibitor to gain FDA approval, and is indicated for BRCA-deficient advanced ovarian cancer (Stockwell, 2014). Since BRCA1/2 mutations occur in a small subset of breast and ovarian cancers, there has been great interest in identifying 'BRCA-like' cancers that have different mutation signatures but share the phenotypes of defective DNA repair and PARP inhibitor hypersensitivity found in BRCA1/2 mutant cancers (E. J. Park et al., 2014; Rowe & Glazer, 2010). Other attempts to broaden the clinical application of PARP inhibitors include combining them with DNA damaging agents such as ionizing radiation (IR), cisplatin, temozolomide, and gemcitabine (Albert et al., 2007; C. L. Cheng et al., 2005; Jacob et al., 2007; Rajan et al., 2012). Though combination treatment strategies may expand the use of PARP inhibitors, the overall tumor-specificity is likely to decrease with the application of non-specific DNA damaging

agents alongside PARP inhibitors, as normal tissue will also be susceptible to increased DNA damage and inhibited repair.

Combining PARP inhibitors with the highly tumor-specific DNA damaging agent ß-lapachone (ß-lap) results in synergy at non-toxic doses of both drugs in cancer cells that exhibit NAD(P)H:quinone oxidoreductase (NQO1) overexpression: including breast cancer, non-small cell lung cancer (NSCLC), and pancreatic ductal adenocarcinoma (PDA). ß-Lap is in a unique class of quinone therapeutics that are bioactivated by the phase II detoxifying enzyme NQO1 (Bey et al., 2007; X. Huang et al., 2012). NQO1 catalyzes the 2-electron reduction of ß-lap to generate an unstable hydroquinone, which then spontaneously reacts with oxygen to revert back to the quinone form (Bey et al., 2007). This reaction occurs rapidly in a redox futile cycle: NADH or NADPH is oxidized by NQO1 to reduce ß-lapachone, and reactive oxygen species (ROS) are generated as the hydroquinone reacts with oxygen (Pink, Planchon, et al., 2000). Hydrogen peroxide produced as a result of this redox cycle diffuses into the nucleus and causes DNA single strand breaks and base oxidation. At lethal doses of ß-lap, the rapid accumulation of DNA damage overwhelms the repair capacity of the cell and causes hyperactivation of PARP1, resulting in extensive generation of PAR, inhibited DNA repair, and severe depletion of NAD^+ and ATP (X. Huang et al., 2012). When used as a single agent, ß-lap induces caspase-independent programmed cell death called NAD^+-Keresis, which is characterized by glycolytic inhibition, µ-calpain activation, atypical (60 kDa) PARP1 and p53 cleavage, and nuclear translocation of apoptosis inducing factor (AIF) (Bentle et al., 2006; Bey et al., 2007; Pink, Planchon, et al., 2000; Tagliarino et al., 2001; Tagliarino et al., 2003). Though ß-lap is currently in Phase I

clinical trials (ARQ761), improving its efficacy at lower doses would prevent its dose-limiting toxicity, methemoglobinemia, and increase its potential efficacy in the clinic (Gerber et al.; L. P. Hartner, 2007).

Combining PARP inhibitors with ß-lapachone resulted in robust tumor-specific cell kill both *in vitro* and *in vivo*. Using low doses of ß-lap caused DNA damage in tumor cells that must be repaired through the activity of PARP1. When PARP1 was inhibited, repair did not occur and these SSBs were converted to lethal DSBs, triggering apoptotic cell death. The differentiating factor between ß-lap compared to other DNA damaging agents when used in combination with PARP inhibitors is that the DNA damage caused by ß-lap is exquisitely tumor-specific due to the requirement for NQO1 bioactivation. Marked overexpression of NQO1 in NSCLC, breast cancer, and PDA tumor tissue relative to normal tissue was also observed, thereby maintaining a wide therapeutic window and offering the potential to expand the application of PARP1 inhibitors and ß-lap to treat a wide variety of solid tumors.

3.4 Results

High NQO1:Catalase ratio establishes a therapeutic window for ß-lap in NSCLC and PDA. Individually comparing gene expression in matched samples showed high expression of NQO1 (**Figure 3-1A**) and low expression of catalase (**Figure 3-1B**) in NSCLC tumor compared to normal lung tissue from the same patient. Consistent with limited prior reports that NQO1 expression is high in human NSCLC, there was a significant ($p = 2.2x10^{-38}$) elevation in expression of NQO1 in NSCLC tissue compared to normal lung tissue by gene expression microarray analysis (**Figure 3-1C**) (Bey et al.,

2007; D. Siegel et al., 1998). These findings may be explained by the frequency of dysregulation of the NRF2-KEAP1 signaling pathway in NSCLC, which can drive NQO1 expression (Singh et al., 2006). Paradoxically, catalase expression is significantly ($p = 5.6x10^{-48}$) lower in tumor tissue compared to normal lung tissue (**Figure 3-1D**). It is unclear what drives the divergent expression patterns of NQO1 and catalase, which both contain antioxidant response elements (ARE) in their promoters (Cho et al., 2002). However, high NQO1 and low catalase levels (a high NQO1/Catalase ratio) in NSCLC tumor tissue makes it an ideal target for ß-lap treatment, as NQO1 is required to initiate the redox futile cycle, and low catalase levels in tumor tissue prevents neutralization of the generated H_2O_2 that causes DNA damage and cell death (**Figure 3-1E**).

Similar results were observed in pancreatic cancer. PDA tumor tissue exhibits high NQO1 expression compared to paired normal tissue (**Figure 3-2A**). Catalase expression follows the opposite trend (**Figure 3-2B**). Combined quantification of NQO1 expression yields a p value of $4.2x10^{-31}$ for tumor overexpression, and even higher expression in cancer cell lines (**Figure 3-2C**). The reduced catalase expression in tumor tissue (**Figure 3-2D**) was not as substantial as noted in NSCLC, though the findings are still highly significant ($p = 1.3x10^{-7}$). For the ß-lap therapeutic window, it is more important to have high catalase expression in normal tissue than low catalase in tumors, since the high NQO1 during ß-lap exposure generates enough free radicals to saturate the neutralization ability of even high catalase levels (Bey et al., 2013). On the other hand, a bystander effect in normal cells can be effectively prevented by catalase since the concentration of H_2O_2 that diffuses into surrounding normal cells is much

lower (Cao et al., 2014). Additionally, the NQO1 to catalase ratio in PDA tumor tissue was similarly elevated as in NSCLC (**Figure 3-2E**), suggesting a high therapeutic window for ß-lap in both NSCLC and PDA.

NQO1 protein levels are elevated in patient-derived tumor samples. Tumor and normal tissue from NSCLC patients was analyzed for NQO1 and catalase protein levels (**Figure 3-3A**), which demonstrated the same trend observed with mRNA expression data: high NQO1 levels and low catalase levels in tumor tissue compared to associated normal tissue. NQO1 enzymatic activity assays also showed high NQO1 activity in NSCLC tissue (**Figure 3-3A**). NQO1 expression data from NSCLC patients before therapy was divided into two groups: those who experienced a complete response to chemotherapy (CR), and those who had progressive disease (PD) despite chemotherapy (**Figure 3-3B**). Patients who were resistant to chemotherapy had higher NQO1 expression than those who experienced a complete response ($p = .006$). This suggests that NQO1 is an actionable target in chemoresistant NSCLC tumors, and that ß-lap may be effective in these recalcitrant cases.

ß-lap sensitivity is only dependent on NQO1 status. To determine the dependence of ß-lap efficacy on NQO1 polymorphisms and other driver mutations in NSCLC, the sensitivity of a panel of cell lines to 2 h ß-lap treatment was determined with long-term survival assays (**Figure 3-4A**). Restriction fragment length polymorphism (RFLP) analysis was used to determine which cell lines were homozygous or heterozygous for

the common *2 (C609T) or *3 (C465T) NQO1 polymorphisms, both of which cause loss of NQO1 activity (**Figure 3-4A**). The ß-lap LD_{50} of all cell lines tested was ~4 μM or less regardless of other mutations or deletions as long as they had at least one wild type allele of NQO1. Cells without a wild-type NQO1 allele were resistant to 2 h ß-lap treatment. Accordingly, the variety of mutational profiles in pancreatic cancer cells is independent of ß-lap and IB-DNQ (another NQO1-bioactivatable drug) sensitivity, with the exception of NQO1 status (**Figure 3-5A**). Panc1 and S2-013 cells, which are homozygous for NQO1*2 polymorphisms, were resistant to ß-lap, and sensitivity was increased by expressing wild-type NQO1 in these cells (**Figure 3-5A**).

Synergy is observed between PARP inhibitors and ß-lap. A549 cells were pre-treated with PARP inhibitors AG014699 (rucaparib) (**Figure 3-6A**)**,** AZD2281 (olaparib) (**Figure 3-6B**), or AG14631 (**Figure 3-6C**) for 2 h followed by co-treatment with ß-lap for 2 h and removal of both drugs. These PARP inhibitors markedly increased ß-lap sensitivity in A549 and this effect was blocked dicoumarol (DIC, a specific inhibitor of NQO1 (**Figure 3-6D**). A dose-response of AG014699 demonstrated that synergy was most effective at 15 μM or higher doses (**Figure 3-6E**). MCF-7 breast cancer cells also showed sensitivity to ß-lap and AG014699 combination treatment (**Figure 3-6F**). Synergy was observed between PARP inhibitors and ß-lap despite a near complete lack of toxicity caused by treatment with these PARP inhibitors as single agents (**Figure 3-7A-C**). As a positive control for PARP inhibition, sensitivity to AG014699 was observed in BRCA2-deficient CAPAN-1 cells as expected (**Figure 3-7D**).

Synergy is dependent on NQO1 expression in NSCLC, PDA, and breast cancer cell lines. After establishing synergy between PARP inhibitors and ß-lap, NQO1 expression was modulated by overexpression or knockdown in various cancer cell types to establish the NQO1 dependence of combination treatment. This genetic approach to addressing NQO1 specificity reinforces the findings noted with dicoumarol, which could exhibit off-target effects since it is a small molecule inhibitor which functions as an NAD^+ analog. MiaPaca2 is a PDA cell line that normally overexpresses NQO1; it was sensitive to combination treatment with ß-lap and AG014699, and toxicity was blocked by dicoumarol (**Figure 3-8A**). When NQO1 expression was knocked down by shRNA as described by *Li et al*. (Li et al., 2011), cells were resistant to ß-lap and AG014699 + ß-lap, even at high doses (**Figure 3-8B**). Knockdown of NQO1 was confirmed at the protein level (**Figure 3-9A**), and an additional knockdown clone exhibited similar sensitivity to ß-lap and AG014699 + ß-lap treatment (**Figure 3-9B**). In contrast, S2013 is a PDA cell line with no NQO1 expression due to a homozygous *2 NQO1 polymorphism (Moore et al., 2015). These cells were sensitive to AG014699 + ß-lap treatment if NQO1 was introduced with an expression vector (**Figure 3-8C**) but were otherwise resistant (**Figure 3-8D**). Likewise, the NSCLC line H596 and triple negative breast cancer cell line MDA-MB-231 also carry NQO1 polymorphisms that cause lack of NQO1 expression and therefore were sensitive to combination treatment only when NQO1 was overexpressed (**Figure 3-8E-H**). Knockdown of PARP1 by shRNA in MCF-7 cells increased sensitivity to ß-lap (**Figure**

3-9C). These cell lines were unaffected by short-term (4 h) single agent treatment with AG014699 at up to 25 μM (**Figure 3-9D**), reinforcing the true synergy observed with combination treatment. In cells from a variety of cancer types, NQO1 expression is both necessary and sufficient for sensitivity to combination treatment with ß-lap and AG014699.

PAR formation and ATP depletion is abrogated with ß-lap in combination with PARP inhibition. During ß-lap treatment, PARP1 hyperactivation results from single strand breaks and base oxidation caused by ROS generated in the NQO1 catalyzed redox futile cycle. There was a rapid increase of high molecular weight PARylated protein after ß-lap treatment, which began to dissipate after 10 minutes, as a result of PARP1 exhaustion and PAR glycohydrase (PARG) activity (**Figure 3-10A**) (Bentle et al., 2006; Bey et al., 2007). As expected with AG014699 treatment in combination with ß-lap, PAR formation was not observed since PARP1 activity was inhibited (**Figure 3-10A**). To confirm that this was an on-target effect of PARP1 inhibitors, PARP1 levels were depleted with shRNA in MCF7 and the same effects were observed (**Figure 3-10B**). Furthermore, an earlier induction of γH2AX when PARP1 was depleted suggests that the single strand breaks detected by PARP1 were more rapidly converted to double strand breaks in its absence (**Fig 3-10B**). PARP1 knockdown in MDA-MB-231 cells similarly reduced protein levels (**Figure 3-11A**) and inhibited PAR formation and accelerated the formation of γH2AX after ß-lap treatment (**Figure 3-11B**). In survival assays, synergy was also observed between PARP1 knockdown and ß-lap treatment in

NQO1+ cells, similar to when PARP inhibitors are used (**Figure 3-11C**). Additionally, AG014699 treatment in PARP knockdown cells resulted in additional synergy compared to the either knockdown or inhibitor use alone, suggesting that neither of these techniques completely blocked PARP activity independently (**Figure 3-11D,E**). In order to synthesize PAR, PARP1 consumes NAD^+, a critical energy currency of the cell (Luo & Kraus, 2012). As a result of the close link between NAD^+ and ATP, ATP levels are also depleted when PARP1 is hyperactivated during ß-lap treatment (Bey et al., 2007). ATP levels were completely depleted with lethal doses of ß-lap treatment in MCF-7 cells within an hour of treatment, but ATP levels were retained when PARP1 was knocked down during ß-lap treatment (**Figure 3-10C**). Even at lower doses of ß-lap, significant ATP depletion was blocked with PARP1 knockdown (**Figure 3-10D**). Prevention of ATP depletion with PARP1 loss occurred despite increased cell death with PARP1 depletion or inhibition, suggesting that the ATP loss caused ß-lap is a result of PARP1 activity, but is not required for cell death in the long-term.

Synergy occurs downstream of the NQO1-mediated ß-lap futile cycle. A series of experiments were performed to determine whether the increased lethality observed with PARP1 inhibition and PARP1 knockdown in combination with ß-lap treatment was due to an effect on the NQO1 mediated futile cycle. First, treatment of cells with AG01499 followed by NQO1 recycling assays did not yield any change of the consumption of NADH, suggesting that AG014699 does not have a direct or indirect effect on cellular NQO1 activity (**Figure 3-12A**). Likewise, H_2O_2 levels produced during

2 h combination treatments with AG014699 and ß-lap were similar to those produced by ß-lap alone, and in both cases were blocked by dicoumarol (**Figure 3-12B**). Oxygen consumption was monitored in A549 cells during ß-lap treatment, which occurs as oxygen reacts with the hydroquinone form of ß-lap to generate ROS during the NQO1-mediated futile cycle, independent of oxidative phosphorylation in the mitochondria (Bey et al., 2007). ß-lap treatment alone at an effective synergy dose (3 μM) or in combination with AG014699 resulted in equivalent rates of sustained oxygen consumption over 2 h (**Figure 3-12C**). These data suggest that the synergy between PARP inhibition and ß-lap treatment does not occur at the level of the NQO1-mediated futile redox cycle and ROS generation, but downstream, at the response to DNA damage. Total levels of NAD^+ and NADH decreased after single agent ß-lap treatment as a direct result of PARP1 activity and were rescued with AG014699 co-treatment (**Figure 3-12D**), which correlates with ATP depletion noted in **Figure 3-10C**. At supralethal doses of ß-lap (8 μM), the oxygen consumption quickly reached a peak of about 400% of the basal level and then decreased. However, this peak oxygen consumption was maintained for a longer period of time with AG014699 co-treatment (**Figure 3-12B**). In the case of ß-lap single agent treatment at high doses, NAD^+ is substantially consumed by PARP1 at high ß-lap doses (**Figure 3-12D**), so it is not available to be reduced back to NADH and drive the futile cycle, resulting in a decrease of oxygen consumption over time. However, it is important to note that at high doses of ß-lap (8 μM) + AG014699, the sustained oxygen consumption allowed by the lack of NAD^+ depletion is not relevant to cell death, since 8 μM ß-lap is already above the LD90 of ß-lap as a single agent. At ß-lap doses where synergy is observed (3 μM),

moderate oxygen consumption and reactive oxygen species formation caused by the futile cycle was maintained for the entire 2 h treatment time since there was enough remaining NAD^+ and NADH to fuel the futile cycle, even during single agent ß-lap treatment (**Figure 3-12B**). This supports the hypothesis that NAD^+ depletion and the ß-lap futile cycle with NQO1 do not contribute to the synergy observed with ß-lap + PARP inhibitor treatment at low doses of ß-lap.

PARP inhibition rescues NAD^+ and ATP loss but amplifies the DNA damage caused by ß-lap. The similarity in ROS generation but abrogation of PAR formation observed with PARP inhibitor + ß-lap versus single agent ß-lap treatment suggested that there may be a downstream enhancement of DNA damage as a result of PARP1 inhibition. Alkaline comet assays were used to detect total DNA damage (single strand breaks, double strand breaks, and abasic sites), which showed that total DNA damage is much higher with 3 μM ß-lap + AG014699 compared to 3 μM ß-lap alone (**Figure 3-13A**). Similarly, the DNA double strand break response with 2 μM ß-lap + AG014699 was similar to 5 μM of ß-lap alone (a lethal single-agent dose) as measured by γH2AX foci formation (**Figure 3-13B**). Increased DNA damage was observed despite the similar levels of ROS formation noted in **Figure 3-12**, suggesting that the inability of inhibited PARP1 to properly repair the damage caused by a low dose of ß-lap resulted in greater accumulation of damage and conversion to double strand breaks. The pathway of cell death initiated by ß-lap is driven by PARP1-mediated loss of NAD^+ and ATP followed by μ-calpain activation, nuclear AIF translocation, and is caspase-

independent despite similarities to apoptosis, such as TUNEL positive staining (Bentle et al., 2006; Bey et al., 2007; X. Huang et al., 2012; Moore et al., 2015; Tagliarino et al., 2003). Less PAR formation was noted with PARP inhibitor + ß-lap treatment along with reduced NAD^+/NADH and ATP loss, yet more DNA damage occurred, which raised the question of whether cells died through the same caspase-independent mechanism as with ß-lap treatment alone. MCF-7 cells treated with AG014699 + ß-lap showed cleavage of caspase-7 and caspase-3, and the 89 kDa cleavage fragment of PARP1, which was prevented by the pan-caspase inhibitor Z-VAD (**Figures 3-13C, 3-14A**). This is in stark contrast to the 60 kDa cleavage fragment of PARP1, cleavage of p53, and lack of caspase-7 activation observed with single agent ß-lap treatment, which could not be blocked with Z-VAD (**Figures 3-13C**). These results indicate that combination treated cells died through caspase-dependent apoptosis instead of the NAD^+-Keresis caused by single agent ß-lap treatment. This is consistent with my findings in Chapter 2 that NAD^+-Keresis is primarily driven by energy depletion in the form of NAD^+/ATP loss, which does not occur with ß-Lap + PARP inhibitor treatment (Moore et al., 2015).

Combination treatment with ß-lap and PARP inhibitors in NSCLC tumor-bearing mice decreased tumor growth and increased overall survival. A549 orthotopic tumors were established in female NOD/SCID mice as described in the methods. On day 8 after tumor cell injection, treatment began. ß-Lap was administered I.V. (22 mg/kg) every other day for 10 days, and AG014699 (rucaparib) was given I.P. (10 mg/kg) every day for 10 days. Significant reduction in tumor growth was observed for both ß-lap treated and PARPi treated mice, with an enhanced effects in mice treated

with the combination of both drugs (**Figure 3-15A, B**). Kaplan-Meier survival analysis yielded a statistically significant survival benefit with ß-lap, and surprisingly also with AG014699, despite its lack of *in vitro* efficacy against A549 cells (**Figure 3-15C**). However, the survival extension was significantly greater with ß-lap + AG014699 combination treatment, supporting the *in vitro* synergy results described above. Notably, there was no increased toxicity observed with these drugs used in combination exceeding the brief (5-20 minutes) lethargy and rapid breathing that occurs with ß-lap single agent treatment.

3.5 Discussion

The above findings demonstrate a robust synergy between PARP inhibition and NQO1-bioactivatable drugs like ß-lap. The ability to use both of these drugs at low doses is a result of the interplay between their mechanisms of action. Though PARP inhibitors typically have little to no effect on cells that do not carry genetic aberrations rendering them hypersensitive, the inhibition of PARP1 in tumor cells that have been treated with ß-lap substantially reduced their ability to repair the specific type of DNA damage (single strand breaks) that ß-lap causes. Unlike other DNA damaging agents, the damage caused by ß-lap is restricted to NQO1-overexpressing tumor cells. Without this added specificity, DNA damaging agents may enhance cancer cell lethality in combination with PARP inhibitors but similarly increase toxicity to normal cells. In contrast, high NQO1, and more importantly, high NQO1 to catalase ratios in tumor tissue from NSCLC, PDA, and breast cancer define a large therapeutic window for the application of this combination treatment in a variety of tumor types for which PARP

inhibitors are normally not effective. Though the levels of catalase in tumor tissue varies between NSCLC and PDA, this is likely not relevant to ß-lap sensitivity since even partial rescue from ß-lap in NQO1+ cells with catalase was only achieved with catalase overexpression at much higher than physiologic levels (Bey et al., 2013). Instead, the high catalase expression in normal tissues is likely more important from a therapeutic standpoint; lower levels of catalase are capable of rescuing a bystander effect caused by H_2O_2 diffusing from NQO1+ cancer cells to NQO1- surrounding normal cells, since the H_2O_2 concentration rapidly decreases as a function of the distance squared, and potentially even faster as it is relatively unstable (Cao et al., 2014). Based on the NQO1 specificity of combination treatment with ß-lap and PARP inhibitors and reports of NQO1 elevation in a variety of other solid tumors, such as prostate and colon cancer, it is anticipated that this combination treatment could expand the effective use of PARP inhibitors even further (D. Siegel & Ross, 2000).

In addition to expanding the expanding the application of PARP inhibitors and improving the efficacy of both of these drugs through tumor-specific synergy, combination treatment with PARP inhibitors and ß-lap also provides a better understanding of the mechanism of death induced by ß-lap. By using NAMPT inhibitors to prevent PAR formation while promoting NAD^+ and ATP depletion In chapter 2, I showed that cell death induced by ß-lap was precipitated primarily by energy depletion rather than signaling driven by PAR polymer, which may be a component of calpain and AIF induced cell death in other contexts (Tagliarino et al., 2001; van Wijk & Hageman, 2005; Vanden Berghe et al., 2014; Virag et al., 2013; Zhang et al., 2014). Results with PARP inhibitors in combination with ß-lap confirm this. When

PARP1 was inhibited, ATP/NAD^+ depletion did not occur from ß-lap treatment; DNA damage (especially in the form of double strand breaks) increases, and cells die through caspase-mediated apoptosis instead of NAD^+-Keresis. At low doses of ß-lap and PARP inhibitors, energy depletion did not occur and lethal DNA double strand breaks led to apoptosis, but at supralethal doses of ß-lap without PARP inhibitors, the ATP and NAD^+ depletion dominate to drive NAD^+-Keresis, despite similar levels of DNA damage.

There is immediate potential for clinical innovation through the application of these findings. ß-lap is still relatively new in clinical trials, but has demonstrated promising tolerability and PK (Gerber et al.). Additionally, a multitude of previous and ongoing trials have shown PARP inhibitors to be well-tolerated and target-specific in clinical use (E. J. Park et al., 2014). In the described *in vivo* studies, there was no combination toxicity above that for the individual agents as expected based on the *in vitro* target specificity findings, and the synergy between ß-lap and AG014699 markedly decreased tumor growth and improved survival compared to either agent alone. This signifies that this combination therapy strategy has a high therapeutic index and will achieve better anti-tumor efficacy than either agent alone without increasing normal tissue toxicity.

Chapter 3 Figures

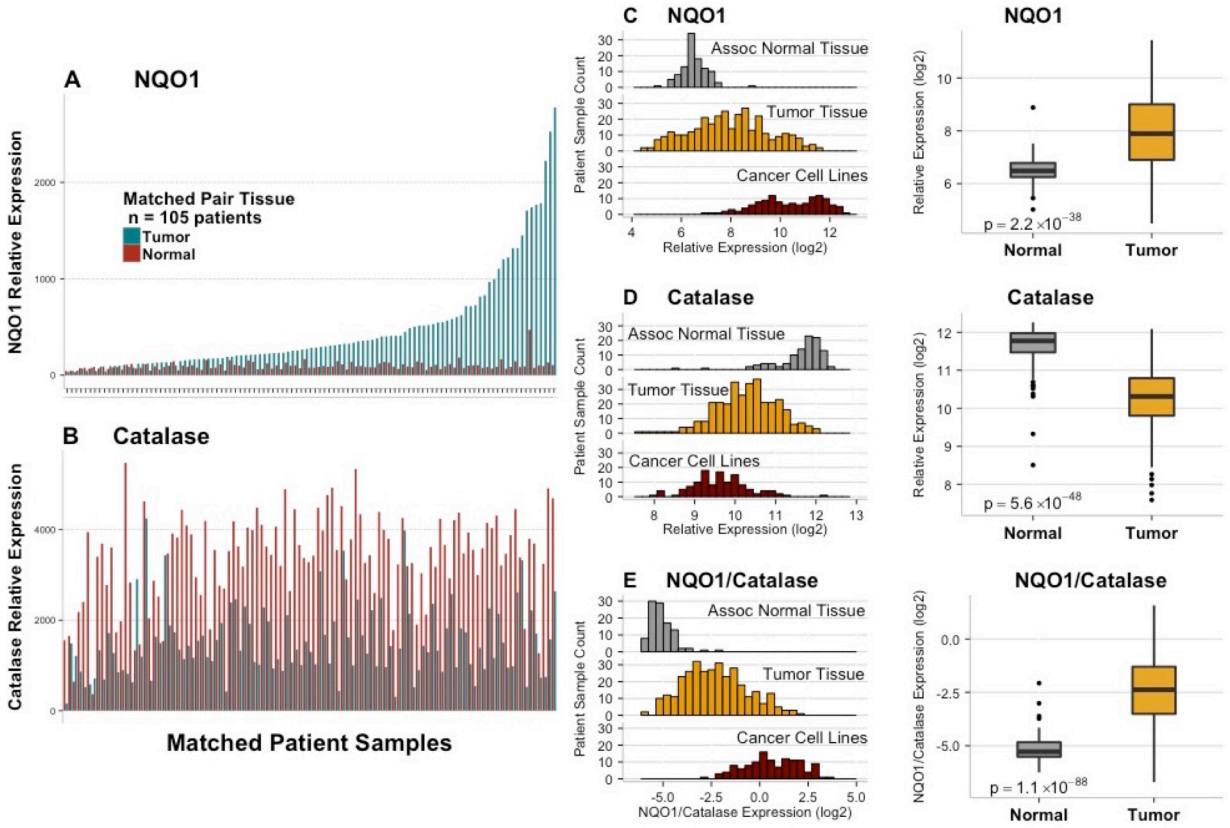

Figure 3-1. NQO1 expression is elevated and catalase expression is reduced in NSCLC tumor tissue compared to associated normal tissue. Gene expression from 105 matched NSCLC and associated normal lung samples were analyzed for **(A)** NQO1 and **(B)** catalase expression as described in the methods section. Analysis of **(C)** NQO1 and **(D)** catalase expression in a total of 327 NSCLC and 105 normal samples was compared, demonstrating high NQO1 and low catalase levels in tumor tissue versus normal tissue, resulting in a high **(E)** NQO1 to catalase ratio in tumor tissue ($p = 1.1x10^{-88}$).

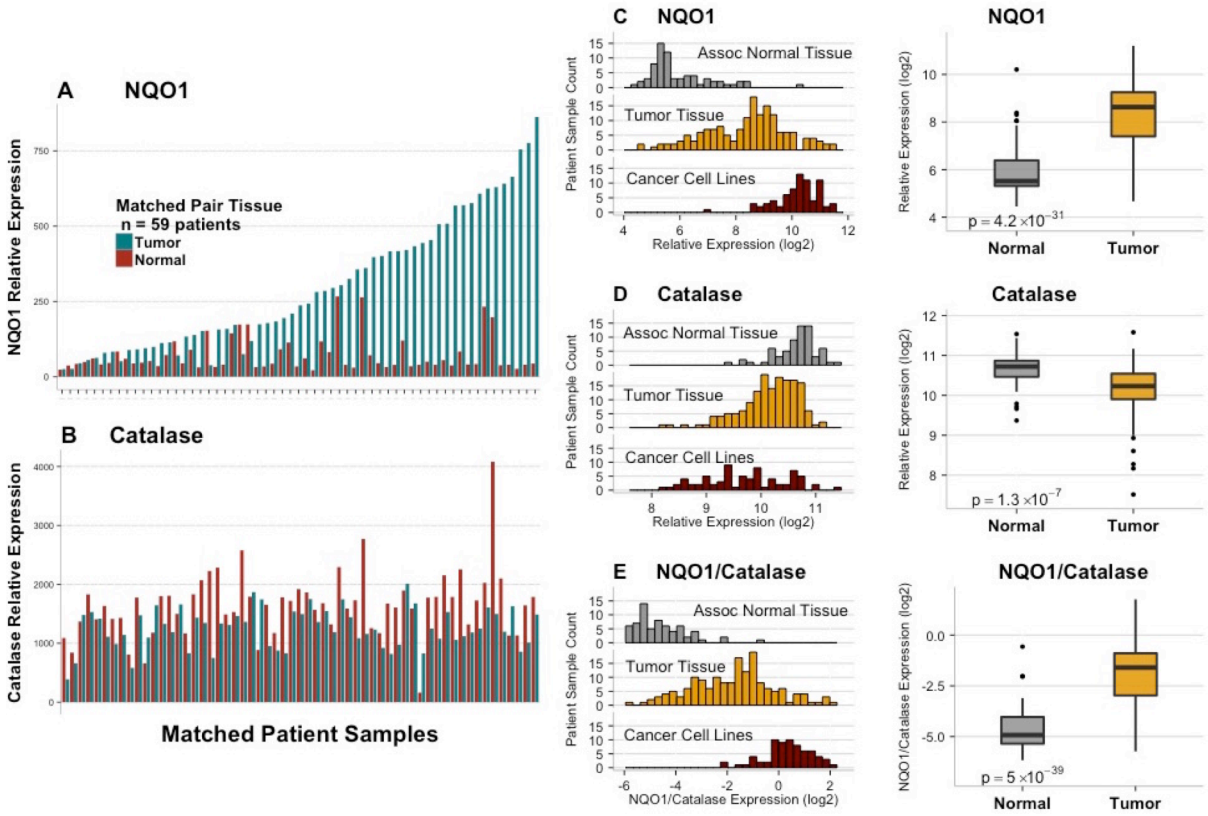

Figure 3-2. NQO1 expression is elevated and catalase expression is reduced in PDA tumor tissue compared to associated normal tissue. Gene expression from 59 matched NSCLC and associated normal lung samples were analyzed for **(A)** NQO1 and **(B)** catalase expression as described in the methods section. Analysis of **(C)** NQO1 and **(D)** catalase expression in patient samples along with PDA cell lines showed high NQO1 and low catalase levels in tumor tissue versus associated normal tissue, resulting in a high **(E)** NQO1 to catalase ratio in tumor tissue ($p = 5x10^{-39}$).

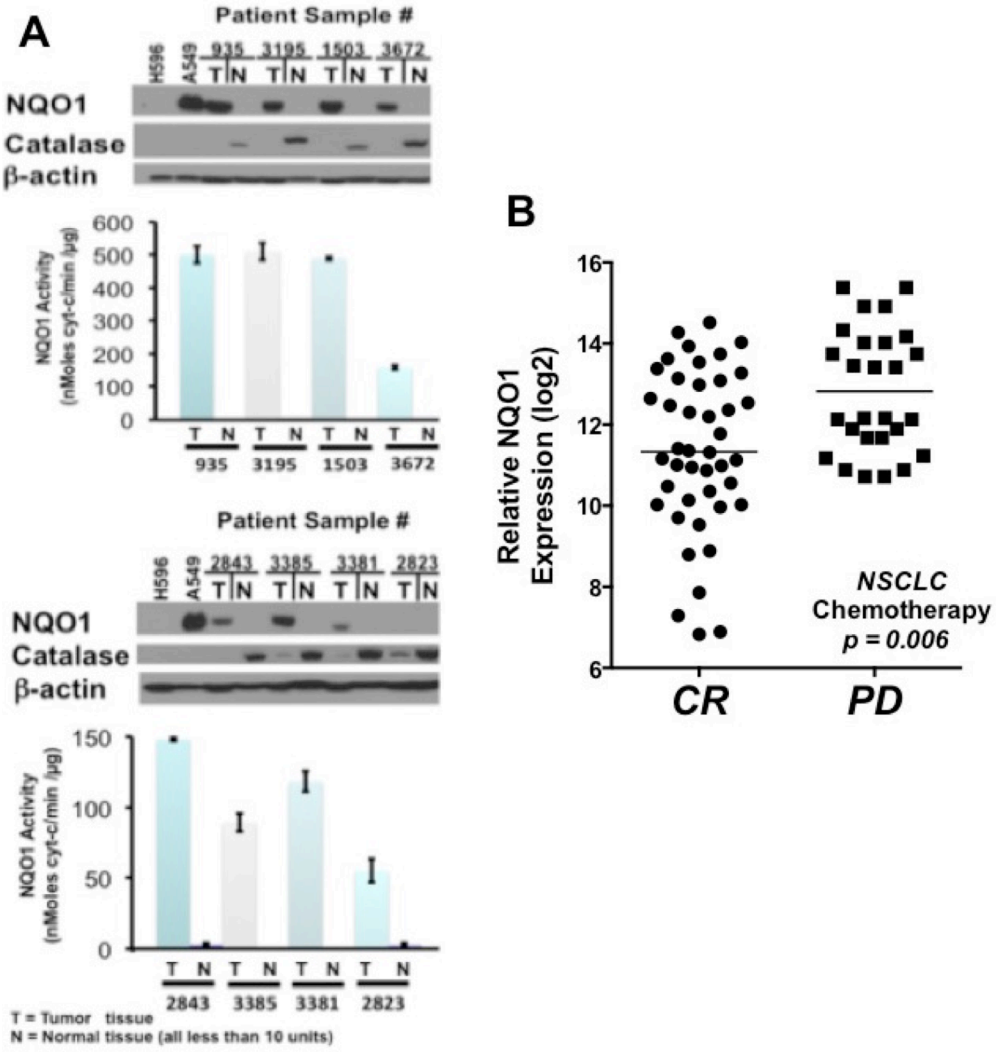

Figure 3-3. NQO1 protein level and enzyme activity is elevated in NSCLC tumor tissue and is associated with treatment-resistant disease. A) Western blots for NQO1 and catalase were performed on NSCLC tumor and associated normal patient samples. NQO1 enzyme assays confirmed high NQO1 activity in tumor tissue samples. **B)** NQO1 expression data from NSCLC patients before chemotherapy was divided into two groups: those who experienced a complete response (CR) and those who exhibited progressive disease (PD) despite treatment. Mean NQO1 expression was higher in patients that did not respond to chemotherapy (p = .006).

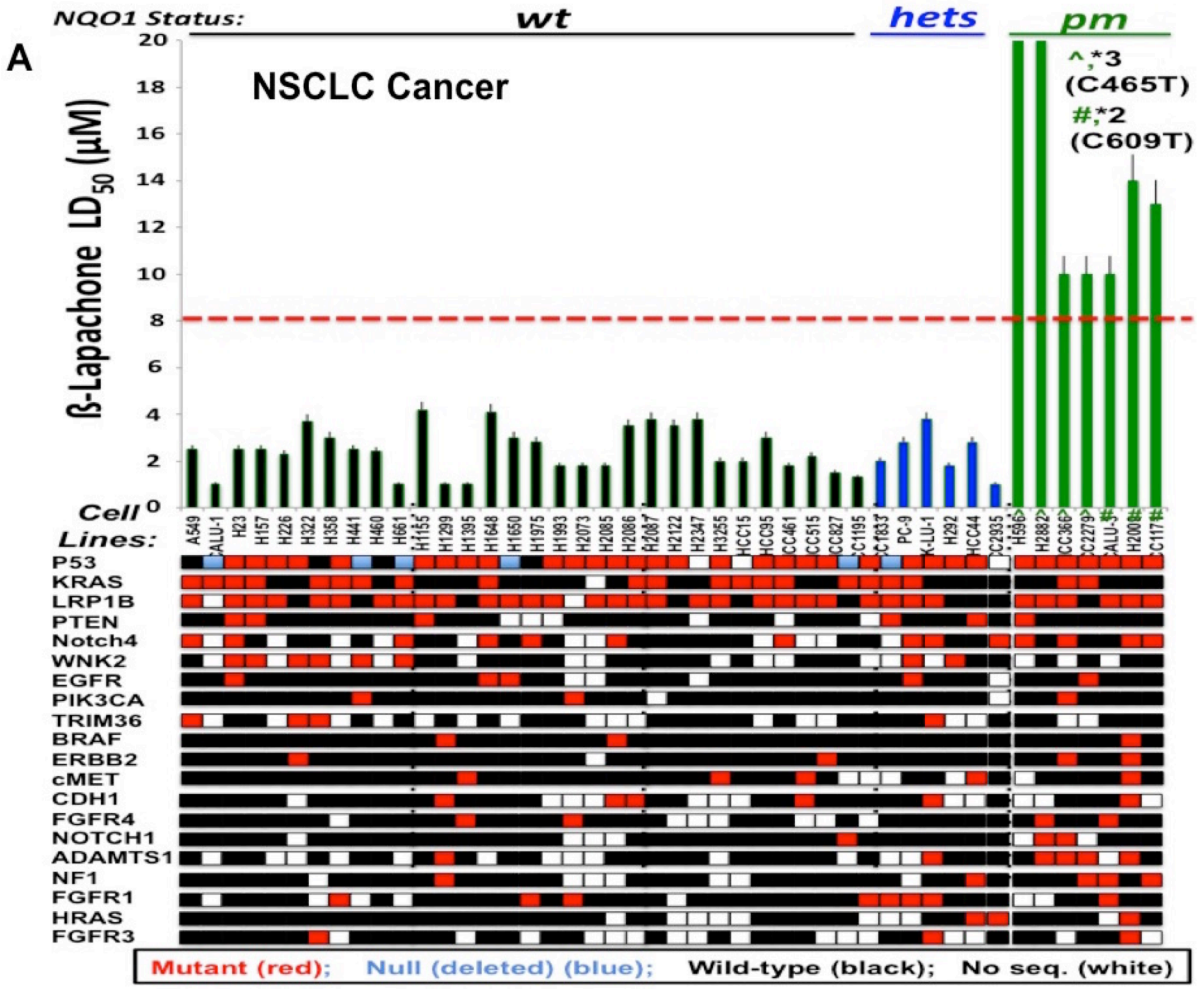

Figure 3-4. ß-lap sensitivity is dependent only on NQO1 status in NSCLC and not on any other known mutation profile. A) A panel of NSCLC cell lines is shown based on the status of common NQO1 polymorphisms detected by SNP analysis (wt (wild-type): no *2(C609T) or *3 (C465T) polymorphisms, hets: wt and *2 or *3 polymorphism-containing alleles present, pm: only *2 or *3 polymorphic alleles detected (no wild-type allele). The sensitivity to ß-lap (LD_{50} in µM) is ~4 or less when at least at least one copy of wt NQO1 is present, but is $\geq$ 10 µM when no wild-type NQO1 sequence is present. Other known mutations in these cells lines are listed in the grid below (red: mutant, blue: null (deletion), black: wild-type, white: no sequence available). ß-lap sensitivity assays were repeated three times and calculated LD_{50} values were averaged and plotted +/- SD.

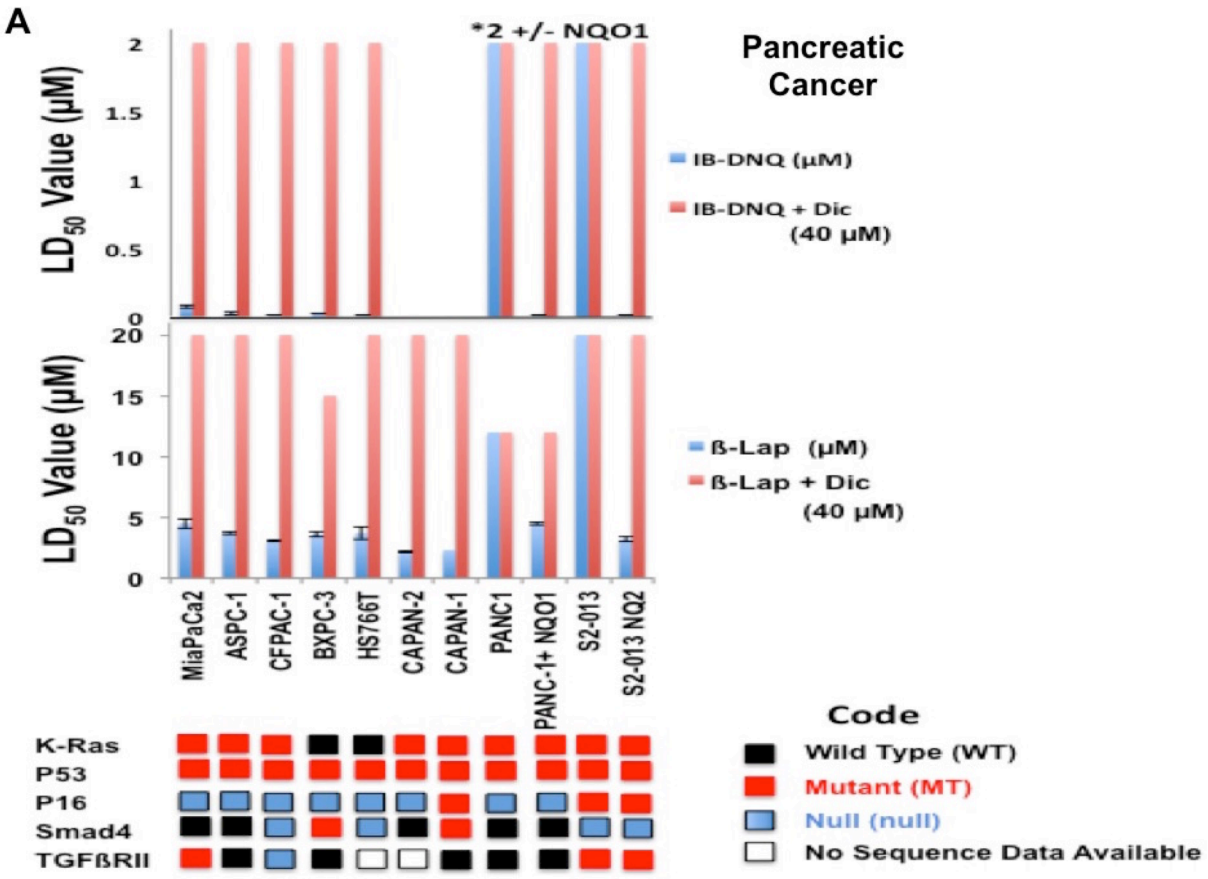

Figure 3-5. ß-lap sensitivity is dependent on NQO1 status in PDA and is not affected by other mutations. A) The sensitivity to ß-lap and IB-DNQ is shown in a panel of PDA cell lines based on the status of common NQO1 polymorphisms detected by SNP analysis (all cell lines express functional NQO1 except PANC1 and S2013, which are homozygous for the *2(C609T) polymorphism and were corrected for NQO1 expression with a CMV-NQO1 vector). The sensitivity to ß-lap (LD_{50} in µM) is ~4 or less when at least at least one copy of wt NQO1 is present, but is $\geq$ 10 µM when no wild-type NQO1 sequence is present. Other known mutations in these cells lines are listed in the grid below (red: mutant, blue: null (deletion), black: wild-type, white: no sequence available). Sensitivity assays were repeated three times and calculated LD_{50} values were averaged and plotted +/- SD.

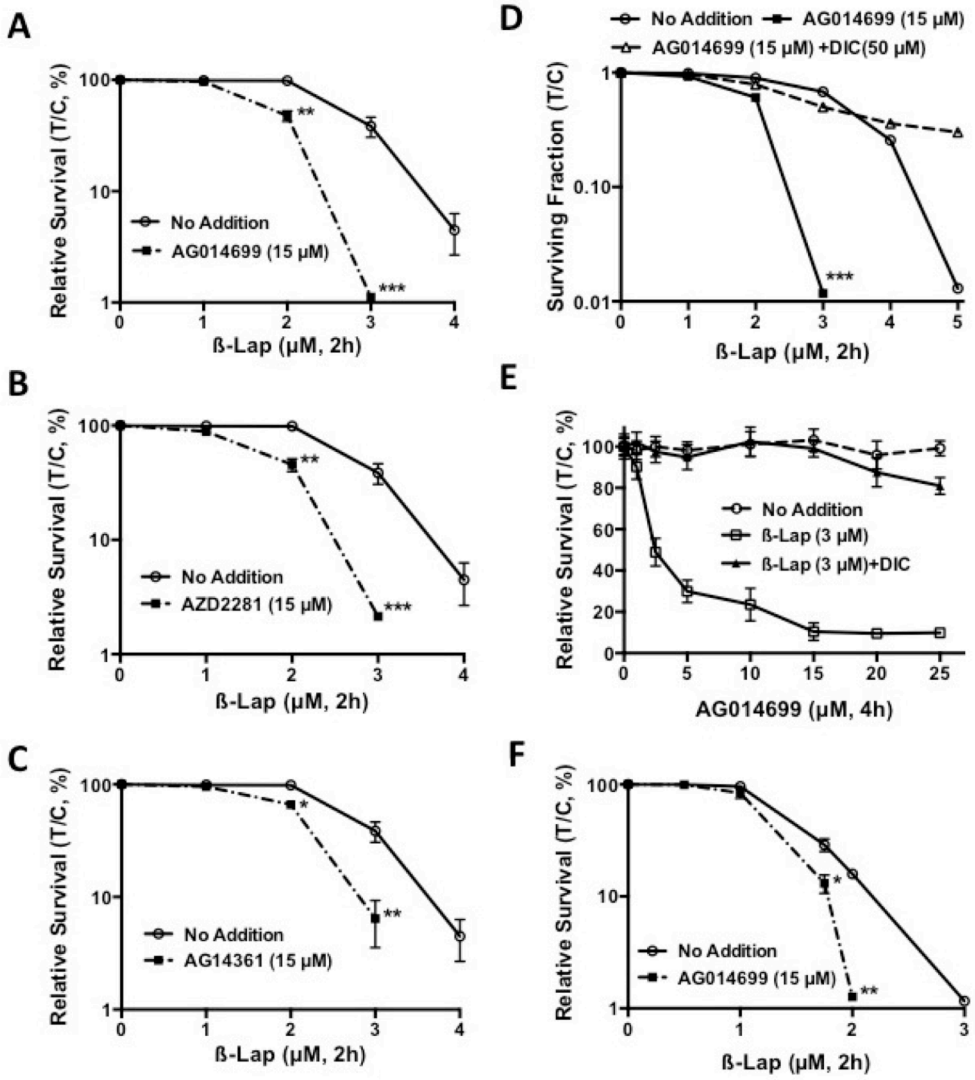

Figure 3-6. PARP inhibitors exhibit synergy with low doses of ß-lap. A549 cells were pretreated with **(A)** AG014699 **(B)** AZD2281 **(C)** AG14361 at 15 μM for 2 h followed by co-treatment with ß-lap at the indicated doses for 2 h. Both drugs were then removed and total DNA was measured 7 days later. **(D)** Cells were treated with AG014699 and ß-lap with or without dicoumarol (DIC) in a colony formation assay. **E**) A549 cells were pre-treated 2 h with various doses of AG014699 followed by co-treatment with a single dose of ß-lap (3 μM) for a total treatment time of 4 h. Total DNA was measured 7 days later. **F)** AG014699 and ß-lap also synergized in MCF7 cells. Results are representative of experiments repeated at least three times.

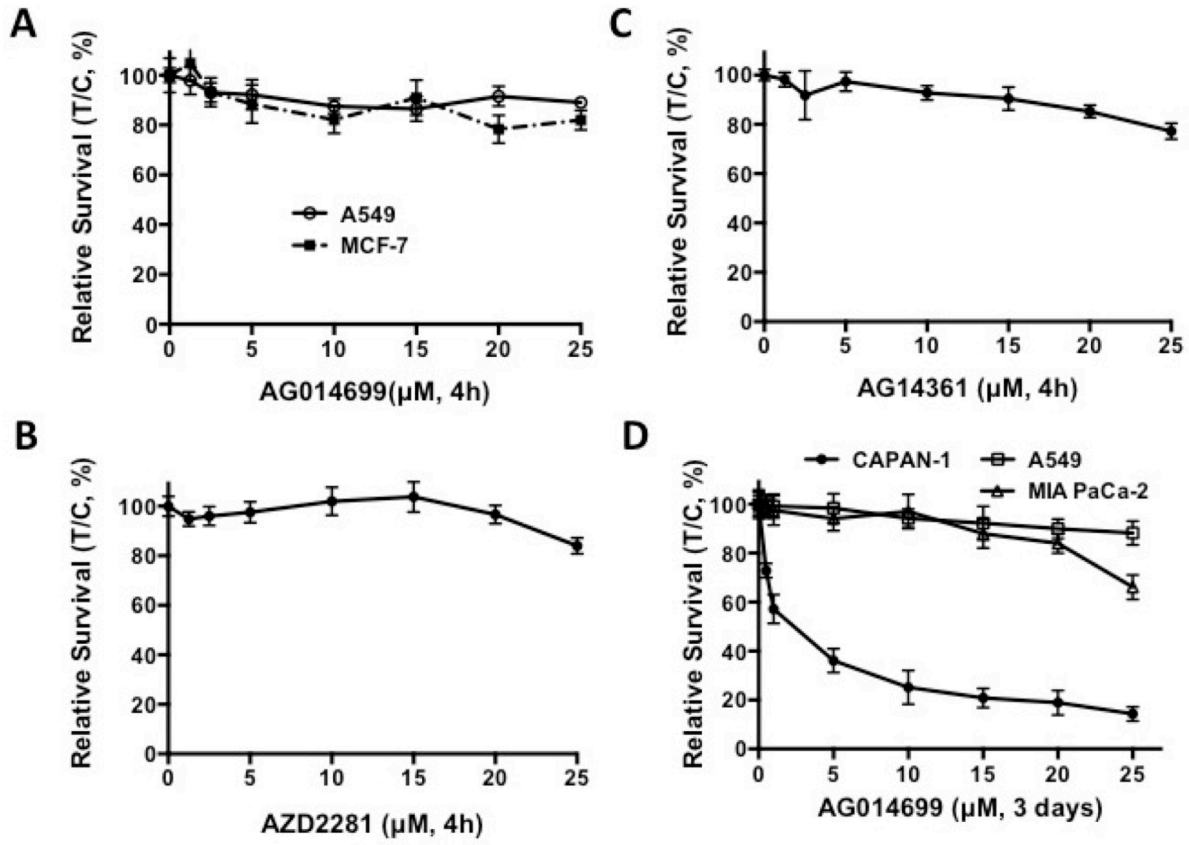

Figure 3-7. PARP inhibitors are not toxic to cells without BRCA mutations in single agent treatment A) A549 and MCF7 cells were treated with AG014699 for 4 h and assayed for survival 7 days later. **B)** PARP inhibitors AZD2281 and **(C)** AG14361 also did not significantly decrease survival of A549 cells after a 4 h treatment. **D)** Long-term (3 day) treatment with AG014699 reduced survival in BRCA2-mutant CAPAN-1 cells but not in A549 or MiaPaca2. Assays were repeated three times and results are plotted as mean +/- SD.

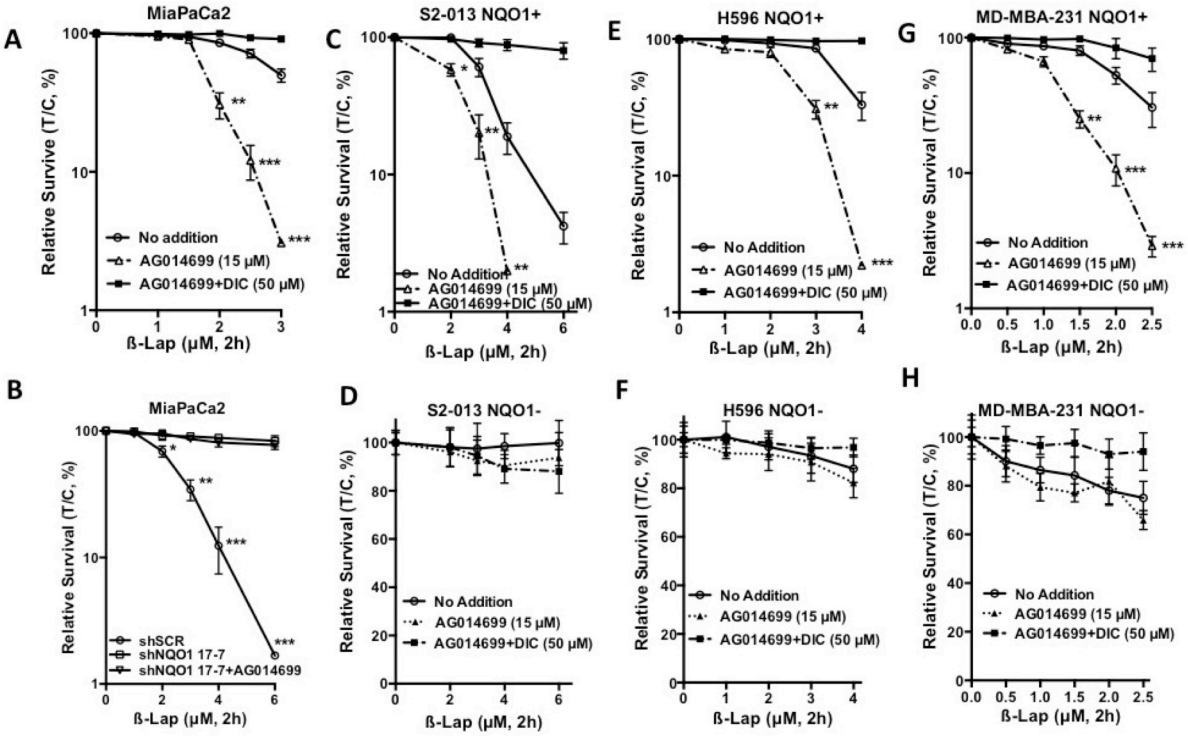

Figure 3-8. Synergy between ß-lap and PARP inhibitors occurs with NQO1 specificity in a variety of tumor cell lines. A) Synergy between ß-lap and AG014699 was blocked by dicoumarol and **(B)** by stable knockdown of NQO1. **C)** S2013 cells with a CMV-NQO1 overexpression vector were sensitive to ß-lap and exhibited synergy with AG014699. **D)** S2013 cells with an empty expression vector do not have a wild-type NQO1 allele and were not sensitive to ß-lap or combination treatment. **E)** NQO1 was overexpressed in H596 NSCLC cells followed by treatment with AG014699 and ß-lap with or without dicoumarol. **F)** H596 cells containing an empty expression vector do not express NQO1 and were resistant to treatment. **G)** NQO1 was overexpressed in MDA-MB-231 TNBC cells and they were treated with AG014699 and ß-lap with or without Dic. **H)** MDA-MB-231 cells containing an empty expression vector do not express NQO1 and were resistant to treatment.

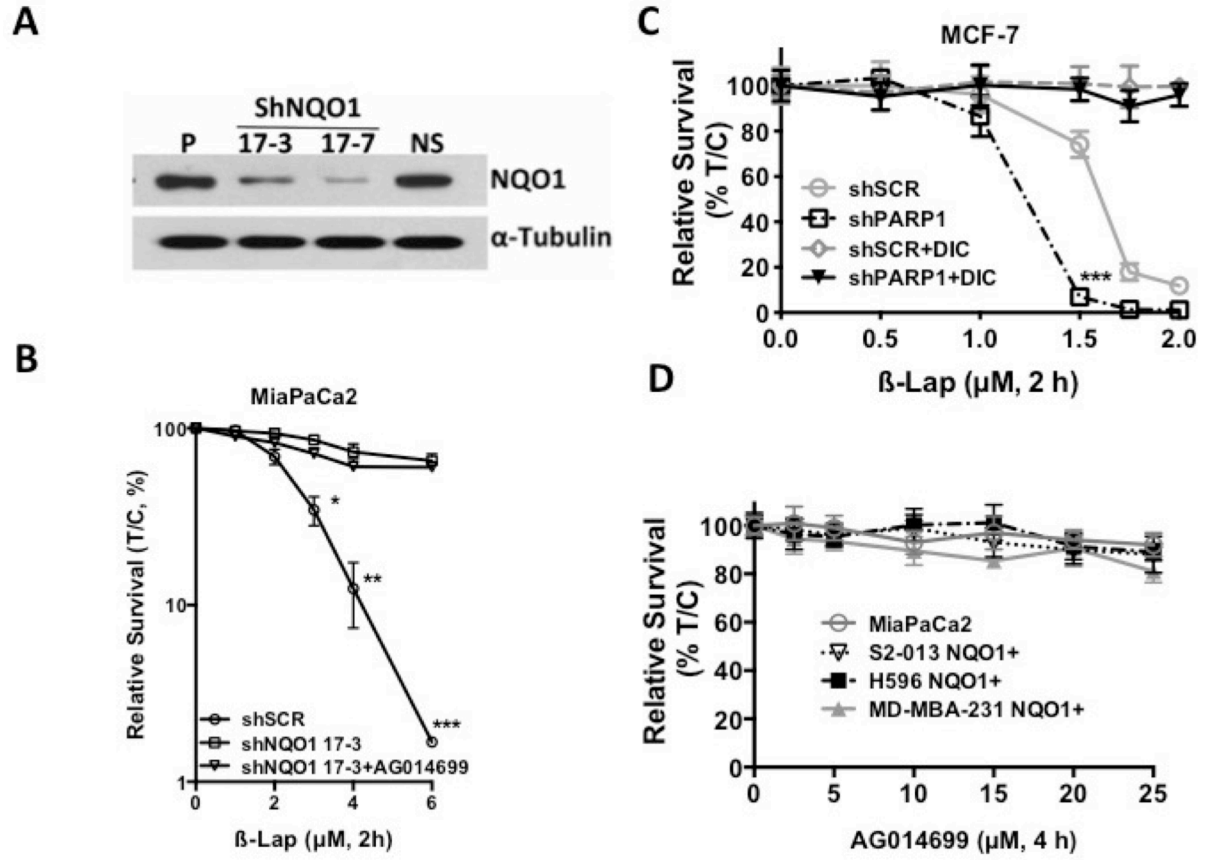

Figure 3-9. Genetic depletion of NQO1 prevents synergy, and PARP1 depletion synergizes with ß-lap. A) NQO1 protein level in clones of stable shRNA knockdown in MiaPaca2. **B)** An alternative stable PARP1 knockdown clone of MiaPaca2 cells also failed to exhibit synergy with PARP1 inhibition, as in '**3-9B**'. **C)** Stable PARP1 depletion with shRNA in MCF-7 increased ß-lap sensitivity. **D)** NQO1 overexpression in NQO1 deficient (homozygous NQO1*2 polymorphic) cell lines did not result in sensitivity to single agent AG014699

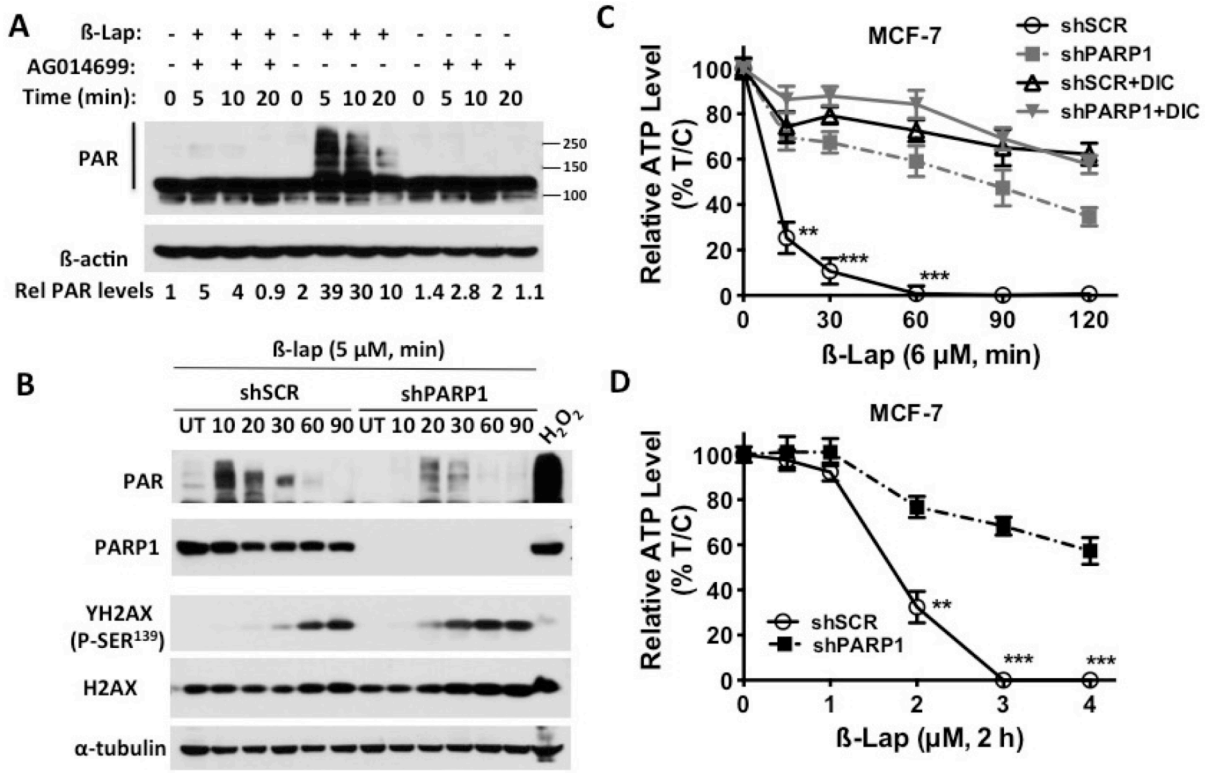

Figure 3-10. PARP inhibition abrogates PAR formation and ATP depletion with ß-lap treatment. **A)** ß-lap (5 µM) was added to A549 cells pretreated with AG014699 for co-treatment at the indicated times. PARP1 activity was evident in the formation of PAR, which occurred with ß-lap treatment but was blocked by dicoumarol and AG014699. **B)** Stable knockdown of PARP1 in MCF-7 cells with shRNA also blocked PAR formation caused by ß-lap and resulted in more rapid γH2AX induction **C)** ATP levels were measured at indicated times during ß-lap treatment in shSCR and shPARP1 transfected MCF-7 cells with or without dicoumarol. **D)** ATP levels were measured after 2 h of treatment at the indicated doses of ß-lap. Results are representative of experiments performed at least three times.

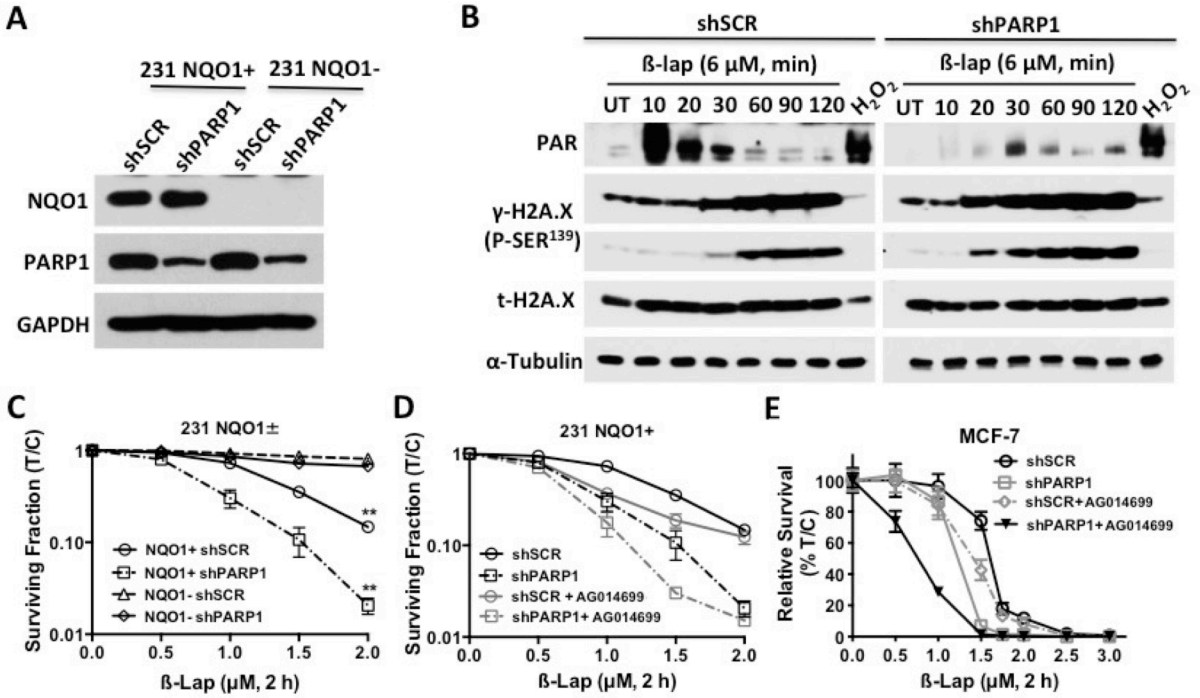

Figure 3-11. PARP depletion prevents PAR formation, enhances γH2AX induction, and synergizes with ß-lap in other cancer cell lines. **A)** Stable knockdown of PARP1 decreased PARP1 protein levels in both MDA-MB-231 NQO1- and NQO1+ cells. **B)** PARP1 depletion prevented PAR formation and resulted in earlier γH2AX induction with ß-lap treatment in MDA-MD-231 NQO1+ cells. **C)** PARP1 depletion synergized with ß-lap in MDA-MB-231 NQO1+ cells but not in NQO1- 231 cells **D)** Combining shRNA mediated PARP1 depletion and AG014699 mediated PARP1 inhibition resulted in increased ß-lap synergy in both MDA-MB-231 NQO1+ and **(E)** MCF7 cells since neither technique fully abrogated PARP1 activity independently.

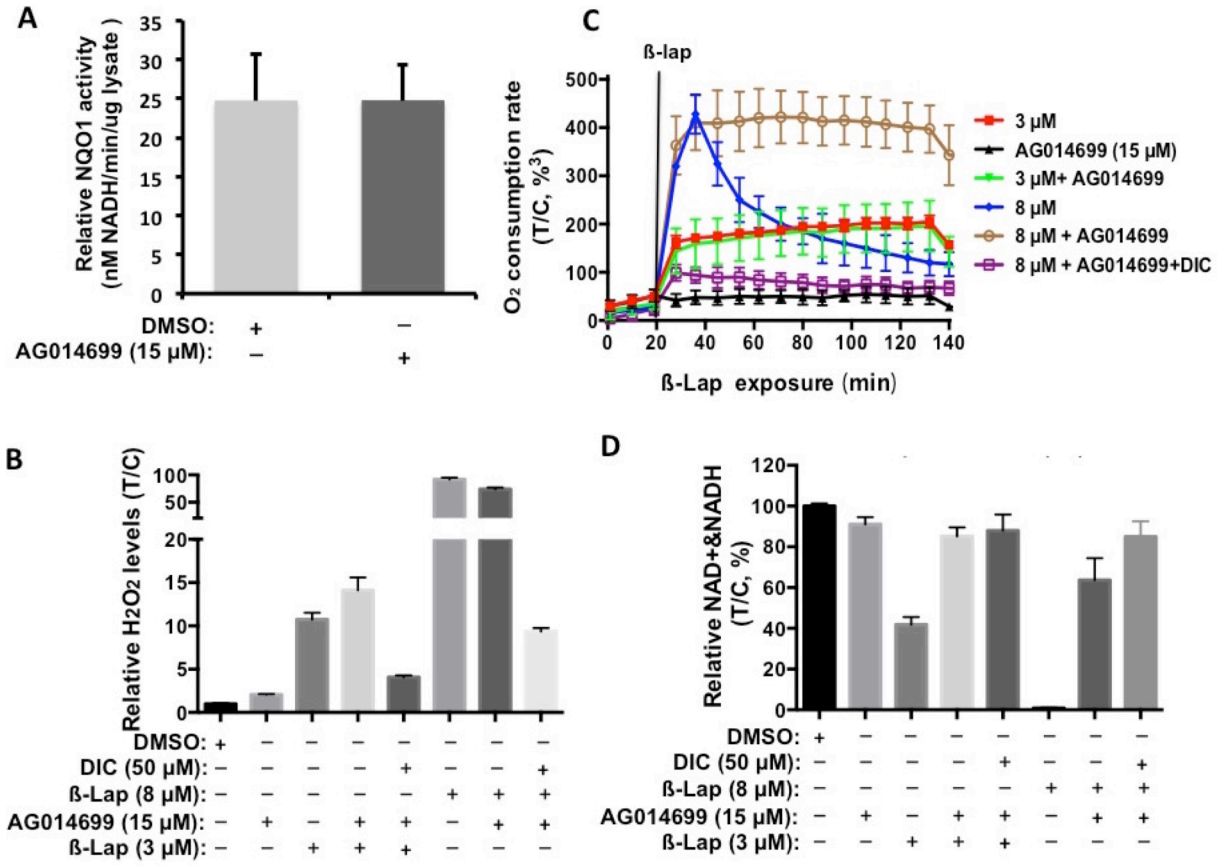

Figure 3-12. PARP inhibition does not affect NQO1 activity and co-treatment generates similar ROS levels at low doses of ß-lap. A) NQO1 activity assays were performed with lysates after A549 cells were treated for 2 h with DMSO or AG014699. **B)** H_2O_2 levels were measured over 2 h treatments with AG014699 and ß-lap at synergy doses (3 μM) or supralethal doses (8 μM) of ß-lap. **C)** Real time oxygen consumption caused by the NQO1 mediated futile cycle with ß-lap was measured with the Seahorse XF following 2 h pre-treatment with AG014699 and ß-lap addition at t=20 min. **D)** Total NAD^+ and NADH levels were measured after pre-treatment with AG014699 and co-treatment with ß-lap. Results are representative of experiments repeated at least two times.

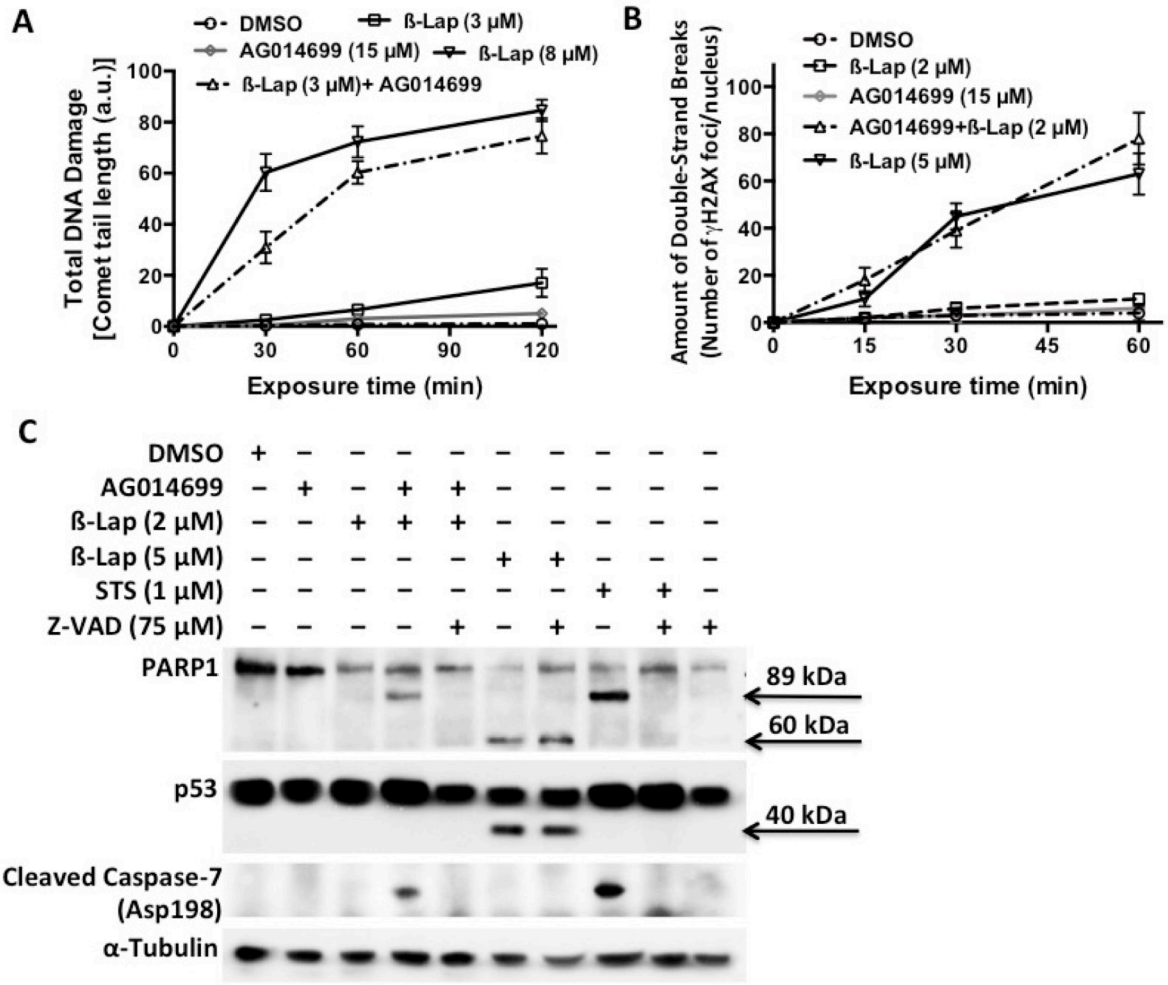

Figure 3-13. Combination treatment with AG014699 and ß-lap results in more DSBs and a switch from NAD⁺-Keresis to caspase-mediated apoptosis. A) Total DNA damage was measured with alkaline comet assays after single agent or combination treatment with AG014699 and ß-lap. **B)** The response to DNA double strand breaks was quantified by immunofluorescence for γH2AX foci after the indicated ß-lap or combination treatment times. **C)** After pre-treating cells with or without AG014699 for 2 h, ß-lap was added for a 2 hr co-treatment and then replaced with fresh media. After 24 h, lysates were processed for SDS-PAGE, and membranes were probed for PARP1, p53, caspase 7, or tubulin. Caspase-mediated PARP1 cleavage (89 kDa) occurred during apoptosis, as shown in the staurosporine (STS) treated control, and was blocked by the pan-caspase inhibitor Z-VAD. High doses of ß-lap induced NAD⁺-Keresis, which resulted in atypical cleavage of PARP1 (60 kDa) and p53, which was not blocked by Z-VAD.

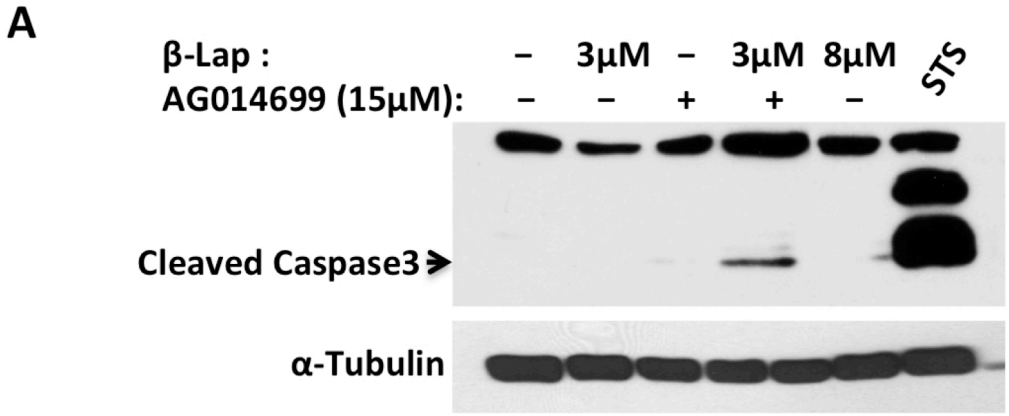

Figure 3-14. Confirmation of alternative death mechanism in combination treated cancer cells. A) Activation of caspase-3 as indicated by its cleavage, which occurred in STS treated and ß-lap + AG014699 treated A549 cells, but not after treatment with a lethal dose of ß-lap alone.

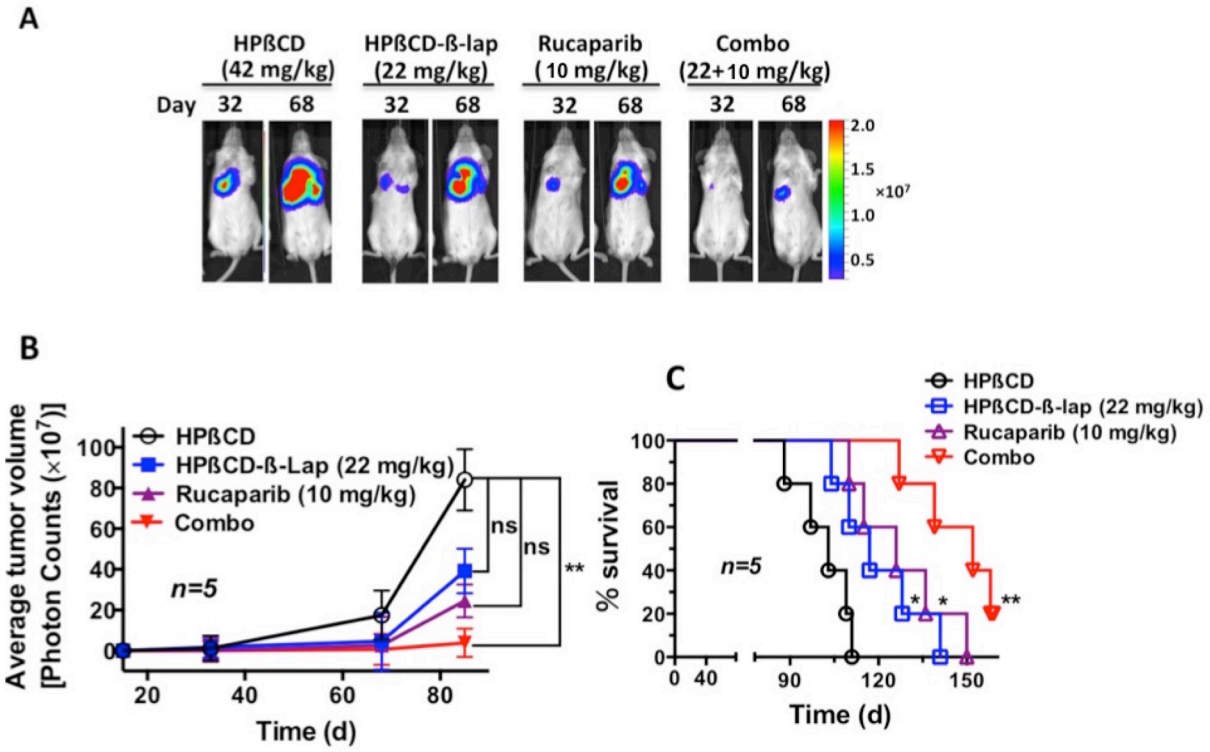

Figure 3-15. ß-lap and AG014699 (rucaparib) increased survival and decreased tumor growth in mice. Female NOD/SCID Mice were injected with A549 luciferase-expressing cells I.V. to establish orthotopic tumors in the lung. Starting on day 8 after injection, mice were treated every other day with ß-lap (22 mg/kg) or HPßCD vehicle alone for a total of 5 injections. **A**) Luciferase-expressing A549 tumors were imaged by BLI on day 32 and 68 after tumor cell injection following treatment with ß-lap, rucaparib, both drugs, or vehicle alone as described in the methods. **B)** Quantification of BLI signal intensity demonstrated a significant reduction in tumor burden in combination treated mice. **C)** Overall survival was improved in both single agent treatment groups, but a significantly greater advantage was observed in mice receiving both ß-lap and rucaparib in combination.

Chapter 4
NQO1 elevation in atypical teratoid rhabdoid tumors (ATRT) is susceptible to targeting with NQO1 bioactivatable therapeutics

4.1 Notes and Acknowledgements

The following chapter was adapted from a manuscript in preparation for submission. Sarai Stuart performed immunohistochemistry (IHC), culture of ATRT cell lines, and ß-lap sensitivity DNA assays. Dr. Dinesh Rakheja provided ATRT cell lines and analyzed IHC staining. Dr. Farjana Fattah performed NQO1 SNP analysis. Agnieszka Cholka performed *in vivo* tumor growth experiments including ß-lap treatments for efficacy and pharmacodynamics. I completed all other experiments, data analysis, figure preparation, and manuscript composition.

4.2 Abstract

Atypical teratoid rhabdoid tumors (ATRTs) are aggressive malignant neoplasms that most commonly occur in the CNS of children less than 3 years of age. Despite intensive chemoradiotherapy and surgery, the outcomes for patients with this disease remain dismal, with approximately 75% of patients dying at a median of 10 months after diagnosis. Therefore, it is critical to identify and validate novel ATRT targets for new therapies. The enzyme NAD(P)H:quinone oxidoreductase 1 (NQO1) is highly expressed in ATRTs, leading to the prediction that ATRTs will be vulnerable to drugs, such as ß-lapachone (ß-lap), that selectively kill NQO1-expressing cells. A panel of ATRT cell lines exhibited overall high NQO1 expression and low micromolar sensitivity

to ß-lap, with the exception of cell lines that were homozygous for the C609T NQO1 polymorphism, which exhibited no NQO1 activity and were generally resistant to ß-lap treatment. A two-hour pulse with ß-lap caused a burst of ROS-mediated DNA damage and PARP1 hyperactivation, resulting in NAD^+ and ATP depletion and caspase-independent, μ-calpain mediated apoptosis. Co-treatment with dicoumarol, a specific inhibitor of NQO1, prevented all of these effects by blocking the bioactivation of ß-lap. Low expression of NQO1 in normal brain tissue suggests a wide therapeutic window for ß-lap. These findings encourage the continued study of ß-lap and other NQO1 bioactivated therapeutics for the treatment of this recalcitrant disease

4.3 Introduction

Atypical teratoid rhabdoid tumors (ATRTs) are rare but malignant and highly invasive neoplasms that typically occur in young children (Burger et al., 1998; Rorke, Packer, & Biegel, 1995). Despite surgery and chemotherapy, ATRT has a poor prognosis: the three-year overall survival is only 22% and the median survival is 1.2 years (von Hoff et al., 2011). ATRT is a subset of malignant rhabdoid tumors (MRT), which may also occur in the kidney or soft tissue and share similar histological and genomic characteristics (Roberts & Biegel, 2009). Notably, virtually all ATRT and MRT tumors exhibit biallelic loss of INI1/SNF5/SMARCB1, a component of the SWI/SNF chromatin remodeling complex (Biegel et al., 2002; Biegel et al., 1999; Roberts & Biegel, 2009).

SWI/SNF complexes are large (~1.14 MDa) and composed of 9-12 subunits that utilize energy from ATP hydrolysis to modify chromatin structure (Cairns, Kim, Sayre,

Laurent, & Kornberg, 1994; Smith, Horowitz-Scherer, Flanagan, Woodcock, & Peterson, 2003; Wilson & Roberts, 2011). In contrast to covalent methylation and acetylation of histones and DNA, SWI/SNF slides DNA around histones and can also eject histones to influence higher order chromatin structure and accessibility for transcription factors (Saha, Wittmeyer, & Cairns, 2006a, 2006b). In yeast, the SWI/SNF complex contributes to the regulation of 5% of the genome, and can function to either increase or decrease transcription of targets based on variations in SWI/SNF subunit composition, interactions with transcription factors, and associations with other chromatin-modifying proteins like HDACs (Sudarsanam, Iyer, Brown, & Winston, 2000; Wilson & Roberts, 2011).

INI1 (integrase interactor-1, also known as SNF5 or SMARCB1) was originally named in humans for its role in promoting genomic integration of HIV-1 DNA via interaction with retroviral integrase (Kalpana, Marmon, Wang, Crabtree, & Goff, 1994). The biochemical function of INI1 within the SWI/SNF complex is difficult to determine due to its low sequence homology with other proteins, but it is thought to be an integral component since it is present in all characterized SWI/SNF complexes and is highly conserved (Smith et al., 2003; Wilson & Roberts, 2011). Homozygous knockout of INI1 is lethal early in embryonic development in mice, but heterozygous mice are prone to developing rhabdoid-like tumors similar to human ATRTs and MRTs (Roberts, Galusha, McMenamin, Fletcher, & Orkin, 2000). Furthermore, INI1 loss cooperates with p53 loss to drive rapid tumorigenesis with even higher penetrance (Isakoff et al., 2005). These findings, along with the cell cycle arrest and growth inhibition documented after INI1 re-expression in ATRT cells, have characterized INI1 as a tumor suppressor

obeying the two-hit hypothesis (McKenna et al., 2008; Roberts et al., 2000; Roberts, Leroux, Fleming, & Orkin, 2002).

The mechanism of carcinogenesis that occurs as a result of INI1 loss is not well understood, nor is the cell of origin in ATRT. Though there are some reports that loss of INI1 may interfere with the mitotic checkpoint or have effects on the DNA damage response (Ray et al., 2009; Vries et al., 2005), genetic and genomic analysis of ATRT tumors shows virtually no chromosomal abnormalities and an SNP profile that is almost indistinguishable from normal cells, besides alterations in chromosome 22 at the INI1 locus (Jackson et al., 2009; McKenna et al., 2008; Darmood Wei & Weissman, 2001). Rather than resulting from genomic instability, these tumors appear to arise due to altered gene expression caused by dysregulated epigenomic modifications. INI1 is important for expression of $P16^{ink4a}$ and to provide a functional pRB mediated G1/S cell cycle checkpoint; it is also directly involved in regulating the expression of myc target genes (Betz, Strobeck, Reisman, Knudsen, & Weissman, 2002; S. W. Cheng et al., 1999; Roberts & Biegel, 2009). The SWI/SNF complex is still functional after INI1 loss, but appears to drive expression of genes associated with stem cells as opposed to differentiation, so altered SWI/SNF complex composition and modified transcription factor interactions likely play a role in ATRT carcinogenesis (Doan et al., 2004; D. Wei et al., 2014).

The lack of classic oncogene and tumor suppressor signatures has made tumor-specific therapy for ATRT difficult to develop. Since these cancers are thought to develop through modulation of chromatin structure, one strategy is to use therapeutics that can affect the epigenetic landscape of cancer cells, such as histone

methyltransferase inhibitors and histone deacetylase inhibitors (Knipstein et al., 2012; Knutson et al., 2013; Watanabe et al., 2009). However, the complexity of epigenetic regulation and potential effects of these inhibitors on normal cells are not well understood. Gene expression analysis has been performed on ATRT and other MRT tumors to identify potential biomarkers and treatment targets, revealing that NQO1 was elevated in MRT relative to other pediatric cancers (Gadd, Sredni, Huang, Perlman, & Renal Tumor Committee of the Children's Oncology, 2010; C. C. Huang et al., 2006).

The results in this chapter show substantial elevation of NQO1 in ATRT tumor samples and cell lines versus normal tissue. NQO1 elevation in ATRT makes it an excellent candidate for treatment with NQO1-bioactivated drugs, such as ß-lap, which engage in a futile redox cycle with NQO1 to rapidly deplete ATP and NAD(H) and induce severe DNA damage in a tumor-specific fashion (Bey et al., 2013; Li et al., 2011; Pink, Planchon, et al., 2000). NQO1-bioactivated drugs are highly effective in killing ATRT cells *in vitro* and *in vivo*. ß-lap (ARQ761) is currently in phase I clinical trials for late stage solid tumors in adults, and these findings suggest that further preclinical and clinical characterization of these drugs in pediatric patients may provide a much-needed effective treatment option for ATRT (Gerber et al.).

4.4 Results

NQO1 expression is elevated in ATRT. Analysis of NQO1 mRNA expression levels in ATRT patient samples showed significant elevation of NQO1 relative to both normal brain and glioma, in which high NQO1 expression was not observed (**Figure 4-1A**). These findings were supported at the protein level by staining ATRT patient tissue and

normal pediatric brain tissue for NQO1 by immunohistochemistry (IHC). Dark cytoplasmic staining in cancer cells was observed with virtually no staining present in normal brain cells (**Figure 4-1B**).

ATRT cell lines exhibit high NQO1 protein level and enzyme activity. Cell lines derived from ATRT tumors were tested for NQO1 enzyme activity levels based on dicoumarol-inhibited reduction of menadione in whole-cell lysates (**Figure 4-2A**). NQO1 activity varied substantially between cell lines but was generally elevated with a few exceptions. CHLA-266 and CMC1073-RT exhibited virtually no NQO1 activity, so restriction fragment length polymorphism analysis was performed to identify the two most common NQO1 polymorphisms, NQO1*2 and NQO1*3. Both of these SNPs lead to a lack of NQO1 enzyme activity due to either a truncated or inactive enzyme. However, only homozygosity at the NQO1*2 loci was associated with loss of NQO1 activity, which was the case for both CHLA-266 and CMC1073-RT (**Figure 4-2A**). NQO1 activity values are plotted in **Figure 4-2B**. Protein levels of NQO1 were in agreement with enzyme activity findings (**Figure 4-2C**).

ß-Lap sensitivity is NQO1 dependent in ATRT. ATRT cell lines were tested for ß-lap sensitivity in long-term DNA content assays after 2 h treatments with ß-lap. NQO1 positive CHLA-69 (**Figure 4-3A**) and BT-12 (**Figure 4-3B**) cells exhibited sensitivity to ß-lap with LD50 values below 4 μM. Co-treatment with dicoumarol, a specific small molecule inhibitor of NQO1, protected cells from ß-lap treatment. A panel of ATRT cell

lines exhibited similar sensitivity to ß-lap, with LD50s in the 3.1-6.2 μM range in cells with elevated NQO1 expression (**Figure 4-3C**). Treatment time required for maximum ß-lap-induced cell kill was found to be 2 h, with longer treatments failing to induce additional cell death at lethal doses (**Figure 4-3D**). Two notable exceptions to the NQO1 specificity described above were observed in this panel of cell lines. First, CHLA-07 was found to be resistant to ß-lap despite the absence of homozygous NQO1 polymorphisms (**Figures 4-2A, 4-3C**). However, the NQO1 enzyme activity in CHLA-07 is relatively low, likely below the threshold required for efficiently catalyzing the futile cycle with ß-lap. Additionally, CHLA-266, which is homozygous for the NQO1*2 polymorphism and does not express functional NQO1 (**Figure 4-2**) was sensitive to ß-lap. This cell line also exhibited hypersensitivity to H_2O_2 (**Figure 4-3E**) and was not substantially spared from ß-lap with dicoumarol co-treatment (**Figure 4-3C**), suggesting that CHLA-266 may have increased susceptibility to the low levels of ROS generated by ß-lap through non-NQO1 mediated mechanisms.

Other NQO1-bioactivated drugs are also effective against ATRT cells. GB59 is a ß-lap derivative that was more effective at lower doses than ß-lap (**Figure 4-4A**). Similarly, GB153 is a variant of GB59 with increased water solubility and also shows efficacy against BT-12, with NQO1 specificity demonstrated with dicoumarol rescue (**Figure 4-4B**). However, sensitivity to both of these compounds was not rescued with dicoumarol to the same extent compared to high doses of ß-lap with dicoumarol, suggesting that either non-NQO1 dependent mechanisms may contribute to cell death

or that dicoumarol does not completely block the NQO1-mediated futile cycle with these compounds.

Induced NQO1 overexpression supports the NQO1 specificity of ß-lap in ATRT. CHLA-07 cells, which express low NQO1 levels and are not sensitive to ß-lap, were transfected with a CMV driven NQO1 expression vector (**Figure 4-5A**). ATP depletion was observed after a 2h ß-lap treatment to a greater extent in cells transfected with NQO1 compared to the empty vector, and could be blocked with dicoumarol, further supporting NQO1 specificity (**Figure 4-5B**). The statistically significant increase in ATP depletion at 6μM ß-lap with NOQ1 overexpression is shown in **Figure 4-5C**.

Acute NAD^+ and ATP depletion occurs following ß-lap treatment. Both BT-12 and CHLA-69 cells exhibited substantial depletion of NAD^+ and NADH in a dose-dependent manner after only 2 h of ß-lap treatment (**Figures 4-6A, 4-6B**). NAD^+ depletion was a result of PARP1 hyperactivation and occurred with NQO1 specificity, since it was completely blocked by co-treatment with dicoumarol. ATP depletion also occurred after 2 h ß-lap treatment, likely a result of the inability of cells to maintain normal metabolism under conditions of substantial NAD(H) restriction (**Figure 4-6C, 4-6D**). However, though the depletion of ATP mirrored NAD(H) in CHLA-69, BT-12 cells showed substantially less ATP depletion, despite similar levels of cell death observed in long-term assays.

Rapid PARP1 hyperactivation, delayed DSBs, and caspase-independent cell death occur with ß-lap treatment. During ß-lap treatment, large molecular weight PAR formation occurred very rapidly (within 5 min), evidence of PARP1 hyperactivation in response to single strand breaks caused by ß-lap (**Figure 4-7A**). Rapid PARylation of PARP1 and depletion of NAD^+ inhibits further PARP1 activity, and residual PAR is removed by poly(ADP ribose) glycohydrase (PARG), seen by the loss of PAR after 15 minutes. Concomitant with the loss of PAR, single strand breaks were converted to double strand breaks, since SSB repair was inhibited by PARP1 hyperactivation. This resulted in the delayed formation of γH2AX in both BT-12 and CHLA-69 (**Figure 4-7A**). After 2 h ß-lap treatment, ATRT cells die within about 48 h. Caspase 7 cleavage was not observed during this cell death process, but μ-calpain cleavage did occur, in accordance with findings in other cell lines that ß-lap-induced cell death does not occur through canonical apoptosis, but NAD^+-Keresis, a form of programmed necrosis (**Figure 4-7B**) (Bey et al., 2007; Moore et al., 2015).

ATRT cells undergo cell cycle independent NAD^+-Keresis after ß-lap treatment. To confirm that cell death after ß-lap treatment was occurring through NAD^+-Keresis and not necrosis, I performed cell cycle analysis and terminal deoxynucleotidyl transferase nick end labeling (TUNEL) analysis on cells after treatment. Untreated cells exhibited a typical cycle distribution and had a low basal level of TUNEL positive staining (**Figure 4-8A**). After 48 h of ß-lap treatment, BT-12 cells experienced a marked increase in TUNEL positive cells in all phases of the cell cycle and a large sub-G1 cell cycle

population (**Figure 4-8B**). The increase in both TUNEL positive and sub-G1 cells was completely blocked by dicoumarol (**Figure 4-8C**). Furthermore, the time frame of cell death after treatment was evident in the increasing TUNEL positive and sub-G1 cells between 24 and 48 h (**Figure 4-8D**).

A notable feature of cell death induced by ß-lap is cell cycle independence. The cell cycle distribution before and after treatment is seen in **Figure 4-9A** and **Figure 4-9B**, respectively. After treatment, it is evident that cells from G1, S, and G2 are all contributing to the increase in the sub-G1 population, with wider, less distinct peaks as DNA content is lost. Dicoumarol prevented all changes in cell cycle distribution induced by ß-lap treatment (**Figure 4-9C**).

Application of NQO1-bioactivated therapeutics to an *in vivo* model of ATRT. BT-12 cells were established in subcutaneous tumors in athymic nude mice. Treatment of mice with 25 mg/kg of ß-lap in HPßCD vehicle yielded mean tumor sizes that were lower than vehicle treated tumors over time, but statistical significance was not achieved at any individual time point by Student's t tests (**Figure 4-10A**). Cells in these tumors nevertheless maintained an ATRT-like morphology and high NQO1 expression (**Figure 4-10B**). Analysis of PAR in tumor tissue at various time points after ß-lap injection demonstrated that PAR formation did occur but was delayed relative to previously reported pharmacodynamics, where PAR was visible at 30 minutes to 1 hour in orthotopic tumor models (**Figure 4-10C**) (Ma et al., 2015).

4.5 Discussion

Analysis of NQO1 levels and ß-lap sensitivity in ATRT patient samples and cell lines has revealed it to be a promising target for NQO1-bioactivated therapeutics. NQO1 expression was very high overall in tumor cell lines and patient samples relative to normal tissue, establishing a high therapeutic window. Furthermore, no NQO1 expression was observed in cases of homozygous NQO1*2 polymorphisms, which could serve as a good clinical predictor of ß-lap response. Sensitivity of cell lines to ß-lap falls into the range of other tumor cell types exhibiting NQO1 expression (Chapter 3), with LD50s in the range of 1-6 μM in NQO1 expressing cells. The level of NQO1 activity required for sensitivity in ATRT is between 150-250 units, as evidenced by the sensitivity of CHLA-69 but resistance of CHLA-07. A sharp cutoff in sensitivity, with virtually no sensitivity at lower NQO1 levels but no additional increase in sensitivity even at very high NQO1 levels, is characteristic of the futile cycle mechanism of ß-lap; once the ability of cells to neutralize ROS is saturated, the cell is rapidly overwhelmed with ROS and DNA damage (Li et al., 2011). The exception to the NQO1 requirement for ß-lap sensitivity, CHLA-266, did not exhibit rescue with dicoumarol and was also hypersensitive to H_2O_2, suggesting that this particular cell line lacks the ability to neutralize even nominal ROS stress. Further support for NQO1 specificity came from the findings that ß-lap sensitivity could be increased in CHLA-07 by overexpressing NQO1.

Other NQO1 bioactivatable drugs also show promise for treating ATRT. Cells were sensitive to both GB59 and GB153 with lower LD50s, but dicoumarol did not completely rescue toxicity at higher doses. This suggests that dicoumarol does not

completely block NQO1 from the futile cycle, which may occur if compounds have higher NQO1 affinity than ß-lap. This is likely the case for deoxyniboquinone in other cell lines (X. Huang et al., 2012). Alternatively, a mechanism of cell death independent of NQO1 may occur with these ß-lap derivatives, which will require further study to rule out. In either case, a wide therapeutic window still exists with these ß-lap derivatives at lower doses.

Despite the fact that the genetic landscape of ATRT cells is more similar to normal cells than typical cancers that exhibit genomic instability, ATRT cells respond to and die after ß-lap exposure through the same mechanism as other cancer cells. Rapid DNA damage induced PARP1 hyperactivation and PAR formation, resulting in substantial energy depletion and the conversion of single strand breaks to double strand breaks. NAD^+ and ATP depletion both occur within two hours. Though ATP depletion does not occur to the same extent in BT-12 as in CHLA-69, in both cases the levels of acute NAD^+ depletion follows the same dose response trend as the overall survival of cells, supporting the relationship between NAD^+ depletion and ß-lap induced cell death previously reported in other cell types (Bey et al., 2007; Moore et al., 2015). Cells died through NAD^+-Keresis, which was characterized by extensive TUNEL positive staining and reduction of DNA content, but μ-Calpain cleavage instead of caspase activation. Notably, death induced by ß-lap was independent of the cell cycle status of treated cells. Cells were only treated for a maximum of 4 hours, which is not enough time for cells to progress through each phase, but cells in all phases of the cell cycle became TUNEL positive and shifted toward the sub-G1 population.

In the context of *in vivo* application, ß-lap was not very effective in the subcutaneous ATRT model tested. Though the cancer cells retain high NQO1 levels when grown *in vivo*, delayed PAR formation relative to orthotopic models tested with ß-lap suggest that the issue is likely suboptimal drug delivery to a poorly vascularized subcutaneous tumor. This is consistent with previous findings that ß-lap was not effective in subcutaneous tumor models except at the highest tolerated doses, unless combined with other treatment modalities, such as ionizing radiation (Dong et al., 2010). ß-lap has shown much greater efficacy in other cancer models, so orthotopic ATRT models will be pursued for future study, since ß-lap can cross the blood-brain barrier (X. Huang et al., 2012; Li et al., 2011). More potent ß-lap derivatives, prodrugs, and micelles will also be used to increase *in vivo* efficacy (X. Huang et al., 2012; Ma et al., 2015; Reinicke et al., 2005).

In sum, ATRT is a cancer that shows early promise for targeting with NQO1-bioactivated therapeutics. The studies above establish substantial NQO1 activity in these cancer cells and high sensitivity to ß-lap. Further preclinical studies to optimize the efficacy of ß-lap and other NQO1-bioactivated drugs both as single agents and in combination with other synergistic treatment modalities will be pursued to advance clinical application of new treatment strategies for this rare but deadly disease.

Chapter 4 Figures

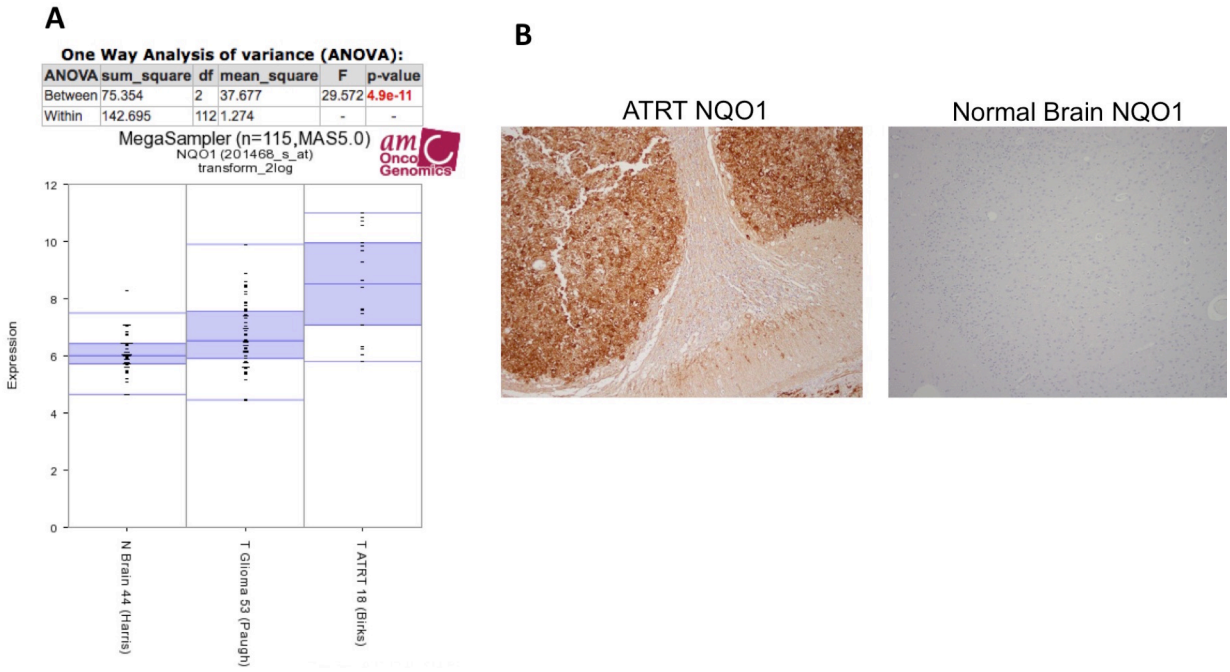

Figure 4-1. Overexpression of NQO1 in ATRT patient samples. A) Expression analysis performed in the R2 genomics analysis platform showed increased expression of NQO1 in ATRT samples compared to normal brain and glioma ($p=4.9x10^{-11}$). **B)** A representative tissue sample from a patient with ATRT exhibited high NQO1 in tumor tissue by IHC compared to normal pediatric brain tissue.

A

Cell line	*2 (609)	*3(465)	NQO1 Act.
CHLA-266	Hom	WT	18
CHLA-07	WT	WT	134
CHLA-69	Het	WT	236
CMC1383-RT	WT	WT	2040
CMC799-RT	Het	WT	1100
BT-12	WT	Het	2100
CMC935-RT	WT	WT	393
CMC958-RT	WT	WT	1360
CMC197-RT	WT	WT	967
CMC1025-RT	Het	WT	632
CMC1073-RT	Hom	WT	10

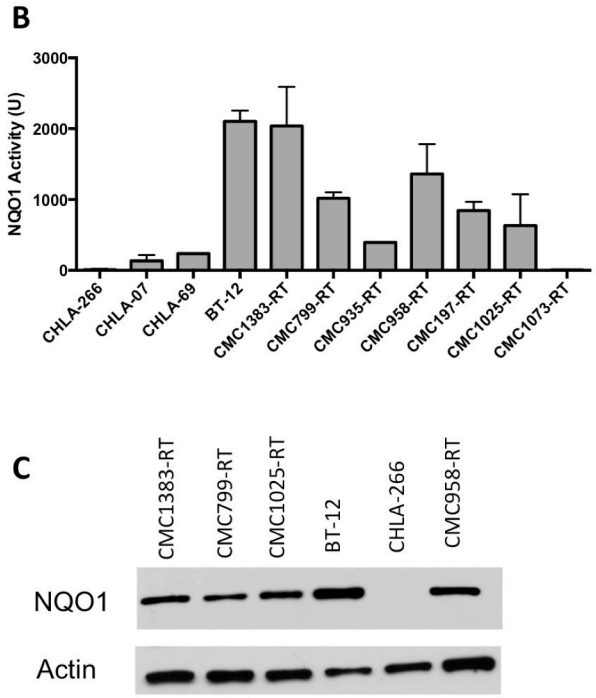

Figure 4-2. NQO1 overexpression is linked to SNP status and enzyme activity in ATRT cell lines. A) Analysis for *2 and *3 NQO1 SNPs, which both lead to loss of functional NQO1, was performed by RFLP. A panel of ATRT cell lines was classified based on whether they were wild type (WT), heterozygous (Het), or homozygous (Hom) for these two common NQO1 polymorphisms. Loss of NQO1 activity was associated with homozygous *2 polymorphisms. **B)** NQO1 enzyme activity assays were performed to quantify total NQO1 activity in cell lysates as described in the methods section. C) Western blots were used to compare relative NQO1 protein levels in ATRT cells.

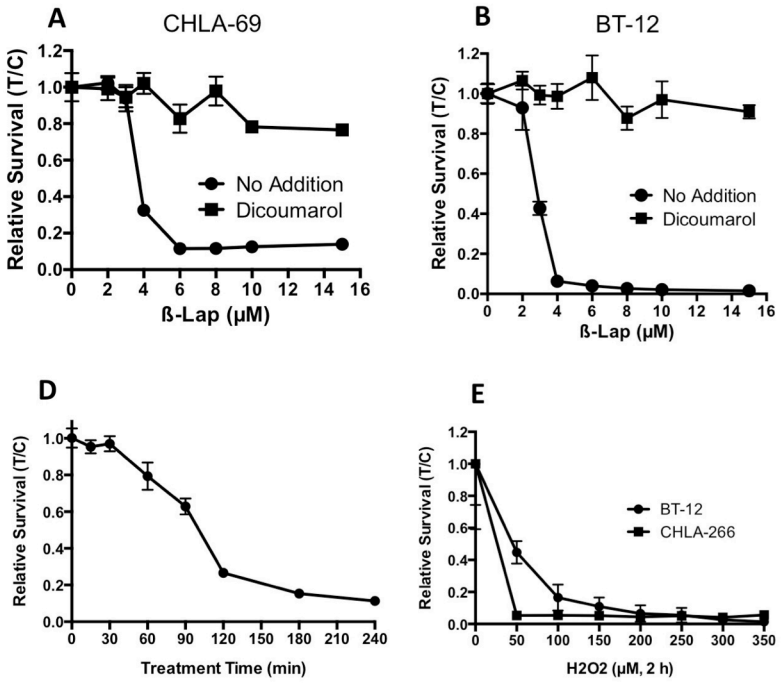

C

Cell line	ß-Lap LD50 (μM)	ß-Lap+ Dic LD50 (μM)
CHLA-266	1.6	3.2
CHLA-07	>15	>15
CHLA-69	3.8	>15
CMC1383-RT	3.4	>15
CMC799-RT	6.2	11
BT-12	3.1	>15
CMC935-RT	3.4	10
CMC958-RT	2.6	>15
CMC197-RT	3.8	>15
CMC1073-RT	>15	>15

Figure 4-3. NQO1 expression is associated with ß-lap sensitivity in ATRT. A) CHLA-69 and **(B)** BT-12 cells were tested for long-term survival after 2 h ß-lap exposure with total DNA quantification assays. Dicoumarol (50 μM) blocked NQO1 and abrogated ß-lap sensitivity. **C)** Analogous survival assays were completed with other ATRT cell lines and LD50s were calculated with and without dicoumarol addition. **D)** BT-12 cells were treated for various times with lethal doses of ß-lap (6 μM) followed by long-term survival assays. The minimum treatment time required to induce maximal cell death is ~2 h. **E)** CHLA-266, which exhibited NQO1-independent ß-lap sensitivity, also exhibited hypersensitivity to H_2O_2 in long-term survival assays compared to BT-12.

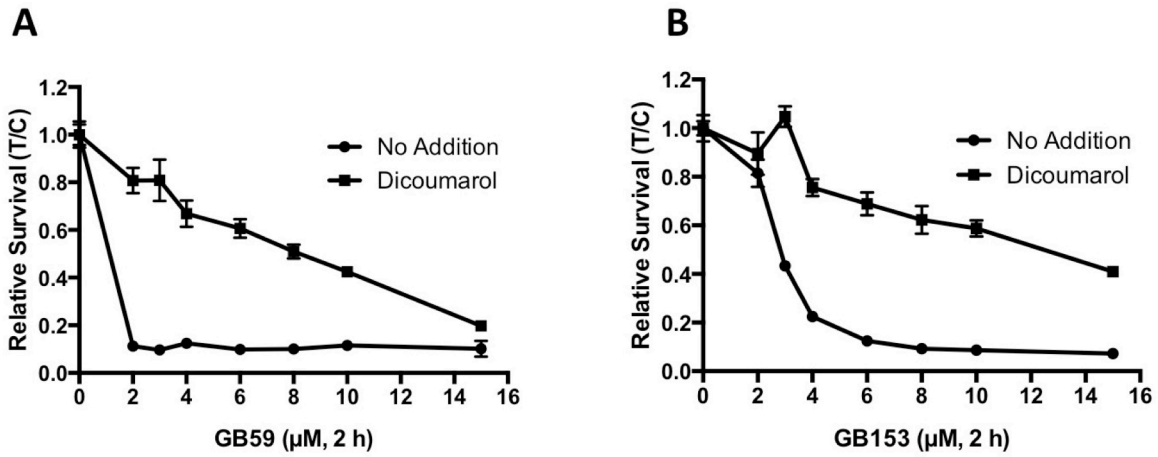

Figure 4-4. Alternative NQO1-bioactivated drugs show efficacy against BT-12. A) Long-term survival assays were performed after 2 h treatments with GB59, a more potent derivative of ß-lap. Cell kill was markedly increased at lower doses, but at high doses dicoumarol did not completely block GB59-induced cell death. **B)** GB153 is a water-soluble derivative of GB59 that elicited a similar dose-response curve against BT-12 as ß-lap and more effective rescue with dicoumarol (50 μM) than GB59.

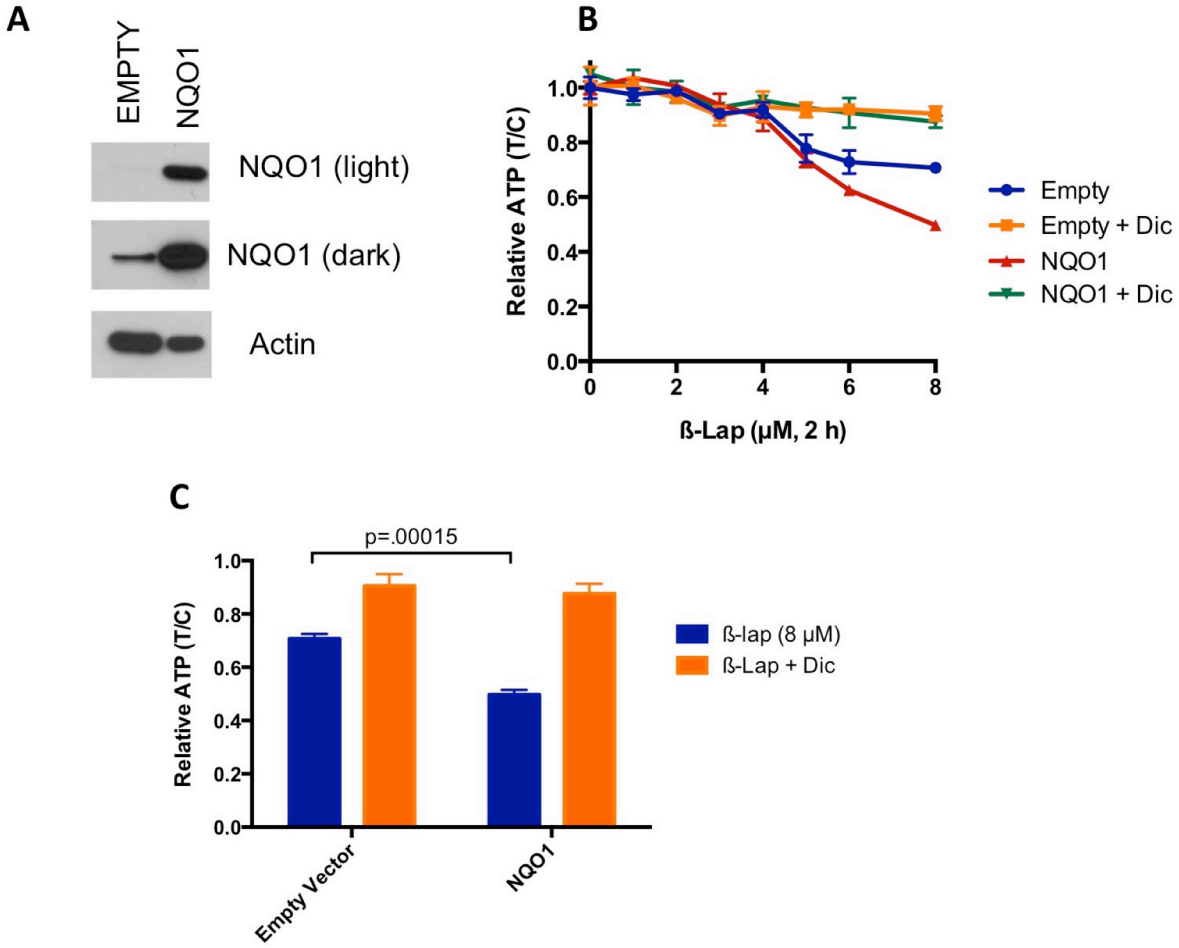

Figure 4-5. Overexpressing NQO1 in NQO1-deficient cells increases response to ß-lap. A) CHLA-07 cells, which express low NQO1 levels, were transfected with a CMV-NQO1 overexpression vector, which increased NQO1 expression compared to empty vector control transfections. **B)** 72 h after transfection, cells were treated with various doses of ß-lap with or without dicoumarol for 2 h followed immediately by ATP assays (CellTiter-Glo). **C)** ATP depletion after 2 h treatment at 8 µM ß-lap was plotted, showing increased NQO1-dependent ATP depletion after NQO1 overexpression.

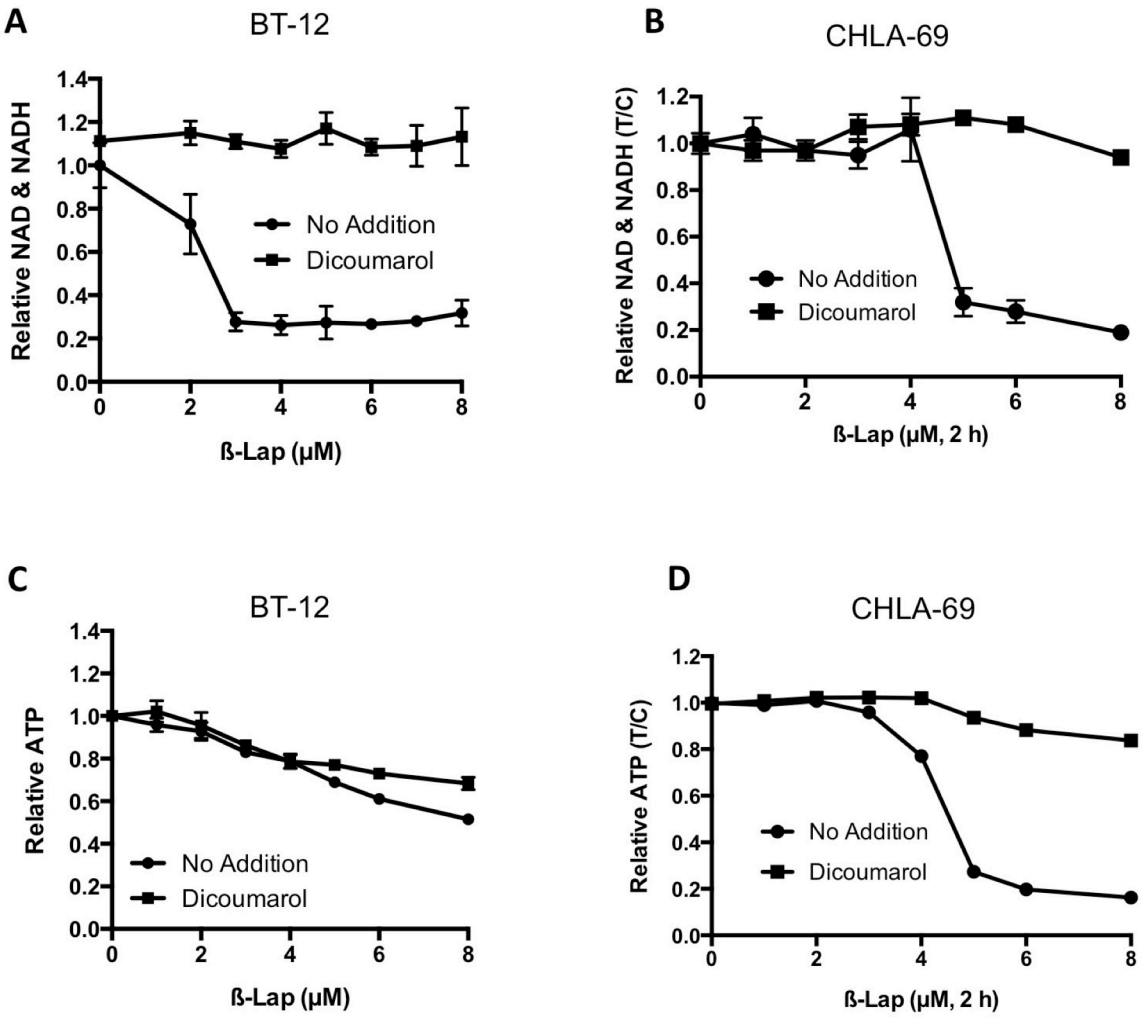

Figure 4-6. Rapid NAD$^+$ and ATP depletion occurs after ß-lap treatment A) BT-12 and **(B)** CHLA-69 cells were treated with various doses of ß-lap with or without dicoumarol for 2 h followed immediately by NAD$^+$/NADH-Glo assays to quantify total NAD$^+$ and NADH. **C)** BT-12 and **(D)** CHLA-69 were treated under the same conditions followed by CellTiter Glo assays to determine total short-term ATP depletion caused by ß-lap.

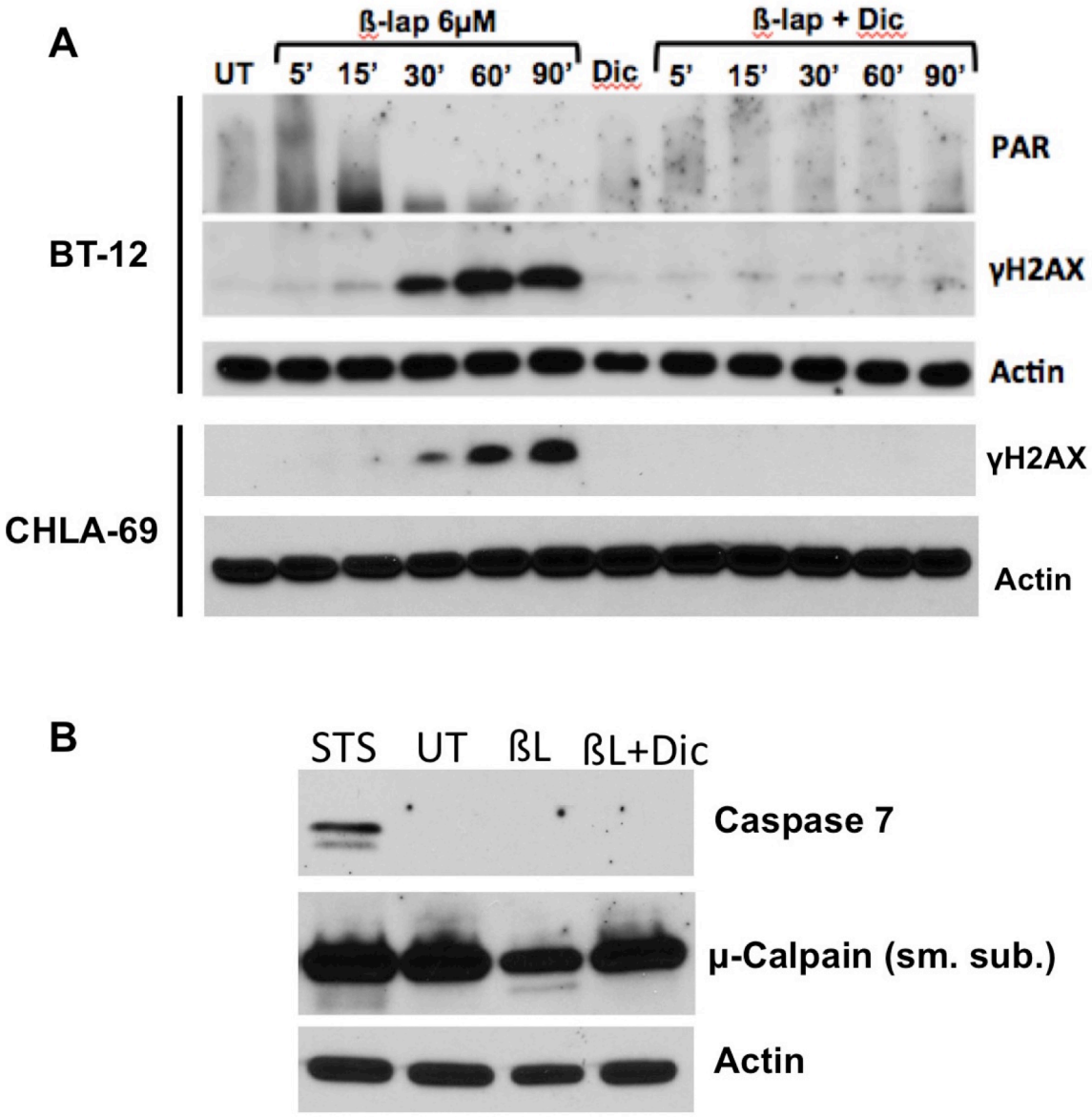

Figure 4-7. PAR formation, DSBs, and programmed necrosis occur after ß-lap treatment. A) BT-12 and CHLA-69 lysates were prepared after indicated treatment times with ß-lap alone or with dicoumarol (50 μM). PAR formation occurred at early time points followed by its dissipation and induction of γH2AX. **B)** 48 h after treatment with ß-lap for 2 h, Caspase 7 cleavage did not occur, in contrast with the staurosporine treated control, but μ-Calpain cleavage did occur and was blocked with dicoumarol.

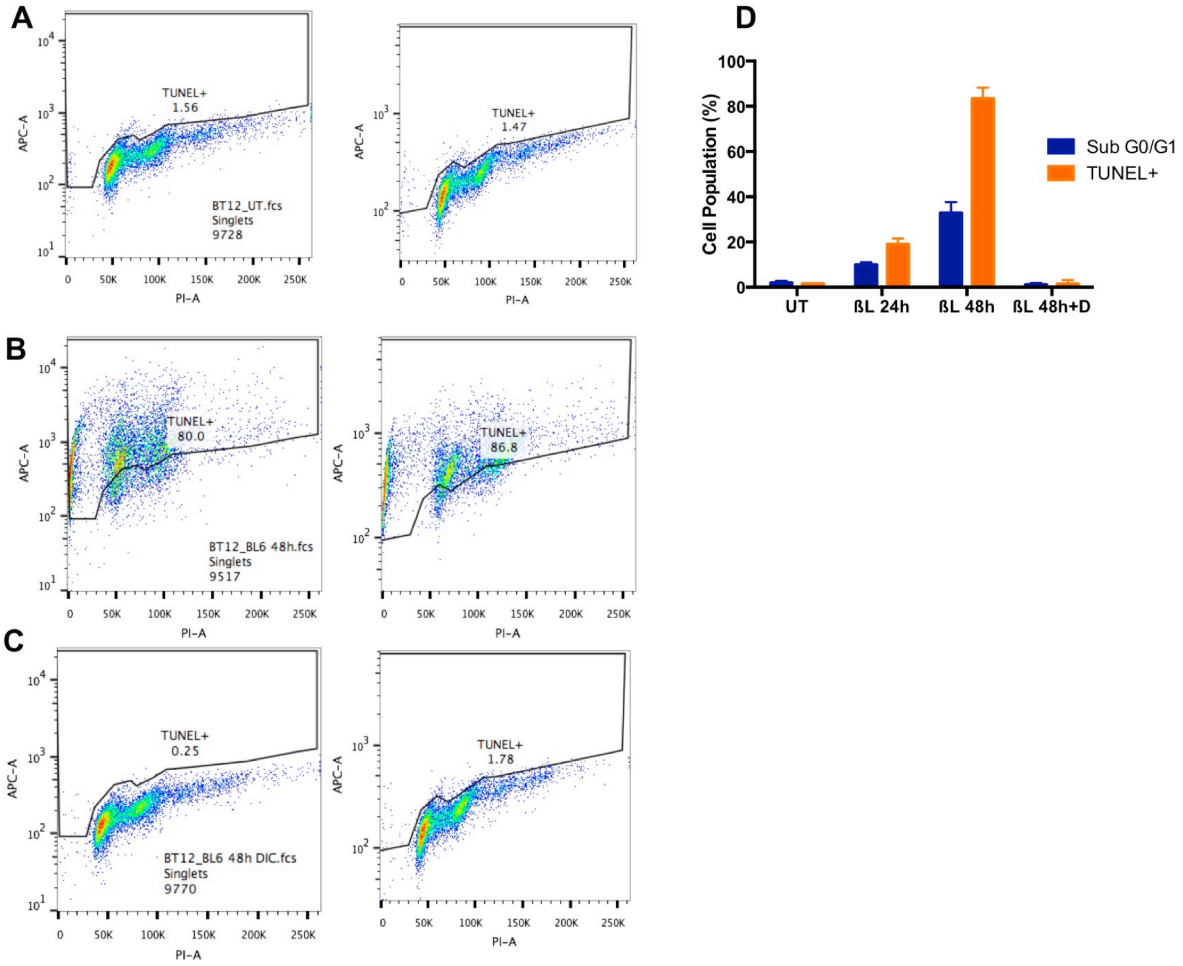

Figure 4-8. ß-lap treatment results in TUNEL positive staining and a large sub-G1 population. At 24 and 48 h after treatment with ß-lap for 4 h, BT-12 cells were analyzed for total DNA content with PI and TUNEL staining (x axis – PI, y axis-TUNEL). Side-by side replicates from separate experiments are shown for **(A)** untreated cells, **(B)** 48 h after ß-lap treatment and **(C)** 48 h after ß-lap + dicoumarol treatment. **D)** Sub-G1 and TUNEL positive cells were quantified 24 and 48 h after treatment with ß-lap or ß-lap and dicoumarol.

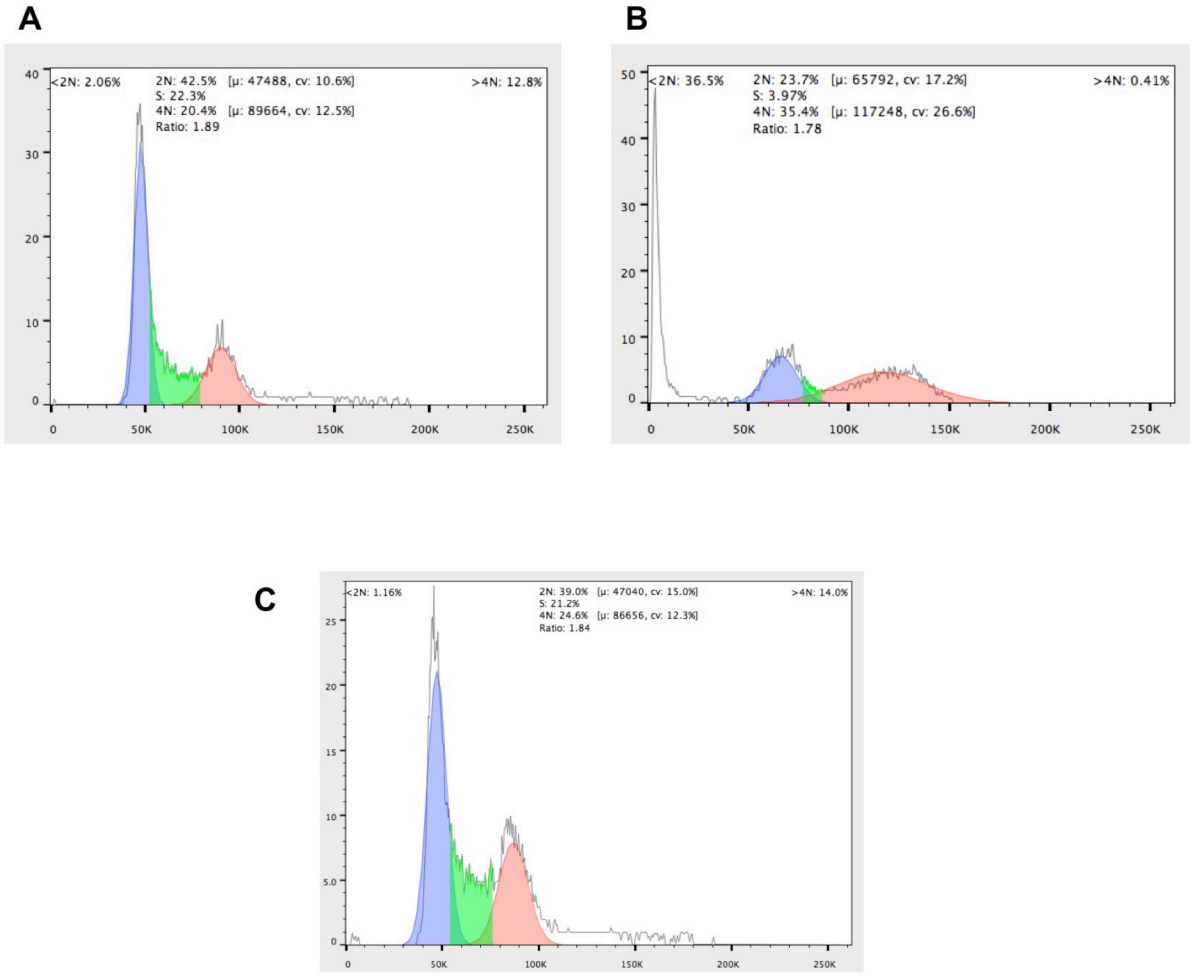

Figure 4-9. Cell death is independent of cell cycle status during treatment. A) A histogram depicting the DNA content of untreated cells by PI staining shows a typical cell cycle distribution for BT-12 cells. **B)** 48 h after 4 h ß-lap treatments, there was a reduction of cells in the G1, S, and G2 phases and an increase in sub-G1 cells. **C)** Dicoumarol completely spared the effects of ß-lap.

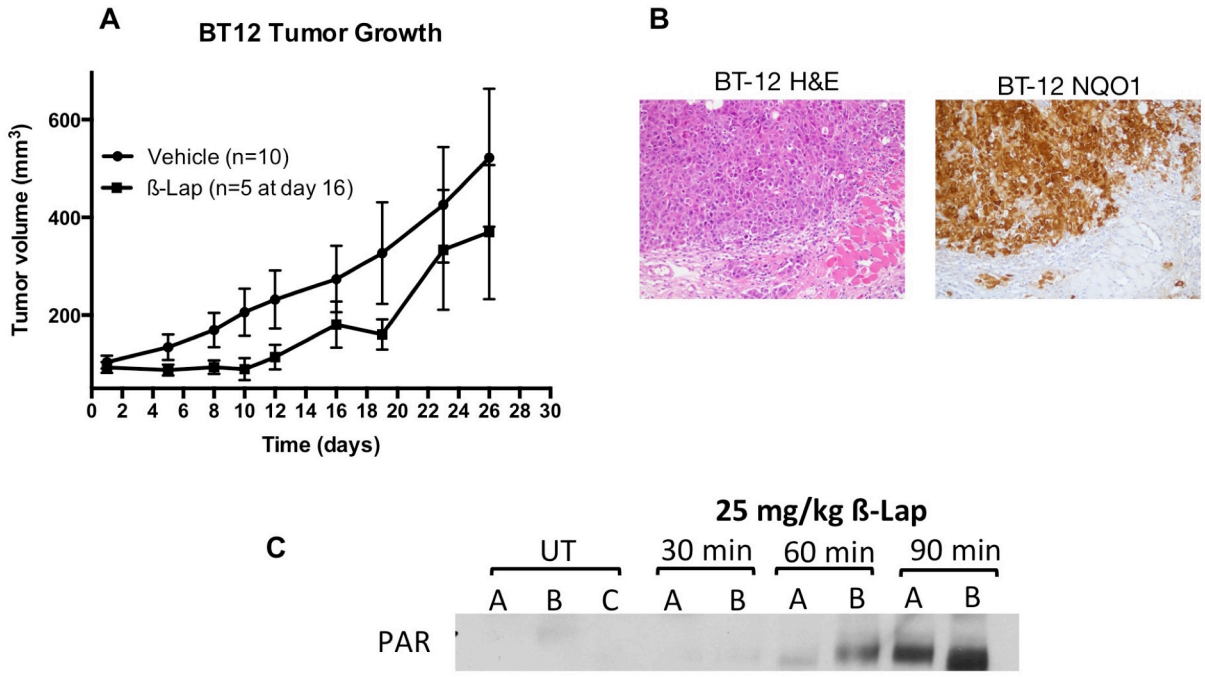

Figure 4-10. Application of ß-lap to an *in vivo* model of ATRT A) Mice bearing established BT-12 subcutaneous xenografts were treated with ß-lap I.V. three times a week for two weeks (30 mg/kg for first two injections, reduced to 25 mg/kg for subsequent treatments) or vehicle alone. **B)** IHC performed on subcutaneous xenografts showed high NQO1 levels. **C)** Mice with established tumors were treated I.V. with 25 mg/kg of ß-lap and tumors were collected at the indicated time points after treatment. PAR formation occurred with a substantial delay compared to *in vitro* results.

Chapter Five
Integrative Discussion and Future Direction

5.1 Integrative Discussion

The previous chapters describe the application of NQO1-bioactivatable drugs in a variety of cancer cell types, including PDA, NSCLC, breast, and ATRT. The broad application of ß-lap and other drugs that work through the same mechanism demonstrates how robust the NQO1-mediated futile redox is in inducing cell death. Mutations in both oncogenes and tumor suppressors have no bearing on sensitivity, with the exception of the complete loss of NQO1 through homozygous NQO1*2 or NQO1*3 polymorphisms. The NQO1 specificity of ß-lap provides a high therapeutic window for single agent treatment, and even greater efficacy at lower doses for the tested combination treatments of NAMPT inhibitors and PARP inhibitors. However, without NQO1 present in tumor cells, both single agent and combination treatments are ineffective, so screening for polymorphism status and the presence of NQO1 in tumor tissue will be critical for determining if patients would benefit from ß-lap or combination treatment.

The combination treatment strategies presented in chapters 2 and 3 demonstrate that NAMPT and PARP inhibitors can be applied much more broadly (to all NQO1 positive tumors) and achieve greater tumor specificity when combined with low doses of ß-lap. The efficacy of ß-lap is also improved in combination treatment conditions by increasing tumor cell death with lower doses and shorter treatment

times, thereby potentially reducing toxicity caused by methemoglobinemia and hemolytic anemia known to occur at high ß-lap doses.

By testing combination treatment strategies, important questions about the mechanism of ß-lap have been answered. In concordance with my initial hypothesis, NAMPT co-treatment demonstrated that severe energy depletion and metabolic catastrophe is a primary driver of NAD^+-Keresis, a form of programmed necrosis caused by ß-lap. This occurs as a secondary effect of the substantial single strand DNA damage and subsequent PARP1 hyperactivation that ß-lap induces; the PAR polymer itself is not necessary for signaling in this death pathway.

Combination treatment with PARP inhibitors further supported this hypothesis. Without PARP1 activity, energy depletion did not occur and cancer cells did not die through NAD^+-Keresis but through caspase-mediated apoptosis. On the other hand, these studies have shown that choosing combination treatment agents to promote NAD^+-Keresis is not the only effective way to identify synergistic therapeutic strategies. In the case of PARP inhibition combined with ß-lap, DNA damage was enhanced at low ß-lap doses due to the lack of PARP1-mediated repair.

The divergent cell death pathways caused by these two treatment strategies may appear to be a mechanistic detail with the same result – more cancer cell death at lower drug doses, but this distinction may be relevant when moving toward clinical application. There are a variety of possible combination treatment strategies to achieve synergy with NQO1-bioactivated therapeutics through promoting DNA damage, inhibiting repair, or enhancing the metabolic effects of treatment, but they will all have their own therapeutic niche. For example, applying PARP inhibitors in combination with

ß-lap may not be a viable option for treating tumors with known disruptions in apoptotic pathways. Likewise, the metabolic status of both the tumor and the patient could guide the application of NAMPT inhibitors and other metabolism-influencing drugs in combination with ß-lap. Preclinical and clinical development of a variety of the most promising combination treatment strategies alongside new NQO1 bioactivatable drugs will contribute to a more complete toolbox for personalized care.

5.2 Future Direction

Many opportunities exist for continued study of the topics presented in this text. Several of the fundamental characteristics of ß-lap induced cell death have been previously elucidated, but the relevance of other components of the pathway is not yet fully defined. The development of practical combination treatment strategies would be promoted by a better understanding of how the death pathway initiated by ß-lap is influenced by NAD^+ and ATP depletion, especially with regard to mitochondrial membrane potential disruption and calcium signaling, which have immediate connections to cellular metabolism. Just as NAMPT increase NAD^+ depletion and PARP inhibitors prevent NAD^+ depletion but prevent DNA repair, a variety of other small molecule inhibitors and RNAi knockdowns could be applied at various points of the pathway to modulate the cell death program and identify the critical steps.

For example, the involvement of calcium signaling in ß-lap-induced cell death is still underexplored outside of its requirement for PARP1 hyperactivation and μ-calpain cleavage (Bentle et al., 2006; Tagliarino et al., 2003). Determining the direct cause and source of Ca^{2+} release would better establish its role in NAD^+-Keresis. Relevant Ca^{2+}

channels in the ER could be inhibited or knocked down and the roles of ROS, lipid peroxidation, and ATP loss on calcium localization after treatment could be determined. Downstream roles of Ca^{2+} signaling will also likely prove to be important, since it has widespread effects on metabolism, cell death, and other signaling processes in cancer (Hajnoczky, Davies, & Madesh, 2003; Monteith, Davis, & Roberts-Thomson, 2012).

The evidence of severe metabolic dysfunction after ß-lap treatment I presented in chapter 2 opens other paths for future exploration. Deregulated cellular energetics is a hallmark of cancer, and using NQO1-bioactivated drugs as a tumor-specific means of targeting overactive glycolysis and the generation of TCA cycle intermediates used in anapleurotic reactions is an appealing prospect (Hanahan & Weinberg, 2011). Additional metabolic inhibition and rescue experiments coupled with high-content metabolomics will clarify the pathways most relevant to energy depletion at lethal doses of ß-lap. Knockdown of genes in metabolic pathways combined with exposure to sublethal doses of ß-lap in NQO+ and NQO1- cancer cell lines would elucidate those pathways that are critical for recovery after treatment. These studies could inform tumor-specific combination treatment strategies and facilitate a better understanding of responses to metabolic stress in cancer cells.

Additional work in the realm of clinical development should focus on the delivery and derivatization of NQO1-bioactivated therapeutics. The binary NQO1 specificity of ß-lap observed *in vitro* is complicated by dose-limiting methemoglobinemia and hemolysis that has occurred in the clinic and in mouse models (Gerber et al.). These issues were partially resolved through a reduction of HPßCD used to solubilize the drug

in the ARQ761 versus ARQ501 formulation (Blanco et al., 2010). Ideally, the hemolytic effects of HPßCD could be avoided entirely by utilizing alternative delivery agents, such as nanoparticles to facilitate the solubility of ß-lap (Ma et al., 2015). A micelle/nanoparticle delivery system has the additional benefit of protecting RBCs from hemoglobin oxidation through non-NQO1 mediated ROS generation if drug carriers preferentially release ß-lap in tumor cells or the tumor microenvironment but not in the bloodstream.

The development of new NQO1-bioactivated therapeutics will be critical for improving clinical outcomes. The discovery of DNQ and IB-DNQ, which have markedly different structures compared to ß-lap but kill cancer cells through the same NQO1-mediated futile cycle, show that there is a wide diversity of quinone structures that the flexible binding pocket of NQO1 can accommodate (Faig et al., 2001; X. Huang et al., 2012). Developing new derivatives with higher NQO1 affinity has the potential to increase the specificity and decrease the doses required for clinical efficacy. Novel NQO1 bioactivatable drugs can also be used to better understand the redox chemistry of the futile cycle. In addition to increasing the NQO1 affinity, it is critical for new compounds to spontaneously oxidize from the hydroquinone form back to the parent compound in order to generate a lethal burst of ROS. The chemical properties of the hydroquinone that destabilize it and facilitate this futile cycle are still unclear, but are likely just as important as NQO1 affinity for inducing cell death.

Clinical application of NAMPT inhibition in combination treatment with ARQ761 will be promoted by the preclinical development of new NAMPT inhibitors and optimized *in vivo* treatment strategies. As described in chapter 2, initial PD results

appear to show tumor response for both FK866 and ß-lap, but an effective treatment strategy with these two agents still needs to be optimized. Ideally, ß-lap treatment would be completed every other day while FK866 would be administered twice a day. However, the short half-life of FK866 in circulation along with potential bone marrow suppression associated with continuous treatment will make it difficult to avoid additive hematologic toxicity. Shorter treatment regimes with ß-lap treatment every day for 4-5 days on established subcutaneous tumors (300-400 $mm^{\wedge 3}$) may provide a better opportunity to see combination effects with shorter treatment times. The continued development of new NAMPT inhibitors with high specificity and better PK profiles should also be applied to *in vivo* studies.

Determining the mechanism of methemoglobinemia produced by ß-lap will also be useful in the development of new NQO1 bioactivatable drugs. Candidate enzymes in RBCs that can facilitate ROS formation from quinones include b5R and P450r, so analyzing the reactivity of these enzymes with ß-lap and new derivatives could help maximize the NQO1 reactivity while minimizing other redox reactions that contribute to the dose limiting toxicity. Currently, more potent NQO1 bioactivated drugs also generate more methemoglobin despite the lack of NQO1 in RBCs, so whether it is possible to increase the NQO1 specificity and futile cycle activity yet reduce non-specific ROS generation is still an open question. If an individual redox enzyme is found to be primarily responsible for methemoglobinemia, a specific inhibitor could be co-administered with ß-lap to prevent toxicity without influencing NQO1-mediated tumor cell death.

Additional studies will also be required to promote the clinical translation of ß-lap in ATRT and combination treatment with ß-lap along with NAMPT inhibitors or PARP inhibitors. Since the *in vitro* mechanisms have been established herein for these treatment strategies, future work should focus on optimizing delivery and dosing of these agents in a variety of xenograft, orthotopic, and GEM cancer models. These studies should include extensive monitoring of both pharmacokinetics and pharmacodynamics. In ATRT orthotopic models, it will be important to ensure that adequate levels of tested therapeutics arrive to tumors in the brain. For combination treatments, fine tuning dosing schedules will help align the pharmacokinetics of complementary drugs to achieve optimal doses for pre-treatment and co-treatment. Additionally, normal tissue toxicity should be monitored to identify and address any combination toxicity. Going forward, these studies will help identify the best combination treatment strategies to bring to future clinical trials.

Chapter Six
Materials and Methods

Chemicals and Reagents

We synthesized and purified ß-lap and GB59 and prepared stock solutions at 50 mM in DMSO. DNQ and IB-DNQ were provided by Paul Hergenrother. FK866 hydrochloride hydrate, GMX1778, dicoumarol, catalase-polyethylene glycol, BAPTA-AM and all other reagents, unless otherwise specified, were purchased from Sigma-Aldrich (St Louis, MO).

Cell Culture

Pancreatic cancer cell lines were obtained from ATCC. They were cultured in DMEM (Life Technologies, Carlsbad, CA) containing 10% FBS (Fisher Scientific, Waltham, MA) in a 37° incubator with 5% CO_2. NSCLC lines were provided by John Minna and cultured in DMEM or RPMI with 10% FBS. Cells were tested monthly to confirm absence of mycoplasma contamination. Lipofectamine RNAiMAX (Life Technologies) was used for siRNA transfections. Cells were transfected with one of two siRNAs purchased from Sigma-Aldrich to target NAMPT (NAMPT #1: SASI_Hs02_00340191, NAMPT #2: SASI_Hs02_00340192), NQO1, PARP1, or a non-targeting control siRNA). After 48 h of incubation with RNAiMax and siRNA in OptiMEM (Life Technologies), cells were detached with trypsin/EDTA (Life Technologies) and seeded for treatment assays or lysed for analysis of knockdown efficiency. For NAMPT inhibition combination drug treatments, cells were treated for 24 h with FK866 followed by co-treatment with ß-lap in complete media. Two h after ß-lap addition, the drug-

containing media was removed and replaced with fresh media. For PARP inhibitor combination treatment, cells were pretreated for 2 h with PARP inhibitors, co-treated for 2 h with ß-lap, and then both drugs were removed and replaced with fresh media.

DNA Assay

For long-term survival and proliferation analysis, cells were seeded at 6,000-15,000 cells per well in 48 well plates. Various doses of ß-lap or combination treatment agents were applied in 6 wells per treatment condition for indicated treatment times, followed by removal and replacement with 1 mL of fresh media per well. Cells were allowed to grow for 4-12 days until vehicle treated wells reached confluence. At this time, media was removed and wells were washed with PBS. High salt TNE buffer was added at 250 µL per well, and plates were frozen at -80° C. Lysate was thawed at room temperature and Hoechst dye (Sigma-Aldrich, 14530), diluted in TNE at 0.1 mg/mL, was added to each well followed by a 2 h incubation at room temperature to allow DNA binding. Fluorescence at 460 nm was read in a Victor X3 (Perkin-Elmer) plate reader to measure total DNA content. Raw values were averaged among replicates and normalized to vehicle treated cells.

Clonogenicity

After ß-lap, NAMPT inhibitor, PARP inhibitor or combination treatment in 60 mm plates at 60% confluency, cells were trypsinized, counted with a Coulter Counter, and diluted in single cell suspension. Cells were then seeded at 100, 500, or 1000 cells per plate on 60mm culture dishes with three replicates for each treatment condition and

allowed to proliferate for seven days in 5 mL of complete culture media. Plates were washed with PBS and cells were fixed and dyed with methanol/crystal violet for 2 minutes. Colonies of fifty or more cells with normal appearance were counted and results were normalized to the colonies formed without drug treatment.

Comet Assay

Alkaline comet assays (Trevigen) were performed to measure total DNA damage, including both single strand breaks and double strand breaks (Bey et al., 2007). Slides were stained with SYBR green, and images were captured using a Leica DM5500 microscope. Comet tail length was quantified in ImageJ.

Nucleotide, Glutathione, and H_2O_2 Assays

CellTiter-Glo (Promega, Madison, WI) was used for cell viability assays (24 h after treatment) and ATP assays (at indicated time points during or after treatment). The following assays were purchased from Promega: GSH/GSSG-Glo, NAD^+/NADH-Glo, $NADP^+$/NADPH-Glo, and ROS-Glo and were used as indicated. For NAD^+, GSH, and $NADP^+$ assays, drug-containing media was removed from cells and replaced with PBS to prevent interactions between ß-lap or dicoumarol with the redox recycling enzymes in these assays. Unless otherwise noted, all raw luminescent values for treatment conditions were normalized to the signal from untreated cells (T/C). Standard curves were generated to ensure linearity.

Immunoblotting

Cells were lysed in ice-cold RIPA with protease and phosphatase inhibitors (Santa Cruz, Dallas, TX). Whole-cell extracts were prepared by centrifugation at 14,000 x g to remove insoluble components. Protein concentration was determined by BCA assay (Thermo Scientific, Waltham, MA) and loading concentration was normalized. Extracts were run on 8% or 4-20% (Bio-Rad, Hercules, CA) gradient acrylamide SDS-PAGE gels and transferred to PVDF membrane. Primary hybridization was carried out in Sigma casein blocking buffer or 5% NFDM in PBS-T at 4° overnight. Following primary antibody hybridization, blots were washed three times for 5 minutes each in PBS-T. Secondary HRP conjugated antibodies were incubated for 1 h at room temperature, followed by detection with SuperSignal West Pico or Dura (Thermo Scientific). Bands were quantified by measuring mean intensity in ImageJ and normalized to actin band intensity to control for loading variation.

Antibodies

Antibodies used for immunofluorescence and western blot include: NQO1 (A180), Actin (C4, Santa Cruz), PAR (Trevigen), Cleaved caspase 7 (D6H1, Cell Signaling), cleaved caspase 3 (5A1E, Cell Signaling), p53 (DO-1, Santa Cruz), Catalase (D4P7B, Cell Signaling), γH2AX (Millipore, JBW301), α-tubulin (Santa Cruz), PARP1 (F-2 and C2-10, Santa Cruz), visfatin/NAMPT (rabbit polyclonal, Abcam, Cambridge, UK), small subunit calpain (EPR3324, Abcam), FLAG (M2, Sigma-Aldrich).

Glycolytic Flux

A Seahorse XF24 bioanalyzer (Seahorse Bioscience, MA) was used for glycolytic stress tests. Cells were seeded at $3x10^4$ cells/well in 24 well plates and were treated with ß-lap at 4μM for two h in complete media and washed with fresh (unbuffered) Seahorse media. The glycolytic stress test kit was used to inject glucose, oligomycin, and 2-deoxy-D-glyucose (2-DG) at the indicated times. Results were normalized using Seahorse XF software.

GAPDH Activity

Cells seeded on 96 well plates were pre-treated with or without FK866 for 24 h, co-treated with ß-lap for 2 h, washed with PBS, and assayed for GAPDH activity using the KDalert GAPDH activity assay (Life Technologies) as directed.

NQO1 Enzyme Activity

NQO1 enzyme activity was determined as described previously by measuring reduction of cytochrome C (Sigma-Aldrich), a terminal electron acceptor, after addition of excess NADH and menadione (Sigma-Aldrich) (Li et al., 2011; Pink, Planchon, et al., 2000). A master reaction solution containing 19.08 mg of cytochrome C, .028 g BSA, 20 uL of menadione (10 mM in ethanol), and 250 μL of NADH (16 mM in water) was prepared in 20 mL 50 mM Tris-HCl pH 7.5. For each reaction 10 μL of S9 cell lysate (lysed by sonication in PBS) was added to 1 mL of the reaction mixture and the absorbance of reduced cytochrome C at 550 nm for 2 minutes. For each sample, a control was performed by adding 10 μL of 5 mM dicoumarol to block NQO1 activity.

Using GraphPad Prism, the slope of the linear portion of the reaction for each sample was calculated, the slope of the dicoumarol containing sample was subtracted, and results were normalized to the lysate concentrations. The extinction coefficient for cytochrome C of EmM = 28.0 was used to calculate the NQO1 enzyme activity in units of moles of cytochrome C reduced per minute per gram of lysate.

Metabolomics

Subconfluent MiaPaca2 cells were pretreated +/- FK866 for 24 h and co-treated with ß-lap for 30 min. Cells were washed twice with ice-cold saline, then scraped in methanol/water (50/50, v/v). Cells were subjected to three freeze-thaw cycles. After rigorous vortexing, cell debris was removed by centrifugation. Pellets were used for protein quantitation (BCA Protein Assay, Thermo). The supernatant was evaporated to dryness using a SpeedVac concentrator (Thermo Savant, Holbrook, NY) and metabolites were reconstituted in 0.03% formic acid in analytical-grade water and centrifuged to remove insoluble debris. Supernatants were transferred to HPLC vials for metabolomics analyses.

Targeted metabolite profiling was performed using a liquid chromatography-mass spectrometry/mass spectrometry (LC/MS/MS) approach. Separation was achieved on a Phenomenex Synergi Polar-RP HPLC column (150 × 2 mm, 4 µm, 80 Å) using a Nexera Ultra High Performance Liquid Chromatograph (UHPLC) system (Shimadzu Corporation, Kyoto, Japan). The mobile phases employed were 0.03% formic acid in water (A) and 0.03% formic acid in acetonitrile (B). The gradient program was as follows: 0-3 min, 100% A; 3-15 min, 100% - 0% A; 15-21 min, 0% A; 21-21.1

min, 0% - 100% A; 21.1-30 min, 100% A. The column was maintained at 35° C and samples were kept in the autosampler at 4° C. The flow rate was 0.5 mL/min, and injection volume 10 µL. The mass spectrometer was an AB QTRAP 5500 (Applied Biosystems SCIEX, Foster City, CA) with electrospray ionization (ESI) source in multiple reaction monitoring (MRM) mode. Sample analyses were performed in positive/negative switching mode. Declustering potential (DP) and collision energy (CE) were optimized for each metabolite by direct infusion of reference standards using a syringe pump prior to sample analysis. The MRM MS/MS detector conditions were set as follows: curtain gas 30 psi; ion spray voltages 5000 V (positive) and -1500 V (negative); temperature 650°C; ion source gas 1 50 psi; ion source gas 2 50 psi; interface heater on; entrance potential 10 V. Dwell time for each transition was set at 3 msec. MRM data was acquired using Analyst 1.6.1 software (Applied Biosystems SCIEX, Foster City, CA). Chromatogram review and peak area integration were performed using MultiQuant software version 2.1 (Applied Biosystems SCIEX, Foster City, CA). The integrated peak area values were used as variables for the statistical data analysis. The chromatographically co-eluted metabolites with shared MRM transitions were shown in a grouped format, i.e., G6P/F6P.

Lactate and Glucose Quantification

Cells were pretreated with FK866 for 24 h and co-treated with ß-lap for 2 h in complete media in 6 well plates. After co-treatment, media was replaced with low glucose, phenol-free DMEM (Invitrogen) with 5% FBS and collected at indicated times for analysis with a BioProfile Automated Analyzer (Nova Biomedical, MA).

Flow Cytometry

Cells were treated as indicated at 40-60% confluence on 10 cm plates. Drug-containing media was removed and cells were incubated in fresh complete media for 48 h. Cells were trypsinized, and both adherent and floating cells were collected by spinning at 300 RCF and washed in PBS containing 1% FBS. Cells were fixed for 30 minutes at room temperature in 1% paraformaldehyde, washed in PBS/FBS, and fixed and permeabilized overnight at -20° C in 70% ethanol. For TUNEL staining, cells were washed and resuspended in master mix containing reaction buffer, TdT enzyme, and AlexaFluor 647 labeled dUTP as described in the ApoDirect protocol (BD Biosciences). The TUNEL reaction was carried out at 37 °C for 4 hours with occasional mixing. Cells were washed and resuspended in BSA/PBS buffer containing propidium iodine, saponin, and RNAse H. Cells were analyzed on a FACSAria (BD Biosciences, San Jose, CA) and cell cycle distribution and TUNEL+ populations were calculated in FlowJo.

Mouse Models

To establish subcutaneous xenograft tumor models, female athymic nude mice between 6-8 weeks of age were used. These mice were injected subcutaneously in the flanks with $2x10^6$ tumor cells in 100 µL of a 1:1 solution of base media (without FBS) and Matrigel. Tumor sizes were calculated by using digital calipers to measure the longest dimension (l) of the tumor and the length orthogonal to the longest dimension (w). Tumor volume was calculated with the formula v= (.5 * l * 2w). Treatment began

when tumor sizes averaged 100 mm^3. To establish orthotopic lung tumors, female NOD/SCID mice were injected IV with 1.2 x 10^6 tumor cells in PBS. One to two hours after injection, luciferin was injected subcutaneously and luminescence was imaged in an IVIS bioluminescent imager to confirm lung localization of luciferase expressing tumor cells. Treatment in this model was started 8 days after tumor cell injection. ß-lap for *in vivo* use was prepared by dissolving it at 14-15 mg/mL in 30% HPßCD by mixing for 2 days at room temperature in the dark. The solution was sterile filtered and stored in aliquots at -80°. Immediately before use, the HPßCD-ß-Lap solution was thawed and diluted in sterile PBS to a working concentration of 5 mg/mL and injected IV in tumor-bearing mice. Tumor volume was followed by caliper measurements in subcutaneous models and by BLI imaging in lung orthotopic models. Mice were sacrificed when tumor volume exceeded 2000 mm^3, ulceration occurred, or mice became moribund.

Statistics

Unless otherwise noted, data points on graphs are plotted as mean with error bars denoting standard deviation. Curve fitting and calculation of IC50 values, ANOVA, and two-tailed Student t-tests for statistical significance with Holm/Sidak multiple comparison correction were performed in GraphPad Prism 6.

Microarray Expression Analysis

NSCLC gene expression data series were extracted from the Gene Expression Omnibus (GEO) subject to the following criteria: public on or before September 30, 2011, more than 50 samples in the full study, Affymetrix HG- U133 Plus 2 platform

used, acceptable data quality. A total of 8 series meeting these criteria were chosen for inclusion in the cohort: GSE2109, GSE8332, GSE10445, GSE10843, GSE14315, GSE18842, GSE19804, GSE31546. Five of these data series were used to support originally published work independent of that presented here: Wagner, et al., *Nat Med* 2007, Broet, et al. *Cancer Res* 2009 (Broet et al., 2009), Stinson, et al. *Sci Signal* 2011 (Stinson et al., 2011), Sanchez-Palencia et al., *Int J Cancer* 2011 (Sanchez-Palencia et al., 2011), Lu, et al. *Cancer Epidemiol Biomarkers Prev* 2010 (Lu et al., 2010). The resulting data cohort includes 327 NSCLC tumor samples, 105 normal lung and 128 NSCLC cell line specimens, for a total of 560 specimens. Within this assembled cohort are 105 matched-pair specimens from two independent studies, in which biopsies were taken from both tumor and associated normal lung for each NSCLC patient studied. The matched-pair specimens represent Spanish and Taiwanese patients. In the context of the genes analyzed in this paper, no significant differences were found between these two patient populations.

Microarray Data Processing and Analysis

The 560 specimen data files included in the cohort were downloaded as raw CEL files for post-processing together, following the standard gene expression data preparation workflow (Irizarry et al., 2003). Data was processed using the linear model from RMA, then fit robustly using probe level models as described (Robinson & Speed, 2007). We used the R package aroma.affymetrix, which uses persistent memory to allow very large datasets to be analyzed. Probe level models are fit to RMA-background corrected and quantile normalized data to get gene-level summaries.

Gene-level summarization used the standard CDF provided by Affymetrix. All data analysis was performed in R.

References

Albert, J. M., Cao, C., Kim, K. W., Willey, C. D., Geng, L., Xiao, D., Wang, H., Sandler, A., Johnson, D. H., Colevas, A. D., Low, J., Rothenberg, M. L., & Lu, B. (2007). Inhibition of poly(ADP-ribose) polymerase enhances cell death and improves tumor growth delay in irradiated lung cancer models. *Clin Cancer Res, 13*(10), 3033-3042. doi: 10.1158/1078-0432.CCR-06-2872

Andrabi, S. A., Umanah, G. K., Chang, C., Stevens, D. A., Karuppagounder, S. S., Gagne, J. P., Poirier, G. G., Dawson, V. L., & Dawson, T. M. (2014). Poly(ADP-ribose) polymerase-dependent energy depletion occurs through inhibition of glycolysis. *Proc Natl Acad Sci U S A*. doi: 10.1073/pnas.1405158111

Asher, G., Lotem, J., Kama, R., Sachs, L., & Shaul, Y. (2002). NQO1 stabilizes p53 through a distinct pathway. *Proc Natl Acad Sci U S A, 99*(5), 3099-3104. doi: 10.1073/pnas.052706799

Awadallah, N. S., Dehn, D., Shah, R. J., Russell Nash, S., Chen, Y. K., Ross, D., Bentz, J. S., & Shroyer, K. R. (2008). NQO1 expression in pancreatic cancer and its potential use as a biomarker. *Appl Immunohistochem Mol Morphol, 16*(1), 24-31. doi: 10.1097/PAI.0b013e31802e91d0

Bauer, A. K., Faiola, B., Abernethy, D. J., Marchan, R., Pluta, L. J., Wong, V. A., Roberts, K., Jaiswal, A. K., Gonzalez, F. J., Butterworth, B. E., Borghoff, S., Parkinson, H., Everitt, J., & Recio, L. (2003). Genetic susceptibility to benzene-induced toxicity: role of NADPH: quinone oxidoreductase-1. *Cancer Res, 63*(5), 929-935.

Beck, C., Robert, I., Reina-San-Martin, B., Schreiber, V., & Dantzer, F. (2014). Poly(ADP-ribose) polymerases in double-strand break repair: Focus on PARP1, PARP2 and PARP3. *Exp Cell Res*. doi: 10.1016/j.yexcr.2014.07.003

Belinsky, M., & Jaiswal, A. K. (1993). NAD(P)H:quinone oxidoreductase1 (DT-diaphorase) expression in normal and tumor tissues. *Cancer Metastasis Rev, 12*(2), 103-117.

Bentle, M. S., Reinicke, K. E., Bey, E. A., Spitz, D. R., & Boothman, D. A. (2006). Calcium-dependent modulation of poly(ADP-ribose) polymerase-1 alters cellular metabolism and DNA repair. *J Biol Chem, 281*(44), 33684-33696. doi: 10.1074/jbc.M603678200

Bentle, M. S., Reinicke, K. E., Dong, Y., Bey, E. A., & Boothman, D. A. (2007). Nonhomologous end joining is essential for cellular resistance to the novel antitumor agent, beta-lapachone. *Cancer Res, 67*(14), 6936-6945. doi: 10.1158/0008-5472.CAN-07-0935

Berger, F., Lau, C., Dahlmann, M., & Ziegler, M. (2005). Subcellular compartmentation and differential catalytic properties of the three human nicotinamide mononucleotide adenylyltransferase isoforms. *J Biol Chem, 280*(43), 36334-36341. doi: 10.1074/jbc.M508660200

Berger, N. A. (1985). Poly(ADP-ribose) in the cellular response to DNA damage. *Radiat Res, 101*(1), 4-15.

Betz, B. L., Strobeck, M. W., Reisman, D. N., Knudsen, E. S., & Weissman, B. E. (2002). Re-expression of hSNF5/INI1/BAF47 in pediatric tumor cells leads to G1 arrest associated with induction of p16ink4a and activation of RB. *Oncogene, 21*(34), 5193-5203. doi: 10.1038/sj.onc.1205706

Bey, E. A., Bentle, M. S., Reinicke, K. E., Dong, Y., Yang, C. R., Girard, L., Minna, J. D., Bornmann, W. G., Gao, J., & Boothman, D. A. (2007). An NQO1- and PARP-1-mediated cell death pathway induced in non-small-cell lung cancer cells by beta-lapachone. *Proc Natl Acad Sci U S A, 104*(28), 11832-11837. doi: 10.1073/pnas.0702176104

Bey, E. A., Reinicke, K. E., Srougi, M. C., Varnes, M., Anderson, V. E., Pink, J. J., Li, L. S., Patel, M., Cao, L., Moore, Z., Rommel, A., Boatman, M., Lewis, C., Euhus, D. M., Bornmann, W. G., Buchsbaum, D. J., Spitz, D. R., Gao, J., & Boothman, D. A. (2013). Catalase abrogates beta-lapachone-induced PARP1 hyperactivation-directed programmed necrosis in NQO1-positive breast cancers. *Mol Cancer Ther, 12*(10), 2110-2120. doi: 10.1158/1535-7163.MCT-12-0962

Bi, T. Q., Che, X. M., Liao, X. H., Zhang, D. J., Long, H. L., Li, H. J., & Zhao, W. (2011). Overexpression of Nampt in gastric cancer and chemopotentiating effects of the Nampt inhibitor FK866 in combination with fluorouracil. *Oncol Rep, 26*(5), 1251-1257. doi: 10.3892/or.2011.1378

Biegel, J. A., Tan, L., Zhang, F., Wainwright, L., Russo, P., & Rorke, L. B. (2002). Alterations of the hSNF5/INI1 gene in central nervous system atypical teratoid/rhabdoid tumors and renal and extrarenal rhabdoid tumors. *Clin Cancer Res, 8*(11), 3461-3467.

Biegel, J. A., Zhou, J. Y., Rorke, L. B., Stenstrom, C., Wainwright, L. M., & Fogelgren, B. (1999). Germ-line and acquired mutations of INI1 in atypical teratoid and rhabdoid tumors. *Cancer Res, 59*(1), 74-79.

Blanco, E., Bey, E. A., Khemtong, C., Yang, S. G., Setti-Guthi, J., Chen, H., Kessinger, C. W., Carnevale, K. A., Bornmann, W. G., Boothman, D. A., & Gao, J. (2010). Beta-lapachone micellar nanotherapeutics for non-small cell lung cancer therapy. *Cancer Res, 70*(10), 3896-3904. doi: 10.1158/0008-5472.CAN-09-3995

Boothman, D. A., Trask, D. K., & Pardee, A. B. (1989). Inhibition of potentially lethal DNA damage repair in human tumor cells by beta-lapachone, an activator of topoisomerase I. *Cancer Res, 49*(3), 605-612.

Boveris, A., Docampo, R., Turrens, J. F., & Stoppani, A. O. (1978). Effect of beta-lapachone on superoxide anion and hydrogen peroxide production in Trypanosoma cruzi. *Biochem J, 175*(2), 431-439.

Broet, P., Camilleri-Broet, S., Zhang, S., Alifano, M., Bangarusamy, D., Battistella, M., Wu, Y., Tuefferd, M., Regnard, J. F., Lim, E., Tan, P., & Miller, L. D. (2009). Prediction of clinical outcome in multiple lung cancer cohorts by integrative genomics: implications for chemotherapy selection. *Cancer Res, 69*(3), 1055-1062. doi: 10.1158/0008-5472.CAN-08-1116

Burger, P. C., Yu, I. T., Tihan, T., Friedman, H. S., Strother, D. R., Kepner, J. L., Duffner, P. K., Kun, L. E., & Perlman, E. J. (1998). Atypical teratoid/rhabdoid tumor of the central nervous system: a highly malignant tumor of infancy and childhood

frequently mistaken for medulloblastoma: a Pediatric Oncology Group study. *Am J Surg Pathol, 22*(9), 1083-1092.

Cadenas, E. (1995). Antioxidant and prooxidant functions of DT-diaphorase in quinone metabolism. *Biochem Pharmacol, 49*(2), 127-140.

Cairns, B. R., Kim, Y. J., Sayre, M. H., Laurent, B. C., & Kornberg, R. D. (1994). A multisubunit complex containing the SWI1/ADR6, SWI2/SNF2, SWI3, SNF5, and SNF6 gene products isolated from yeast. *Proc Natl Acad Sci U S A, 91*(5), 1950-1954.

Cao, L., Li, L. S., Spruell, C., Xiao, L., Chakrabarti, G., Bey, E. A., Reinicke, K. E., Srougi, M. C., Moore, Z., Dong, Y., Vo, P., Kabbani, W., Yang, C. R., Wang, X., Fattah, F., Morales, J. C., Motea, E. A., Bornmann, W. G., Yordy, J. S., & Boothman, D. A. (2014). Tumor-Selective, Futile Redox Cycle-Induced Bystander Effects Elicited by NQO1 Bioactivatable Radiosensitizing Drugs in Triple-Negative Breast Cancers. *Antioxid Redox Signal, 21*(2), 237-250. doi: 10.1089/ars.2013.5462

Cea, M., Zoppoli, G., Bruzzone, S., Fruscione, F., Moran, E., Garuti, A., Rocco, I., Cirmena, G., Casciaro, S., Olcese, F., Pierri, I., Cagnetta, A., Ferrando, F., Ghio, R., Gobbi, M., Ballestrero, A., Patrone, F., & Nencioni, A. (2009). APO866 activity in hematologic malignancies: a preclinical in vitro study. *Blood, 113*(23), 6035-6037; author reply 6037-6038. doi: 10.1182/blood-2009-03-209213

Ceccaldi, R., Liu, J. C., Amunugama, R., Hajdu, I., Primack, B., Petalcorin, M. I., O'Connor, K. W., Konstantinopoulos, P. A., Elledge, S. J., Boulton, S. J., Yusufzai, T., & D'Andrea, A. D. (2015). Homologous-recombination-deficient tumours are dependent on Poltheta-mediated repair. *Nature, 518*(7538), 258-262. doi: 10.1038/nature14184

Chan, M., Gravel, M., Bramoulle, A., Bridon, G., Avizonis, D., Shore, G. C., & Roulston, A. (2014). Synergy between the NAMPT inhibitor GMX1777(8) and pemetrexed in non-small cell lung cancer cells is mediated by PARP activation and enhanced NAD consumption. *Cancer Res*. doi: 10.1158/0008-5472.CAN-14-0809

Chao, C., Zhang, Z. F., Berthiller, J., Boffetta, P., & Hashibe, M. (2006). NAD(P)H:quinone oxidoreductase 1 (NQO1) Pro187Ser polymorphism and the risk of lung, bladder, and colorectal cancers: a meta-analysis. *Cancer Epidemiol Biomarkers Prev, 15*(5), 979-987. doi: 10.1158/1055-9965.EPI-05-0899

Cheng, C. L., Johnson, S. P., Keir, S. T., Quinn, J. A., Ali-Osman, F., Szabo, C., Li, H., Salzman, A. L., Dolan, M. E., Modrich, P., Bigner, D. D., & Friedman, H. S. (2005). Poly(ADP-ribose) polymerase-1 inhibition reverses temozolomide resistance in a DNA mismatch repair-deficient malignant glioma xenograft. *Mol Cancer Ther, 4*(9), 1364-1368. doi: 10.1158/1535-7163.MCT-05-0128

Cheng, S. W., Davies, K. P., Yung, E., Beltran, R. J., Yu, J., & Kalpana, G. V. (1999). c-MYC interacts with INI1/hSNF5 and requires the SWI/SNF complex for transactivation function. *Nat Genet, 22*(1), 102-105. doi: 10.1038/8811

Chiarugi, A., Dolle, C., Felici, R., & Ziegler, M. (2012). The NAD metabolome--a key determinant of cancer cell biology. *Nat Rev Cancer, 12*(11), 741-752. doi: 10.1038/nrc3340

Chini, C. C., Guerrico, A. M., Nin, V., Camacho-Pereira, J., Escande, C., Barbosa, M. T., & Chini, E. N. (2014). Targeting of NAD metabolism in pancreatic cancer cells: potential novel therapy for pancreatic tumors. *Clin Cancer Res, 20*(1), 120-130. doi: 10.1158/1078-0432.CCR-13-0150

Cho, H. Y., Jedlicka, A. E., Reddy, S. P., Kensler, T. W., Yamamoto, M., Zhang, L. Y., & Kleeberger, S. R. (2002). Role of NRF2 in protection against hyperoxic lung injury in mice. *Am J Respir Cell Mol Biol, 26*(2), 175-182. doi: 10.1165/ajrcmb.26.2.4501

Chuang, D. M., Hough, C., & Senatorov, V. V. (2005). Glyceraldehyde-3-phosphate dehydrogenase, apoptosis, and neurodegenerative diseases. *Annu Rev Pharmacol Toxicol, 45*, 269-290. doi: 10.1146/annurev.pharmtox.45.120403.095902

Colussi, C., Albertini, M. C., Coppola, S., Rovidati, S., Galli, F., & Ghibelli, L. (2000). H2O2-induced block of glycolysis as an active ADP-ribosylation reaction protecting cells from apoptosis. *FASEB J, 14*(14), 2266-2276. doi: 10.1096/fj.00-0074com

Conroy, T., Desseigne, F., Ychou, M., Bouche, O., Guimbaud, R., Becouarn, Y., Adenis, A., Raoul, J. L., Gourgou-Bourgade, S., de la Fouchardiere, C., Bennouna, J., Bachet, J. B., Khemissa-Akouz, F., Pere-Verge, D., Delbaldo, C., Assenat, E., Chauffert, B., Michel, P., Montoto-Grillot, C., Ducreux, M., Groupe Tumeurs Digestives of, U., & Intergroup, P. (2011). FOLFIRINOX versus gemcitabine for metastatic pancreatic cancer. *N Engl J Med, 364*(19), 1817-1825. doi: 10.1056/NEJMoa1011923

Cruz, F. S., Docampo, R., & Boveris, A. (1978). Generation of superoxide anions and hydrogen peroxide from beta-lapachone in bacteria. *Antimicrob Agents Chemother, 14*(4), 630-633.

D'Anneo, A., Augello, G., Santulli, A., Giuliano, M., di Fiore, R., Messina, C., Tesoriere, G., & Vento, R. (2010). Paclitaxel and beta-lapachone synergistically induce apoptosis in human retinoblastoma Y79 cells by downregulating the levels of phospho-Akt. *J Cell Physiol, 222*(2), 433-443. doi: 10.1002/jcp.21983

Dantzer, F., de La Rubia, G., Menissier-De Murcia, J., Hostomsky, Z., de Murcia, G., & Schreiber, V. (2000). Base excision repair is impaired in mammalian cells lacking Poly(ADP-ribose) polymerase-1. *Biochemistry, 39*(25), 7559-7569.

Dantzer, F., Schreiber, V., Niedergang, C., Trucco, C., Flatter, E., De La Rubia, G., Oliver, J., Rolli, V., Menissier-de Murcia, J., & de Murcia, G. (1999). Involvement of poly(ADP-ribose) polymerase in base excision repair. *Biochimie, 81*(1-2), 69-75.

David, K. K., Andrabi, S. A., Dawson, T. M., & Dawson, V. L. (2009). Parthanatos, a messenger of death. *Front Biosci (Landmark Ed), 14*, 1116-1128.

Dehn, D., Siegel, D., Moody, C. J., Steiner, M., & Ross, D. (2005). Mechanism based inhibition of NADPH: Quinone oxidoreductase 1 (NQO1) as a potential therapeutic approach in pancreatic cancer. *Proceedings of the American Association for Cancer Research, 2005*(1), 559.

DeNicola, G. M., Karreth, F. A., Humpton, T. J., Gopinathan, A., Wei, C., Frese, K., Mangal, D., Yu, K. H., Yeo, C. J., Calhoun, E. S., Scrimieri, F., Winter, J. M.,

Hruban, R. H., Iacobuzio-Donahue, C., Kern, S. E., Blair, I. A., & Tuveson, D. A. (2011). Oncogene-induced Nrf2 transcription promotes ROS detoxification and tumorigenesis. *Nature, 475*(7354), 106-109. doi: 10.1038/nature10189

Doan, D. N., Veal, T. M., Yan, Z., Wang, W., Jones, S. N., & Imbalzano, A. N. (2004). Loss of the INI1 tumor suppressor does not impair the expression of multiple BRG1-dependent genes or the assembly of SWI/SNF enzymes. *Oncogene, 23*(19), 3462-3473. doi: 10.1038/sj.onc.1207472

Docampo, R., Cruz, F. S., Boveris, A., Muniz, R. P., & Esquivel, D. M. (1979). beta-Lapachone enhancement of lipid peroxidation and superoxide anion and hydrogen peroxide formation by sarcoma 180 ascites tumor cells. *Biochem Pharmacol, 28*(6), 723-728.

Dong, Y., Bey, E. A., Li, L. S., Kabbani, W., Yan, J., Xie, X. J., Hsieh, J. T., Gao, J., & Boothman, D. A. (2010). Prostate cancer radiosensitization through poly(ADP-Ribose) polymerase-1 hyperactivation. *Cancer Res, 70*(20), 8088-8096. doi: 10.1158/0008-5472.CAN-10-1418

Dong, Y., Chin, S. F., Blanco, E., Bey, E. A., Kabbani, W., Xie, X. J., Bornmann, W. G., Boothman, D. A., & Gao, J. (2009). Intratumoral delivery of beta-lapachone via polymer implants for prostate cancer therapy. *Clin Cancer Res, 15*(1), 131-139. doi: 10.1158/1078-0432.CCR-08-1691

Du, X., Matsumura, T., Edelstein, D., Rossetti, L., Zsengeller, Z., Szabo, C., & Brownlee, M. (2003). Inhibition of GAPDH activity by poly(ADP-ribose) polymerase activates three major pathways of hyperglycemic damage in endothelial cells. *J Clin Invest, 112*(7), 1049-1057. doi: 10.1172/JCI18127

El-Khamisy, S. F., Masutani, M., Suzuki, H., & Caldecott, K. W. (2003). A requirement for PARP-1 for the assembly or stability of XRCC1 nuclear foci at sites of oxidative DNA damage. *Nucleic Acids Res, 31*(19), 5526-5533.

Fagerholm, R., Hofstetter, B., Tommiska, J., Aaltonen, K., Vrtel, R., Syrjakoski, K., Kallioniemi, A., Kilpivaara, O., Mannermaa, A., Kosma, V. M., Uusitupa, M., Eskelinen, M., Kataja, V., Aittomaki, K., von Smitten, K., Heikkila, P., Lukas, J., Holli, K., Bartkova, J., Blomqvist, C., Bartek, J., & Nevanlinna, H. (2008). NAD(P)H:quinone oxidoreductase 1 NQO1*2 genotype (P187S) is a strong prognostic and predictive factor in breast cancer. *Nat Genet, 40*(7), 844-853. doi: 10.1038/ng.155

Faig, M., Bianchet, M. A., Winski, S., Hargreaves, R., Moody, C. J., Hudnott, A. R., Ross, D., & Amzel, L. M. (2001). Structure-based development of anticancer drugs: complexes of NAD(P)H:quinone oxidoreductase 1 with chemotherapeutic quinones. *Structure, 9*(8), 659-667.

Farber, S., & Diamond, L. K. (1948). Temporary remissions in acute leukemia in children produced by folic acid antagonist, 4-aminopteroyl-glutamic acid. *N Engl J Med, 238*(23), 787-793. doi: 10.1056/NEJM194806032382301

Farmer, H., McCabe, N., Lord, C. J., Tutt, A. N., Johnson, D. A., Richardson, T. B., Santarosa, M., Dillon, K. J., Hickson, I., Knights, C., Martin, N. M., Jackson, S. P., Smith, G. C., & Ashworth, A. (2005). Targeting the DNA repair defect in BRCA mutant cells as a therapeutic strategy. *Nature, 434*(7035), 917-921. doi: 10.1038/nature03445

Flaherty, K. T., Puzanov, I., Kim, K. B., Ribas, A., McArthur, G. A., Sosman, J. A., O'Dwyer, P. J., Lee, R. J., Grippo, J. F., Nolop, K., & Chapman, P. B. (2010). Inhibition of mutated, activated BRAF in metastatic melanoma. *N Engl J Med, 363*(9), 809-819. doi: 10.1056/NEJMoa1002011

Fong, P. C., Yap, T. A., Boss, D. S., Carden, C. P., Mergui-Roelvink, M., Gourley, C., De Greve, J., Lubinski, J., Shanley, S., Messiou, C., A'Hern, R., Tutt, A., Ashworth, A., Stone, J., Carmichael, J., Schellens, J. H., de Bono, J. S., & Kaye, S. B. (2010). Poly(ADP)-ribose polymerase inhibition: frequent durable responses in BRCA carrier ovarian cancer correlating with platinum-free interval. *J Clin Oncol, 28*(15), 2512-2519. doi: 10.1200/JCO.2009.26.9589

Gadd, S., Sredni, S. T., Huang, C. C., Perlman, E. J., & Renal Tumor Committee of the Children's Oncology, G. (2010). Rhabdoid tumor: gene expression clues to pathogenesis and potential therapeutic targets. *Lab Invest, 90*(5), 724-738. doi: 10.1038/labinvest.2010.66

Gaedigk, A., Tyndale, R. F., Jurima-Romet, M., Sellers, E. M., Grant, D. M., & Leeder, J. S. (1998). NAD(P)H:quinone oxidoreductase: polymorphisms and allele frequencies in Caucasian, Chinese and Canadian Native Indian and Inuit populations. *Pharmacogenetics, 8*(4), 305-313.

Gebel, S., Gerstmayer, B., Bosio, A., Haussmann, H. J., Van Miert, E., & Muller, T. (2004). Gene expression profiling in respiratory tissues from rats exposed to mainstream cigarette smoke. *Carcinogenesis, 25*(2), 169-178. doi: 10.1093/carcin/bgg193

Gerber, D., Arriaga, Y., Beg, M. S., Dowell, J. E., Schiller, J. H., Frankel, A. E., Leff, R., Meek, C., Bolluyt, J., Fatunde, O., Martinez, R. T., Vo, P., Fattah, F., Sarode, V., Zhou, Y., Xie, Y., McLeod, M., Schwartz, B., & Boothman, D. A. 253 Phase 1 correlative study of ARQ761, a β-lapachone analogue that promotes NQ01-mediated programmed cancer cell necrosis. *European Journal of Cancer, 50*, 84-85. doi: 10.1016/S0959-8049(14)70379-X

Gorre, M. E., Mohammed, M., Ellwood, K., Hsu, N., Paquette, R., Rao, P. N., & Sawyers, C. L. (2001). Clinical resistance to STI-571 cancer therapy caused by BCR-ABL gene mutation or amplification. *Science, 293*(5531), 876-880. doi: 10.1126/science.1062538

Gottesman, M. M. (2002). Mechanisms of cancer drug resistance. *Annu Rev Med, 53*, 615-627. doi: 10.1146/annurev.med.53.082901.103929

Grant, C. M., Quinn, K. A., & Dawes, I. W. (1999). Differential protein S-thiolation of glyceraldehyde-3-phosphate dehydrogenase isoenzymes influences sensitivity to oxidative stress. *Mol Cell Biol, 19*(4), 2650-2656.

Haince, J. F., McDonald, D., Rodrigue, A., Dery, U., Masson, J. Y., Hendzel, M. J., & Poirier, G. G. (2008). PARP1-dependent kinetics of recruitment of MRE11 and NBS1 proteins to multiple DNA damage sites. *J Biol Chem, 283*(2), 1197-1208. doi: 10.1074/jbc.M706734200

Hajnoczky, G., Davies, E., & Madesh, M. (2003). Calcium signaling and apoptosis. *Biochem Biophys Res Commun, 304*(3), 445-454.

Hanahan, D., & Weinberg, R. A. (2011). Hallmarks of cancer: the next generation. *Cell, 144*(5), 646-674. doi: 10.1016/j.cell.2011.02.013

Hartner, L., Rosen, L., Hensley, M., Mendelson, D., Staddon, A., Chow, W., Kovalyov, O., Ruka, W., Skladowski, K., & Jagiello-Gruszfeld, A. (2007). Phase 2 dose multi-center, open-label study of ARQ 501, a checkpoint activator, in adult patients with persistent, recurrent or metastatic leiomyosarcoma (LMS). *J Clin Oncol, 25*, 20521.

Hassa, P. O., & Hottiger, M. O. (2008). The diverse biological roles of mammalian PARPS, a small but powerful family of poly-ADP-ribose polymerases. *Front Biosci, 13*, 3046-3082.

Helleday, T., Petermann, E., Lundin, C., Hodgson, B., & Sharma, R. A. (2008). DNA repair pathways as targets for cancer therapy. *Nat Rev Cancer, 8*(3), 193-204. doi: 10.1038/nrc2342

Holen, K., Saltz, L. B., Hollywood, E., Burk, K., & Hanauske, A. R. (2008). The pharmacokinetics, toxicities, and biologic effects of FK866, a nicotinamide adenine dinucleotide biosynthesis inhibitor. *Invest New Drugs, 26*(1), 45-51. doi: 10.1007/s10637-007-9083-2

Holohan, C., Van Schaeybroeck, S., Longley, D. B., & Johnston, P. G. (2013). Cancer drug resistance: an evolving paradigm. *Nat Rev Cancer, 13*(10), 714-726. doi: 10.1038/nrc3599

Houtkooper, R. H., Canto, C., Wanders, R. J., & Auwerx, J. (2010). The secret life of NAD+: an old metabolite controlling new metabolic signaling pathways. *Endocr Rev, 31*(2), 194-223. doi: 10.1210/er.2009-0026

Huang, C. C., Cutcliffe, C., Coffin, C., Sorensen, P. H., Beckwith, J. B., Perlman, E. J., & Renal Tumor Committee of the Children's Oncology, G. (2006). Classification of malignant pediatric renal tumors by gene expression. *Pediatr Blood Cancer, 46*(7), 728-738. doi: 10.1002/pbc.20773

Huang, G., Chen, H., Dong, Y., Luo, X., Yu, H., Moore, Z., Bey, E. A., Boothman, D. A., & Gao, J. (2013). Superparamagnetic iron oxide nanoparticles: amplifying ROS stress to improve anticancer drug efficacy. *Theranostics, 3*(2), 116-126. doi: 10.7150/thno.5411

Huang, X., Dong, Y., Bey, E. A., Kilgore, J. A., Bair, J. S., Li, L. S., Patel, M., Parkinson, E. I., Wang, Y., Williams, N. S., Gao, J., Hergenrother, P. J., & Boothman, D. A. (2012). An NQO1 substrate with potent antitumor activity that selectively kills by PARP1-induced programmed necrosis. *Cancer Res, 72*(12), 3038-3047. doi: 10.1158/0008-5472.CAN-11-3135

Hwang, N. R., Yim, S. H., Kim, Y. M., Jeong, J., Song, E. J., Lee, Y., Lee, J. H., Choi, S., & Lee, K. J. (2009). Oxidative modifications of glyceraldehyde-3-phosphate dehydrogenase play a key role in its multiple cellular functions. *Biochem J, 423*(2), 253-264. doi: 10.1042/BJ20090854

Hynes, N. E., & Lane, H. A. (2005). ERBB receptors and cancer: the complexity of targeted inhibitors. *Nat Rev Cancer, 5*(5), 341-354. doi: 10.1038/nrc1609

Imlay, J. A., Chin, S. M., & Linn, S. (1988). Toxic DNA damage by hydrogen peroxide through the Fenton reaction in vivo and in vitro. *Science, 240*(4852), 640-642.

Irizarry, R. A., Hobbs, B., Collin, F., Beazer-Barclay, Y. D., Antonellis, K. J., Scherf, U., & Speed, T. P. (2003). Exploration, normalization, and summaries of high density

oligonucleotide array probe level data. *Biostatistics, 4*(2), 249-264. doi: 10.1093/biostatistics/4.2.249

Isakoff, M. S., Sansam, C. G., Tamayo, P., Subramanian, A., Evans, J. A., Fillmore, C. M., Wang, X., Biegel, J. A., Pomeroy, S. L., Mesirov, J. P., & Roberts, C. W. (2005). Inactivation of the Snf5 tumor suppressor stimulates cell cycle progression and cooperates with p53 loss in oncogenic transformation. *Proc Natl Acad Sci U S A, 102*(49), 17745-17750. doi: 10.1073/pnas.0509014102

Jackson, E. M., Sievert, A. J., Gai, X., Hakonarson, H., Judkins, A. R., Tooke, L., Perin, J. C., Xie, H., Shaikh, T. H., & Biegel, J. A. (2009). Genomic analysis using high-density single nucleotide polymorphism-based oligonucleotide arrays and multiplex ligation-dependent probe amplification provides a comprehensive analysis of INI1/SMARCB1 in malignant rhabdoid tumors. *Clin Cancer Res, 15*(6), 1923-1930. doi: 10.1158/1078-0432.CCR-08-2091

Jacob, D. A., Bahra, M., Langrehr, J. M., Boas-Knoop, S., Stefaniak, R., Davis, J., Schumacher, G., Lippert, S., & Neumann, U. P. (2007). Combination therapy of poly (ADP-ribose) polymerase inhibitor 3-aminobenzamide and gemcitabine shows strong antitumor activity in pancreatic cancer cells. *J Gastroenterol Hepatol, 22*(5), 738-748. doi: 10.1111/j.1440-1746.2006.04496.x

Janku, F., Stewart, D. J., & Kurzrock, R. (2010). Targeted therapy in non-small-cell lung cancer--is it becoming a reality? *Nat Rev Clin Oncol, 7*(7), 401-414. doi: 10.1038/nrclinonc.2010.64

Kalpana, G. V., Marmon, S., Wang, W., Crabtree, G. R., & Goff, S. P. (1994). Binding and stimulation of HIV-1 integrase by a human homolog of yeast transcription factor SNF5. *Science, 266*(5193), 2002-2006.

Kamb, A., Wee, S., & Lengauer, C. (2007). Why is cancer drug discovery so difficult? *Nat Rev Drug Discov, 6*(2), 115-120. doi: 10.1038/nrd2155

Kelsey, K. T., Ross, D., Traver, R. D., Christiani, D. C., Zuo, Z. F., Spitz, M. R., Wang, M., Xu, X., Lee, B. K., Schwartz, B. S., & Wiencke, J. K. (1997). Ethnic variation in the prevalence of a common NAD(P)H quinone oxidoreductase polymorphism and its implications for anti-cancer chemotherapy. *Br J Cancer, 76*(7), 852-854.

Knipstein, J. A., Birks, D. K., Donson, A. M., Alimova, I., Foreman, N. K., & Vibhakar, R. (2012). Histone deacetylase inhibition decreases proliferation and potentiates the effect of ionizing radiation in atypical teratoid/rhabdoid tumor cells. *Neuro Oncol, 14*(2), 175-183. doi: 10.1093/neuonc/nor208

Knutson, S. K., Warholic, N. M., Wigle, T. J., Klaus, C. R., Allain, C. J., Raimondi, A., Porter Scott, M., Chesworth, R., Moyer, M. P., Copeland, R. A., Richon, V. M., Pollock, R. M., Kuntz, K. W., & Keilhack, H. (2013). Durable tumor regression in genetically altered malignant rhabdoid tumors by inhibition of methyltransferase EZH2. *Proc Natl Acad Sci U S A, 110*(19), 7922-7927. doi: 10.1073/pnas.1303800110

Kobayashi, S., Boggon, T. J., Dayaram, T., Janne, P. A., Kocher, O., Meyerson, M., Johnson, B. E., Eck, M. J., Tenen, D. G., & Halmos, B. (2005). EGFR mutation and resistance of non-small-cell lung cancer to gefitinib. *N Engl J Med, 352*(8), 786-792. doi: 10.1056/NEJMoa044238

L. P. Hartner, L. R., M. Hensley, D. Mendelson, A. P. Staddon, W. Chow, O. Kovalyov, W. Ruka, K. Skladowski, A. Jagiello-Gruszfeld, M. Byakhov. (2007). Phase 2 dose multi-center, open-label study of ARQ 501, a checkpoint activator, in adult patients with persistent, recurrent or metastatic leiomyosarcoma (LMS). *Journal of Clinical Oncology, 25*(18S).

Langelier, M. F., Planck, J. L., Roy, S., & Pascal, J. M. (2012). Structural basis for DNA damage-dependent poly(ADP-ribosyl)ation by human PARP-1. *Science, 336*(6082), 728-732. doi: 10.1126/science.1216338

Lawson, K. A., Woodson, K., Virtamo, J., & Albanes, D. (2005). Association of the NAD(P)H:quinone oxidoreductase (NQO1) 609C->T polymorphism with lung cancer risk among male smokers. *Cancer Epidemiol Biomarkers Prev, 14*(9), 2275-2276. doi: 10.1158/1055-9965.EPI-05-0375

Lewis, A. M., Ough, M., Hinkhouse, M. M., Tsao, M. S., Oberley, L. W., & Cullen, J. J. (2005). Targeting NAD(P)H:quinone oxidoreductase (NQO1) in pancreatic cancer. *Mol Carcinog, 43*(4), 215-224. doi: 10.1002/mc.20107

Li, L. S., Bey, E. A., Dong, Y., Meng, J., Patra, B., Yan, J., Xie, X. J., Brekken, R. A., Barnett, C. C., Bornmann, W. G., Gao, J., & Boothman, D. A. (2011). Modulating endogenous NQO1 levels identifies key regulatory mechanisms of action of beta-lapachone for pancreatic cancer therapy. *Clin Cancer Res, 17*(2), 275-285. doi: 10.1158/1078-0432.CCR-10-1983

Lindahl, T., Satoh, M. S., Poirier, G. G., & Klungland, A. (1995). Post-translational modification of poly(ADP-ribose) polymerase induced by DNA strand breaks. *Trends Biochem Sci, 20*(10), 405-411.

Logsdon, C. D., Simeone, D. M., Binkley, C., Arumugam, T., Greenson, J. K., Giordano, T. J., Misek, D. E., Kuick, R., & Hanash, S. (2003). Molecular profiling of pancreatic adenocarcinoma and chronic pancreatitis identifies multiple genes differentially regulated in pancreatic cancer. *Cancer Res, 63*(10), 2649-2657.

Lu, T. P., Tsai, M. H., Lee, J. M., Hsu, C. P., Chen, P. C., Lin, C. W., Shih, J. Y., Yang, P. C., Hsiao, C. K., Lai, L. C., & Chuang, E. Y. (2010). Identification of a novel biomarker, SEMA5A, for non-small cell lung carcinoma in nonsmoking women. *Cancer Epidemiol Biomarkers Prev, 19*(10), 2590-2597. doi: 10.1158/1055-9965.EPI-10-0332

Luo, X., & Kraus, W. L. (2012). On PAR with PARP: cellular stress signaling through poly(ADP-ribose) and PARP-1. *Genes Dev, 26*(5), 417-432. doi: 10.1101/gad.183509.111

Ma, X., Huang, X., Moore, Z., Huang, G., Kilgore, J. A., Wang, Y., Hammer, S., Williams, N. S., Boothman, D. A., & Gao, J. (2015). Esterase-activatable beta-lapachone prodrug micelles for NQO1-targeted lung cancer therapy. *J Control Release, 200*, 201-211. doi: 10.1016/j.jconrel.2014.12.027

Maloney, D. G., Smith, B., & Rose, A. (2002). Rituximab: mechanism of action and resistance. *Semin Oncol, 29*(1 Suppl 2), 2-9.

Mandir, A. S., Poitras, M. F., Berliner, A. R., Herring, W. J., Guastella, D. B., Feldman, A., Poirier, G. G., Wang, Z. Q., Dawson, T. M., & Dawson, V. L. (2000). NMDA but not non-NMDA excitotoxicity is mediated by Poly(ADP-ribose) polymerase. *J Neurosci, 20*(21), 8005-8011.

Mateos-Gomez, P. A., Gong, F., Nair, N., Miller, K. M., Lazzerini-Denchi, E., & Sfeir, A. (2015). Mammalian polymerase theta promotes alternative NHEJ and suppresses recombination. *Nature, 518*(7538), 254-257. doi: 10.1038/nature14157

McKenna, E. S., Sansam, C. G., Cho, Y. J., Greulich, H., Evans, J. A., Thom, C. S., Moreau, L. A., Biegel, J. A., Pomeroy, S. L., & Roberts, C. W. (2008). Loss of the epigenetic tumor suppressor SNF5 leads to cancer without genomic instability. *Mol Cell Biol, 28*(20), 6223-6233. doi: 10.1128/MCB.00658-08

Medicine, W. I. o. (1998). *Dietary reference intakes for Thiamin, Riboflavin, Niacin, Vitamin B6, Folate, Vitamin B12, Papntothenic Acid, Biotin, and Choline: a report of the Standing Committee on the Scientific Evaluation of Dietary Reference Intakes Food and Nutrition Board, Institute of Medicine*: Nat. Acad. Press.

Meric-Bernstam, F., Farhangfar, C., Mendelsohn, J., & Mills, G. B. (2013). Building a personalized medicine infrastructure at a major cancer center. *J Clin Oncol, 31*(15), 1849-1857. doi: 10.1200/JCO.2012.45.3043

Monteith, G. R., Davis, F. M., & Roberts-Thomson, S. J. (2012). Calcium channels and pumps in cancer: changes and consequences. *J Biol Chem, 287*(38), 31666-31673. doi: 10.1074/jbc.R112.343061

Moore, Z., Chakrabarti, G., Luo, X., Ali, A., Hu, Z., Fattah, F. J., Vemireddy, R., DeBerardinis, R. J., Brekken, R. A., & Boothman, D. A. (2015). NAMPT inhibition sensitizes pancreatic adenocarcinoma cells to tumor-selective, PAR-independent metabolic catastrophe and cell death induced by beta-lapachone. *Cell Death Dis, 6*, e1599. doi: 10.1038/cddis.2014.564

Motohashi, H., & Yamamoto, M. (2004). Nrf2-Keap1 defines a physiologically important stress response mechanism. *Trends Mol Med, 10*(11), 549-557. doi: 10.1016/j.molmed.2004.09.003

Munk Jensen, M., Erichsen, K. D., Johnbeck, C. B., Bjorkling, F., Madsen, J., Bzorek, M., Jensen, P. B., Hojgaard, L., Sehested, M., & Kjaer, A. (2013). [18F]FLT and [18F]FDG PET for Non-invasive Treatment Monitoring of the Nicotinamide Phosphoribosyltransferase Inhibitor APO866 in Human Xenografts. *PLoS One, 8*(1), e53410. doi: 10.1371/journal.pone.0053410

Nahimana, A., Attinger, A., Aubry, D., Greaney, P., Ireson, C., Thougaard, A. V., Tjornelund, J., Dawson, K. M., Dupuis, M., & Duchosal, M. A. (2009). The NAD biosynthesis inhibitor APO866 has potent antitumor activity against hematologic malignancies. *Blood, 113*(14), 3276-3286. doi: 10.1182/blood-2008-08-173369

Nahta, R., Yuan, L. X., Zhang, B., Kobayashi, R., & Esteva, F. J. (2005). Insulin-like growth factor-I receptor/human epidermal growth factor receptor 2 heterodimerization contributes to trastuzumab resistance of breast cancer cells. *Cancer Res, 65*(23), 11118-11128. doi: 10.1158/0008-5472.CAN-04-3841

Natter, K., & Kohlwein, S. D. (2013). Yeast and cancer cells - common principles in lipid metabolism. *Biochim Biophys Acta, 1831*(2), 314-326. doi: 10.1016/j.bbalip.2012.09.003

Nolan, K. A., Timson, D. J., Stratford, I. J., & Bryce, R. A. (2006). In silico identification and biochemical characterization of novel inhibitors of NQO1. *Bioorg Med Chem Lett, 16*(24), 6246-6254. doi: 10.1016/j.bmcl.2006.09.015

O'brien, P. (1991). Molecular mechanisms of quinone cytotoxicity. *Chem Biol Interact, 80*(1), 1-41.

O'Brien, T., Oeh, J., Xiao, Y., Liang, X., Vanderbilt, A., Qin, A., Yang, L., Lee, L. B., Ly, J., Cosino, E., LaCap, J. A., Ogasawara, A., Williams, S., Nannini, M., Liederer, B. M., Jackson, P., Dragovich, P. S., & Sampath, D. (2013). Supplementation of nicotinic acid with NAMPT inhibitors results in loss of in vivo efficacy in NAPRT1-deficient tumor models. *Neoplasia, 15*(12), 1314-1329.

Olesen, U. H., Hastrup, N., & Sehested, M. (2011). Expression patterns of nicotinamide phosphoribosyltransferase and nicotinic acid phosphoribosyltransferase in human malignant lymphomas. *APMIS, 119*(4-5), 296-303. doi: 10.1111/j.1600-0463.2011.02733.x

Park, E. J., Min, K. J., Lee, T. J., Yoo, Y. H., Kim, Y. S., & Kwon, T. K. (2014). beta-Lapachone induces programmed necrosis through the RIP1-PARP-AIF-dependent pathway in human hepatocellular carcinoma SK-Hep1 cells. *Cell Death Dis, 5*, e1230. doi: 10.1038/cddis.2014.202

Park, H. J., Ahn, K. J., Ahn, S. D., Choi, E., Lee, S. W., Williams, B., Kim, E. J., Griffin, R., Bey, E. A., Bornmann, W. G., Gao, J., Park, H. J., Boothman, D. A., & Song, C. W. (2005). Susceptibility of cancer cells to beta-lapachone is enhanced by ionizing radiation. *Int J Radiat Oncol Biol Phys, 61*(1), 212-219. doi: 10.1016/j.ijrobp.2004.09.018

Park, M. T., Song, M. J., Lee, H., Oh, E. T., Choi, B. H., Jeong, S. Y., Choi, E. K., & Park, H. J. (2011). beta-lapachone significantly increases the effect of ionizing radiation to cause mitochondrial apoptosis via JNK activation in cancer cells. *PLoS One, 6*(10), e25976. doi: 10.1371/journal.pone.0025976

Pink, J. J., Planchon, S. M., Tagliarino, C., Varnes, M. E., Siegel, D., & Boothman, D. A. (2000). NAD(P)H:Quinone oxidoreductase activity is the principal determinant of beta-lapachone cytotoxicity. *The Journal of biological chemistry, 275*(8), 5416-5424.

Pink, J. J., Wuerzberger-Davis, S., Tagliarino, C., Planchon, S. M., Yang, X., Froelich, C. J., & Boothman, D. A. (2000). Activation of a cysteine protease in MCF-7 and T47D breast cancer cells during beta-lapachone-mediated apoptosis. *Exp Cell Res, 255*(2), 144-155. doi: 10.1006/excr.1999.4790

Planchon, S. M., Pink, J. J., Tagliarino, C., Bornmann, W. G., Varnes, M. E., & Boothman, D. A. (2001). beta-Lapachone-induced apoptosis in human prostate cancer cells: involvement of NQO1/xip3. *Exp Cell Res, 267*(1), 95-106. doi: 10.1006/excr.2001.5234

Preiss, J., & Handler, P. (1958a). Biosynthesis of diphosphopyridine nucleotide. I. Identification of intermediates. *J Biol Chem, 233*(2), 488-492.

Preiss, J., & Handler, P. (1958b). Biosynthesis of diphosphopyridine nucleotide. II. Enzymatic aspects. *J Biol Chem, 233*(2), 493-500.

Preusch, P. C., Siegel, D., Gibson, N. W., & Ross, D. (1991). A note on the inhibition of DT-diaphorase by dicoumarol. *Free Radic Biol Med, 11*(1), 77-80.

Radjendirane, V., Joseph, P., Lee, Y. H., Kimura, S., Klein-Szanto, A. J., Gonzalez, F. J., & Jaiswal, A. K. (1998). Disruption of the DT diaphorase (NQO1) gene in mice leads to increased menadione toxicity. *J Biol Chem, 273*(13), 7382-7389.

Rajan, A., Carter, C. A., Kelly, R. J., Gutierrez, M., Kummar, S., Szabo, E., Yancey, M. A., Ji, J., Mannargudi, B., Woo, S., Spencer, S., Figg, W. D., & Giaccone, G. (2012). A phase I combination study of olaparib with cisplatin and gemcitabine in adults with solid tumors. *Clin Cancer Res, 18*(8), 2344-2351. doi: 10.1158/1078-0432.CCR-11-2425

Ray, A., Mir, S. N., Wani, G., Zhao, Q., Battu, A., Zhu, Q., Wang, Q. E., & Wani, A. A. (2009). Human SNF5/INI1, a component of the human SWI/SNF chromatin remodeling complex, promotes nucleotide excision repair by influencing ATM recruitment and downstream H2AX phosphorylation. *Mol Cell Biol, 29*(23), 6206-6219. doi: 10.1128/MCB.00503-09

Reddy, S., Li, L., Boothman, D. A., Sumer, B., & Yordy, J. S. NQO1-Mediated Synergistic Lethality in Combination With β-lapachone (β-lap) and Ionizing Radiation (IR) in Head-and-Neck Cancer (HNC). *International Journal of Radiation Oncology • Biology • Physics, 87*(2), S139. doi: 10.1016/j.ijrobp.2013.06.357

Reinicke, K. E., Bey, E. A., Bentle, M. S., Pink, J. J., Ingalls, S. T., Hoppel, C. L., Misico, R. I., Arzac, G. M., Burton, G., Bornmann, W. G., Sutton, D., Gao, J., & Boothman, D. A. (2005). Development of beta-lapachone prodrugs for therapy against human cancer cells with elevated NAD(P)H:quinone oxidoreductase 1 levels. *Clin Cancer Res, 11*(8), 3055-3064. doi: 10.1158/1078-0432.CCR-04-2185

Roberts, C. W., & Biegel, J. A. (2009). The role of SMARCB1/INI1 in development of rhabdoid tumor. *Cancer Biol Ther, 8*(5), 412-416.

Roberts, C. W., Galusha, S. A., McMenamin, M. E., Fletcher, C. D., & Orkin, S. H. (2000). Haploinsufficiency of Snf5 (integrase interactor 1) predisposes to malignant rhabdoid tumors in mice. *Proc Natl Acad Sci U S A, 97*(25), 13796-13800. doi: 10.1073/pnas.250492697

Roberts, C. W., Leroux, M. M., Fleming, M. D., & Orkin, S. H. (2002). Highly penetrant, rapid tumorigenesis through conditional inversion of the tumor suppressor gene Snf5. *Cancer Cell, 2*(5), 415-425.

Robinson, M. D., & Speed, T. P. (2007). A comparison of Affymetrix gene expression arrays. *BMC Bioinformatics, 8*, 449. doi: 10.1186/1471-2105-8-449

Rorke, L. B., Packer, R., & Biegel, J. (1995). Central nervous system atypical teratoid/rhabdoid tumors of infancy and childhood. *J Neurooncol, 24*(1), 21-28.

Ross, D., Kepa, J. K., Winski, S. L., Beall, H. D., Anwar, A., & Siegel, D. (2000). NAD(P)H:quinone oxidoreductase 1 (NQO1): chemoprotection, bioactivation, gene regulation and genetic polymorphisms. *Chem Biol Interact, 129*(1-2), 77-97.

Rovito, H. A., & Oblong, J. E. (2013). Nicotinamide preferentially protects glycolysis in dermal fibroblasts under oxidative stress conditions. *Br J Dermatol, 169 Suppl 2*, 15-24. doi: 10.1111/bjd.12365

Rowe, B. P., & Glazer, P. M. (2010). Emergence of rationally designed therapeutic strategies for breast cancer targeting DNA repair mechanisms. *Breast Cancer Res, 12*(2), 203. doi: 10.1186/bcr2566

Saha, A., Wittmeyer, J., & Cairns, B. R. (2006a). Chromatin remodelling: the industrial revolution of DNA around histones. *Nat Rev Mol Cell Biol, 7*(6), 437-447. doi: 10.1038/nrm1945

Saha, A., Wittmeyer, J., & Cairns, B. R. (2006b). Mechanisms for nucleosome movement by ATP-dependent chromatin remodeling complexes. *Results Probl Cell Differ, 41*, 127-148.

Sanchez-Palencia, A., Gomez-Morales, M., Gomez-Capilla, J. A., Pedraza, V., Boyero, L., Rosell, R., & Farez-Vidal, M. E. (2011). Gene expression profiling reveals novel biomarkers in nonsmall cell lung cancer. *Int J Cancer, 129*(2), 355-364. doi: 10.1002/ijc.25704

Sandhu, S. K., Schelman, W. R., Wilding, G., Moreno, V., Baird, R. D., Miranda, S., Hylands, L., Riisnaes, R., Forster, M., Omlin, A., Kreischer, N., Thway, K., Gevensleben, H., Sun, L., Loughney, J., Chatterjee, M., Toniatti, C., Carpenter, C. L., Iannone, R., Kaye, S. B., de Bono, J. S., & Wenham, R. M. (2013). The poly(ADP-ribose) polymerase inhibitor niraparib (MK4827) in BRCA mutation carriers and patients with sporadic cancer: a phase 1 dose-escalation trial. *Lancet Oncol, 14*(9), 882-892. doi: 10.1016/S1470-2045(13)70240-7

Savage, R. E., Hall, T., Bresciano, K., Bailey, J., Starace, M., & Chan, T. C. (2008). Development and validation of a liquid chromatography-tandem mass spectrometry method for the determination of ARQ 501 (beta-lapachone) in plasma and tumors from nu/nu mouse xenografts. *J Chromatogr B Analyt Technol Biomed Life Sci, 872*(1-2), 148-153. doi: 10.1016/j.jchromb.2008.07.031

Sawyers, C. (2004). Targeted cancer therapy. *Nature, 432*(7015), 294-297. doi: 10.1038/nature03095

Schlager, J. J., & Powis, G. (1990). Cytosolic NAD(P)H:(quinone-acceptor)oxidoreductase in human normal and tumor tissue: effects of cigarette smoking and alcohol. *Int J Cancer, 45*(3), 403-409.

Scott, A. M., Wolchok, J. D., & Old, L. J. (2012). Antibody therapy of cancer. *Nat Rev Cancer, 12*(4), 278-287. doi: 10.1038/nrc3236

Shah, H. R., Conway, R. M., Van Quill, K. R., Madigan, M. C., Howard, S. A., Qi, J., Weinberg, V., & O'Brien, J. M. (2008). Beta-lapachone inhibits proliferation and induces apoptosis in retinoblastoma cell lines. *Eye (Lond), 22*(3), 454-460. doi: 10.1038/sj.eye.6702764

Siegel, D., Franklin, W. A., & Ross, D. (1998). Immunohistochemical detection of NAD(P)H:quinone oxidoreductase in human lung and lung tumors. *Clin Cancer Res, 4*(9), 2065-2070.

Siegel, D., & Ross, D. (2000). Immunodetection of NAD(P)H:quinone oxidoreductase 1 (NQO1) in human tissues. *Free Radic Biol Med, 29*(3-4), 246-253.

Siegel, R., Naishadham, D., & Jemal, A. (2013). Cancer statistics, 2013. *CA Cancer J Clin, 63*(1), 11-30. doi: 10.3322/caac.21166

Siegel, R. L., Miller, K. D., & Jemal, A. (2015). Cancer statistics, 2015. *CA Cancer J Clin, 65*(1), 5-29. doi: 10.3322/caac.21254

Singh, A., Misra, V., Thimmulappa, R. K., Lee, H., Ames, S., Hoque, M. O., Herman, J. G., Baylin, S. B., Sidransky, D., Gabrielson, E., Brock, M. V., & Biswal, S. (2006).

Dysfunctional KEAP1-NRF2 interaction in non-small-cell lung cancer. *PLoS Med, 3*(10), e420. doi: 10.1371/journal.pmed.0030420

Smith, C. L., Horowitz-Scherer, R., Flanagan, J. F., Woodcock, C. L., & Peterson, C. L. (2003). Structural analysis of the yeast SWI/SNF chromatin remodeling complex. *Nat Struct Biol, 10*(2), 141-145. doi: 10.1038/nsb888

Srivastava, M., Khurana, P., & Sugadev, R. (2012). Lung cancer signature biomarkers: tissue specific semantic similarity based clustering of digital differential display (DDD) data. *BMC Res Notes, 5*, 617. doi: 10.1186/1756-0500-5-617

Stinson, S., Lackner, M. R., Adai, A. T., Yu, N., Kim, H. J., O'Brien, C., Spoerke, J., Jhunjhunwala, S., Boyd, Z., Januario, T., Newman, R. J., Yue, P., Bourgon, R., Modrusan, Z., Stern, H. M., Warming, S., de Sauvage, F. J., Amler, L., Yeh, R. F., & Dornan, D. (2011). TRPS1 targeting by miR-221/222 promotes the epithelial-to-mesenchymal transition in breast cancer. *Sci Signal, 4*(177), ra41. doi: 10.1126/scisignal.2001538

Stockwell, S. (2014). FDA Grants Accelerated Approval to Olaparib (Lynparza) to Treat Advanced Ovarian Cancer; Companion Diagnostic Test Also Approved. *Oncology Times*.

Sudarsanam, P., Iyer, V. R., Brown, P. O., & Winston, F. (2000). Whole-genome expression analysis of snf/swi mutants of Saccharomyces cerevisiae. *Proc Natl Acad Sci U S A, 97*(7), 3364-3369. doi: 10.1073/pnas.050407197

Suzuki, M., & Kurata, M. (1992). Effects of ATP level on glutathione regeneration in rabbit and guinea-pig erythrocytes. *Comp Biochem Physiol B, 103*(4), 859-862.

Tagliarino, C., Pink, J. J., Dubyak, G. R., Nieminen, A. L., & Boothman, D. A. (2001). Calcium is a key signaling molecule in beta-lapachone-mediated cell death. *J Biol Chem, 276*(22), 19150-19159. doi: 10.1074/jbc.M100730200

Tagliarino, C., Pink, J. J., Reinicke, K. E., Simmers, S. M., Wuerzberger-Davis, S. M., & Boothman, D. A. (2003). Mu-calpain activation in beta-lapachone-mediated apoptosis. *Cancer Biol Ther, 2*(2), 141-152.

Talalay, P. (2000). Chemoprotection against cancer by induction of phase 2 enzymes. *Biofactors, 12*(1-4), 5-11.

Tan, B., Young, D. A., Lu, Z. H., Wang, T., Meier, T. I., Shepard, R. L., Roth, K., Zhai, Y., Huss, K., Kuo, M. S., Gillig, J., Parthasarathy, S., Burkholder, T. P., Smith, M. C., Geeganage, S., & Zhao, G. (2013). Pharmacological inhibition of nicotinamide phosphoribosyltransferase (NAMPT), an enzyme essential for NAD+ biosynthesis, in human cancer cells: metabolic basis and potential clinical implications. *J Biol Chem, 288*(5), 3500-3511. doi: 10.1074/jbc.M112.394510

Tanigawa, S., Fujii, M., & Hou, D. X. (2007). Action of Nrf2 and Keap1 in ARE-mediated NQO1 expression by quercetin. *Free Radic Biol Med, 42*(11), 1690-1703. doi: 10.1016/j.freeradbiomed.2007.02.017

Terai, K., Dong, G. Z., Oh, E. T., Park, M. T., Gu, Y., Song, C. W., & Park, H. J. (2009). Cisplatin enhances the anticancer effect of beta-lapachone by upregulating NQO1. *Anticancer Drugs, 20*(10), 901-909. doi: 10.1097/CAD.0b013e328330098d

Travelli, C., Drago, V., Maldi, E., Kaludercic, N., Galli, U., Boldorini, R., Di Lisa, F., Tron, G. C., Canonico, P. L., & Genazzani, A. A. (2011). Reciprocal potentiation of the

antitumoral activities of FK866, an inhibitor of nicotinamide phosphoribosyltransferase, and etoposide or cisplatin in neuroblastoma cells. *J Pharmacol Exp Ther, 338*(3), 829-840. doi: 10.1124/jpet.111.184630

Turner, N., Tutt, A., & Ashworth, A. (2005). Targeting the DNA repair defect of BRCA tumours. *Curr Opin Pharmacol, 5*(4), 388-393. doi: 10.1016/j.coph.2005.03.006

Underhill, C., Toulmonde, M., & Bonnefoi, H. (2011). A review of PARP inhibitors: from bench to bedside. *Ann Oncol, 22*(2), 268-279. doi: 10.1093/annonc/mdq322

Vaitkevicius, V. K., Brennan, M. J., Beckett, V. L., Kelly, J. E., & Talley, R. W. (1961). Clinical evaluation of cancer chemotherapy with 5-fluorouracil. *Cancer, 14*, 131-152.

van Wijk, S. J., & Hageman, G. J. (2005). Poly(ADP-ribose) polymerase-1 mediated caspase-independent cell death after ischemia/reperfusion. *Free Radic Biol Med, 39*(1), 81-90. doi: 10.1016/j.freeradbiomed.2005.03.021

Vanden Berghe, T., Linkermann, A., Jouan-Lanhouet, S., Walczak, H., & Vandenabeele, P. (2014). Regulated necrosis: the expanding network of non-apoptotic cell death pathways. *Nat Rev Mol Cell Biol, 15*(2), 135-147. doi: 10.1038/nrm3737

Villanueva, J., Vultur, A., Lee, J. T., Somasundaram, R., Fukunaga-Kalabis, M., Cipolla, A. K., Wubbenhorst, B., Xu, X., Gimotty, P. A., Kee, D., Santiago-Walker, A. E., Letrero, R., D'Andrea, K., Pushparajan, A., Hayden, J. E., Brown, K. D., Laquerre, S., McArthur, G. A., Sosman, J. A., Nathanson, K. L., & Herlyn, M. (2010). Acquired resistance to BRAF inhibitors mediated by a RAF kinase switch in melanoma can be overcome by cotargeting MEK and IGF-1R/PI3K. *Cancer Cell, 18*(6), 683-695. doi: 10.1016/j.ccr.2010.11.023

Virag, L., Robaszkiewicz, A., Rodriguez-Vargas, J. M., & Oliver, F. J. (2013). Poly(ADP-ribose) signaling in cell death. *Mol Aspects Med, 34*(6), 1153-1167. doi: 10.1016/j.mam.2013.01.007

von Heideman, A., Berglund, A., Larsson, R., & Nygren, P. (2010). Safety and efficacy of NAD depleting cancer drugs: results of a phase I clinical trial of CHS 828 and overview of published data. *Cancer Chemother Pharmacol, 65*(6), 1165-1172. doi: 10.1007/s00280-009-1125-3

von Hoff, K., Hinkes, B., Dannenmann-Stern, E., von Bueren, A. O., Warmuth-Metz, M., Soerensen, N., Emser, A., Zwiener, I., Schlegel, P. G., Kuehl, J., Fruhwald, M. C., Kortmann, R. D., Pietsch, T., & Rutkowski, S. (2011). Frequency, risk-factors and survival of children with atypical teratoid rhabdoid tumors (AT/RT) of the CNS diagnosed between 1988 and 2004, and registered to the German HIT database. *Pediatr Blood Cancer, 57*(6), 978-985. doi: 10.1002/pbc.23236

Vries, R. G., Bezrookove, V., Zuijderduijn, L. M., Kia, S. K., Houweling, A., Oruetxebarria, I., Raap, A. K., & Verrijzer, C. P. (2005). Cancer-associated mutations in chromatin remodeler hSNF5 promote chromosomal instability by compromising the mitotic checkpoint. *Genes Dev, 19*(6), 665-670. doi: 10.1101/gad.335805

Wang, M., Wu, W., Wu, W., Rosidi, B., Zhang, L., Wang, H., & Iliakis, G. (2006). PARP-1 and Ku compete for repair of DNA double strand breaks by distinct NHEJ pathways. *Nucleic Acids Res, 34*(21), 6170-6182. doi: 10.1093/nar/gkl840

Wang, W., Elkins, K., Oh, A., Ho, Y. C., Wu, J., Li, H., Xiao, Y., Kwong, M., Coons, M., Brillantes, B., Cheng, E., Crocker, L., Dragovich, P. S., Sampath, D., Zheng, X., Bair, K. W., O'Brien, T., & Belmont, L. D. (2014). Structural basis for resistance to diverse classes of NAMPT inhibitors. *PLoS One, 9*(10), e109366. doi: 10.1371/journal.pone.0109366

Watanabe, M., Adachi, S., Matsubara, H., Imai, T., Yui, Y., Mizushima, Y., Hiraumi, Y., Watanabe, K., Kamitsuji, Y., Toyokuni, S. Y., Hosoi, H., Sugimoto, T., Toguchida, J., & Nakahata, T. (2009). Induction of autophagy in malignant rhabdoid tumor cells by the histone deacetylase inhibitor FK228 through AIF translocation. *Int J Cancer, 124*(1), 55-67. doi: 10.1002/ijc.23897

Wei, D., Goldfarb, D., Song, S., Cannon, C., Yan, F., Sakellariou-Thompson, D., Emanuele, M., Major, M. B., Weissman, B. E., & Kuwahara, Y. (2014). SNF5/INI1 deficiency redefines chromatin remodeling complex composition during tumor development. *Mol Cancer Res, 12*(11), 1574-1585. doi: 10.1158/1541-7786.MCR-14-0005

Wei, D., & Weissman, B. E. (2001). Genetics and Genomics of Malignant Rhabdoid Tumours *eLS*: John Wiley & Sons, Ltd.

Weinstein, I. B., & Joe, A. (2008). Oncogene addiction. *Cancer Res, 68*(9), 3077-3080; discussion 3080. doi: 10.1158/0008-5472.CAN-07-3293

Williams, R. T. (1967). Comparative patterns of drug metabolism. *Fed Proc, 26*(4), 1029-1039.

Wilson, B. G., & Roberts, C. W. (2011). SWI/SNF nucleosome remodellers and cancer. *Nat Rev Cancer, 11*(7), 481-492. doi: 10.1038/nrc3068

Woo, H. J., & Choi, Y. H. (2005). Growth inhibition of A549 human lung carcinoma cells by beta-lapachone through induction of apoptosis and inhibition of telomerase activity. *Int J Oncol, 26*(4), 1017-1023.

Ying, W., Sevigny, M. B., Chen, Y., & Swanson, R. A. (2001). Poly(ADP-ribose) glycohydrolase mediates oxidative and excitotoxic neuronal death. *Proc Natl Acad Sci U S A, 98*(21), 12227-12232. doi: 10.1073/pnas.211202598

Zhang, F., Xie, R., Munoz, F. M., Lau, S. S., & Monks, T. J. (2014). PARP-1 Hyperactivation and Reciprocal Elevations in Intracellular Ca2+ During ROS-Induced Nonapoptotic Cell Death. *Toxicol Sci, 140*(1), 118-134. doi: 10.1093/toxsci/kfu073